Output-only Modal Identification

4

4.1 Fundamental Assumptions in OMA

The expression Operational Modal Analysis means the class of modal identification methods based on response measurements only. This discipline has been systematized in the last two decades but early applications can be traced back to the beginning of modal testing in the 1960s. At that time output-only modal identification was referred to as ambient vibration testing. The first applications of OMA were mainly based on the analysis of PSDs and the identification of *Operational Deflection Shapes* (ODSs). An ODS represents the deflection of a structure at a particular frequency under a generic input and it is usually the result of the contribution of different modes. However, under certain assumptions, which are going to be illustrated in Sect. 4.4.1, ODSs are a close estimate of the actual mode shapes. In the 1990s a number of methods working in time domain were developed and applied in combination with correlation functions, leading to the so-called Natural Excitation Techniques (NExT) for output-only modal testing. In the same period the use of ARMA models for modal parameter estimation, first suggested in the late 1970s, started spreading. An increasing number of applications appeared in the literature but output-only modal identification was not fully developed and widely accepted as a reliable source of information, yet. However, at the end of the 1990s new effective output-only modal identification techniques, such as the Frequency Domain Decomposition (FDD) and the Stochastic Subspace Identification (SSI), became available, overcoming the limitations of the previous techniques in dealing with closely spaced modes and noise. Nowadays, OMA is a widely accepted tool for modal identification, with several successful applications in civil engineering (bridges, buildings, pedestrian bridges, historical structures, offshore platforms, wind turbines, dams, stadia),

Electronic supplementary material: The online version of this chapter (doi: 10.1007/978-1-4939-0767-0_4) contains supplementary material, which is available to authorized users. Supplementary material can also be accessed at http://link.springer.com/chapter/10.1007/978-1-4939-0767-0_4.

C. Rainieri and G. Fabbrocino, *Operational Modal Analysis of Civil Engineering Structures: An Introduction and Guide for Applications*, DOI 10.1007/978-1-4939-0767-0_4,

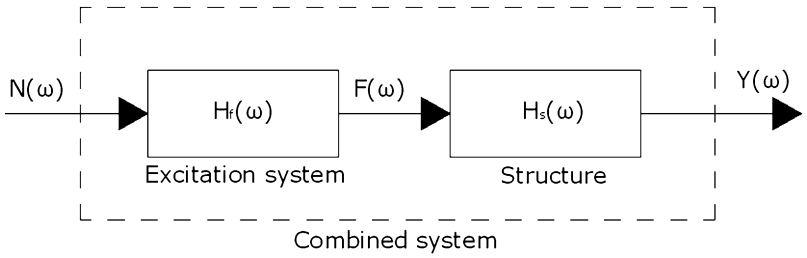

Fig. 4.1 The combined system

mechanical and industrial engineering (ships, trucks, car bodies, engines, rotating machineries), aerospace engineering (in-flight modal identification of aircrafts and shuttles, studies about flutter).

OMA is based on the following assumptions:

- *Linearity* (the response of the system to a given combination of inputs is equal to the same combination of the corresponding outputs),
- *Stationarity* (the dynamic characteristics of the structure do not change over time, so that the coefficients of the differential equations governing the dynamic response of the structure are independent of time),
- *Observability* (the sensor layout has been properly designed to observe the modes of interest, avoiding, for instance, nodal points).

Moreover, unlike traditional modal testing where the input is controlled, OMA is based on the dynamic response of the structure under test to noncontrollable and immeasurable loadings such as environmental and operational loads (traffic, wind, microtremors, and so on). As a consequence, some assumptions about the input are needed. If the structure is excited by white noise, that is to say, the input spectrum is constant, all modes are equally excited and the output spectrum contains full information about the structure. However, this is rarely the case, since the excitation has a spectral distribution of its own. Modes are, therefore, weighted by the spectral distribution of the input and both the properties of the input and the modal parameters of the structure are observed in the response. Additionally, noise and eventual spurious harmonics due to rotating equipment are observed in the response. Thus, in the general case, the structure is assumed to be excited by unknown forces that are the output of the so-called excitation system loaded by white noise (Fig. 4.1). Under this assumption, the measured response can be interpreted as the output of the combined system, made by the excitation system and the structure under test in series, to a stationary, zero mean, Gaussian white noise.

Since the excitation system and the structure under test are in series, the FRF of the combined system is the product their respective FRFs:

$$H_c(\omega) = H_f(\omega)H_s(\omega) \tag{4.1}$$

where $H_c(\omega)$, $H_f(\omega)$, and $H_s(\omega)$ are the FRFs of the combined system, the excitation system, and the structure under test, respectively. In fact, for each subsystem, output and input are related by the following equations:

$$F(\omega) = H_f(\omega)N(\omega) \tag{4.2}$$

$$Y(\omega) = H_s(\omega)F(\omega) \tag{4.3}$$

where N(ω), F(ω), and Y(ω) denote the Fourier transforms of the white noise input to the excitation system, the excitation system output, and the structure output, respectively. In this context, the measured response includes information about the excitation system and the structure under test but the modal parameters of the structure are preserved and identifiable, and the characteristics of the excitation system have no influence on the accuracy of modal parameter estimates (Ibrahim et al. 1996). The discrimination between structural modes and properties of the excitation system is possible since the structural system has a narrowband response and time invariant properties, while the excitation system has a broadband response and it may have either time varying or time invariant properties. The estimation of the modal model (Sect. 4.2.1) of the structure gives the opportunity to estimate also the unknown forces, according to (4.3).

The assumption of *broadband excitation* ensures that all the structural modes in the frequency range of interest are excited. Assuming that the combined system is excited by a random input, the second order statistics of the response carry all the physical information about the system (Chap. 2) and play a fundamental role in output-only modal identification. The focus on second order statistics is justified by the central limit theorem. In fact, the structural response is approximately Gaussian in most cases, no matter of the distributions of the (independent) input loads, which are often not Gaussian. The spatial distribution of the input also affects the performance of OMA methods, in particular in the presence of closely spaced modes (Herlufsen et al. 2005). A distribution of random in time and space inputs provides better modal identification results (Herlufsen et al. 2005). In fact, the identification of closely spaced modes requires that the rank of the excitation PSD matrix is larger than 1 and, therefore, multiple uncorrelated inputs are applied (Chap. 1). The presence of measurement noise and spurious harmonics in response measurements requires appropriate data processing to eventually mitigate their effects and discriminate them from actual structural modes.

4.2 Structural Dynamics Models

4.2.1 Frequency Response and Impulse Response

The dynamic behavior of a structure can be represented either by a set of differential equations in time domain, or by a set of algebraic equations in frequency domain. Equations of motion are traditionally expressed in time domain, thus obtaining, for a general MDOF system, the following set of linear, second order differential equations expressed in matrix form:

$$[M]\{\ddot{y}(t)\} + [C]\{\dot{y}(t)\} + [K]\{y(t)\} = \{f(t)\} \tag{4.4}$$

where $\{\ddot{y}(t)\}$, $\{\dot{y}(t)\}$ and $\{y(t)\}$ are the vectors of acceleration, velocity, and displacement, respectively; [M], [C], and [K] denote the mass, damping, and stiffness matrices; $\{f(t)\}$ is the forcing vector. This matrix equation is written for a linear, time invariant ([M], [C] and [K] are constant), observable system with viscous damping. It describes the dynamics of the N_{DOF} discrete DOFs of the structure and it is usually referred to as the spatial model. The definition of the spatial model (of mass, stiffness, and damping properties) is the first step in theoretical analyses and it usually requires a large number of DOFs (some order of magnitude larger than the number of DOFs required for an accurate experimental model) in order to adequately describe the dynamic behavior of the structure. Equations of motion, which are coupled in this formulation, can be decoupled under the assumption of proportional damping by solving an eigenproblem. As a result, the complete solution is obtained by superposition of eigensolutions. This is a standard formulation of the dynamic problem reported in several structural dynamics and modal analysis books (Chopra 2000, Ewins 2000, Heylen et al. 1998).

The matrix differential equation of (4.4) becomes a set of linear algebraic equations by applying the Fourier transform and its properties (Chap. 2):

$$\left(-\omega^2[M] + i\omega[C] + [K]\right)\{Y(\omega)\} = \{F(\omega)\} \tag{4.5}$$

where $\{Y(\omega)\}$ and $\{F(\omega)\}$ are the Fourier transforms of $\{y(t)\}$ and $\{f(t)\}$, respectively; i is the imaginary unit (Chap. 2). A linear time-invariant system can be, therefore, represented through its FRF, which is given by the ratio between the Fourier transforms of the output and the input. Equation (4.5) can be rewritten as:

$$[Z(\omega)]\{Y(\omega)\} = \{F(\omega)\} \tag{4.6}$$

by adopting the following position:

$$-\omega^2[M] + i\omega[C] + [K] = [Z(\omega)]. \tag{4.7}$$

According to its definition, the FRF is therefore given by:

$$[H(\omega)] = [Z(\omega)]^{-1} = \frac{adj([Z(\omega)])}{|Z(\omega)|} \tag{4.8}$$

with $adj([Z(\omega)])$ and $|Z(\omega)|$ the adjoint matrix and the determinant of the dynamic stiffness matrix $[Z(\omega)]$, respectively; the FRF matrix carries all the information about the inertial, elastic, and energy dissipating properties of the structure ((4.7) and (4.8)). The FRF can be also expressed in terms of modal parameters through a partial fraction expansion as (refer to Ewins 2000, and Heylen et al. 1998 for more details):

$$[H(\omega)] = \sum_{r=1}^{N_m} \frac{[R_r]}{i\omega - \lambda_r} + \frac{[R_r]^*}{i\omega - \lambda_r^*} = \sum_{r=1}^{N_m} \frac{Q_r\{\phi_r\}\{\phi_r\}^T}{i\omega - \lambda_r} + \frac{Q_r^*\{\phi_r\}^*\{\phi_r\}^{*T}}{i\omega - \lambda_r^*} \tag{4.9}$$

where N_m denotes the number of modes, $\{\phi_r\}$ is the mode shape, Q_r holds the information about the modal scaling factor, and $\lambda_r = \sigma_r + i\omega_{d,r}$ is the pole of the r-th mode holding the information about damped frequency $f_{d,r} = \omega_{d,r}/(2\pi)$ and damping ratio $\xi_r = -\sigma_r / \left(\sqrt{\sigma_r^2 + \omega_{d,r}^2} \right)$ of the r-th mode. The structure of the FRF matrix expressed by (4.9) highlights some useful results for modal analysis. First of all, (4.9) shows that each mode gives a contribution to the response of the system at any frequency. Thus, it is impossible to excite only one mode of a structure by means of a single frequency sine wave (Richardson and Schwarz 2003). However, near a resonance this summation can be approximated by the term related to the corresponding mode. SDOF identification methods (Sect. 4.3) are based on this assumption. Moreover, (4.9) shows that every element of the FRF matrix has the same denominator. Thus, the eigenvalues (poles) of the system are given by the common denominator and they can be estimated either from any individual FRF or from multiple FRFs measured on the same structure. The selected approach leads to the classification of modal analysis techniques as local or global, respectively. The residue matrix $[R_r]$, which is a complex-valued matrix basically given by an outer product of the mode shape vector with itself (Heylen et al. 1998):

$$[R_r] = Q_r \{\phi_r\} \{\phi_r\}^T \tag{4.10}$$

holds the information about mode shapes.

The relation between input and output through the FRF matrix:

$$\{Y(\omega)\} = [H(\omega)]\{F(\omega)\} \tag{4.11}$$

can be manipulated to obtain a fundamental equation of OMA. In fact, taking into account the definition of PSD and the properties of transpose (Chap. 2), the product $\{Y(\omega)\}^*\{Y(\omega)\}^T$ can be computed and the following relation between PSD matrix of the output and FRF matrix can be obtained:

$$[S_{YY}(\omega)] = [H(\omega)]^* [S_{FF}(\omega)] [H(\omega)]^T. \tag{4.12}$$

Assuming that the PSD matrix of the input is constant (as reported in Sect. 4.1, in OMA the input to the combined system is a stationary, zero mean Gaussian white noise), the output PSD matrix carries the same information and can be expressed in pole-residue form as the FRF matrix:

$$[S_{YY}(\omega)] = \sum_{r=1}^{N_m} \frac{\{\phi_r\}\{\gamma_r\}^T}{i\omega - \lambda_r} + \frac{\{\phi_r\}^*\{\gamma_r\}^H}{i\omega - \lambda_r^*} + \frac{\{\gamma_r\}\{\phi_r\}^T}{-i\omega - \lambda_r} + \frac{\{\gamma_r\}^*\{\phi_r\}^H}{-i\omega - \lambda_r^*} \tag{4.13}$$

where $\{\gamma_r\}$ is the operational reference vector associated to the r-th mode: it corresponds to the modal participation vector $Q_r\{\phi_r\}^T$ appearing in the pole-residue form of the FRF matrix but, unlike this, it depends on all the modal parameters of the system, the input locations, and the input correlation matrix (Peeters 2000).

In (4.13) the poles hold the information about natural frequencies and damping ratios, while the residues hold the information about the mode shapes. However, since the input is not measured, only un-scaled mode shapes can be obtained. Equation (4.13) clearly shows that, for each mode, the output PSD provides four poles in complex conjugate pairs (λ_r, λ_r^*, $-\lambda_r$, $-\lambda_r^*$).

Taking into account that FRF and IRF on one hand, and spectral density functions and correlation functions on the other hand are Fourier transform pairs, similar analogies are possible between IRFs and correlation functions in the framework of OMA. In fact, in time domain the dynamic response of a structure to a generic input is determined by the IRF, whose mathematical expression:

$$[h(t)] = \sum_{r=1}^{N_m} \left([R_r] e^{\lambda_r t} + [R_r]^* e^{\lambda_r^* t} \right) \tag{4.14}$$

shows evident analogies with the mathematical structure of the FRF reported in (4.9). The poles hold the information about natural frequencies and damping ratios, while the information about the mode shapes is in the $[R_r]$ matrices.

In the output-only case and under the same assumptions about the input as above, it is possible to show (James et al. 1992, James et al. 1995) that also the correlation function can be expressed as a sum of complex exponentials:

$$\left[R_{yy}(\tau)\right] = \begin{cases} \sum_{r=1}^{N_m} \left(\{\phi_r\}\{\gamma_r\}^T e^{\lambda_r \tau} + \{\phi_r\}^*\{\gamma_r\}^H e^{\lambda_r^* \tau} \right) & \tau \geq 0 \\ \sum_{r=1}^{N_m} \left(\{\gamma_r\}\{\phi_r\}^T e^{-\lambda_r |\tau|} + \{\gamma_r\}^*\{\phi_r\}^H e^{-\lambda_r^* |\tau|} \right) & \tau < 0 \end{cases} . \tag{4.15}$$

The poles λ_r provide the natural frequencies and damping ratios, while the information about the mode shapes is in the residue matrices. As with the PSD matrix, only un-scaled mode shapes can be obtained from output-only modal identification based on correlation functions. It is interesting to note that the causal part (positive lags) of the correlation functions contains the stable poles ($\sigma < 0$) while the noncausal part (negative lags) contains the unstable poles ($\sigma > 0$).

Time domain modal identification methods usually identify the modal parameters from the causal part only, thus reducing the total number of poles by a factor 2. Moreover, since the modal decomposition of the causal part of the correlation functions and that of IRFs are very similar, modal parameter estimators traditionally used in the context of input–output modal analysis can be applied also in the context of OMA.

A similar reduction of the number of poles is sometimes carried out also in frequency domain. In fact, the so-called *positive power spectra* are sometimes preferentially adopted in practical applications—for instance, to enhance numerical conditioning in the poly-reference Least Squares Complex Frequency (p-LSCF) method-.

The order $n = 2N_m$ of the positive power spectra is the same as that of the FRF and contains all the necessary information about the structure. The positive power spectra are defined as the DFT of the correlation functions at positive time lags only:

$$\left[S_{YY}^{+}(\omega)\right] = DFT\left(\left[R_{yy}(\tau)\right]\big|_{\tau \geq 0}\right). \tag{4.16}$$

It is worth noting that the positive power spectra are different from the one-sided spectra (Chap. 2). More details about positive power spectra and their role in output-only modal identification are reported in Sects. 4.2.4, 4.4.3.2 and 4.9.

4.2.2 State-Space Models

State space-models are used to convert the second order problem, governed by the differential equation of motion expressed in matrix form in (4.4) into two first order problems, defined by the so-called state equation and observation equation.

The state equation can be obtained from (4.4) by some mathematical manipulations. When the forcing vector $\{f(t)\}$ is factorized into the matrix $[\overline{B}]$, which defines the location of inputs, and the vector $\{u(t)\}$ describing the time variation, (4.4) can be rewritten as follows:

$$[M]\{\ddot{y}(t)\} + [C]\{\dot{y}(t)\} + [K]\{y(t)\} = \left[\overline{B}\right]\{u(t)\} \tag{4.17}$$

or, equivalently:

$$\{\ddot{y}(t)\} + [M]^{-1}[C]\{\dot{y}(t)\} + [M]^{-1}[K]\{y(t)\} = [M]^{-1}\left[\overline{B}\right]\{u(t)\}. \tag{4.18}$$

The definition of the *state vector*:

$$\{s(t)\} = \begin{Bmatrix} \{\dot{y}(t)\} \\ \{y(t)\} \end{Bmatrix} \tag{4.19}$$

and its substitution in the set of equations consisting of (4.18) and the following identity:

$$[M]\{\dot{y}(t)\} = [M]\{\dot{y}(t)\} \tag{4.20}$$

yield:

$$\{\dot{s}(t)\} = \begin{bmatrix} -[M]^{-1}[C] & -[M]^{-1}[K] \\ [I] & [0] \end{bmatrix}\{s(t)\} + \begin{bmatrix} [M]^{-1}\left[\overline{B}\right] \\ [0] \end{bmatrix}\{u(t)\}. \tag{4.21}$$

From (4.21) the *state matrix* [A_c] and the *input influence matrix* [B_c] can be defined as follows:

$$[A_c] = \begin{bmatrix} -[M]^{-1}[C] & -[M]^{-1}[K] \\ [I] & [0] \end{bmatrix}, \tag{4.22}$$

$$[B_c] = \begin{bmatrix} [M]^{-1}[\overline{B}] \\ [0] \end{bmatrix}, \tag{4.23}$$

and the *state equation* can be written as:

$$\{\dot{s}(t)\} = [A_c]\{s(t)\} + [B_c]\{u(t)\} \tag{4.24}$$

where the subscript c denotes continuous time.

In the most general case, the observation equation can be written as:

$$\{y_l(t)\} = [C_a]\{\ddot{y}(t)\} + [C_v]\{\dot{y}(t)\} + [C_d]\{y(t)\} \tag{4.25}$$

under the assumption that measurements of the structural response are taken at l locations and the sensors are accelerometers, velocimeters, and displacement transducers; $\{y_l(t)\}$ is the vector of the measured outputs, $[C_a], [C_v]$ and $[C_d]$ are the output location matrices for acceleration, velocity, and displacement, respectively. In the following, the index l in $\{y_l(t)\}$ will be dropped wherever $\{y_l(t)\}$ cannot be confused with the vector of displacements $\{y(t)\}$. It is worth emphasizing that, while a real structure is characterized by an infinite number of DOFs (which becomes a finite but large number in the lumped mass models usually set for numerical analyses), in a practical vibration test this number decreases down to a few dozens or even less. Substitution of the expression for $\{\ddot{y}(t)\}$ obtained from (4.18) into (4.25) yields the following equation:

$$\begin{aligned} \{y_l(t)\} \quad &= \Big([C_v] - [C_a][M]^{-1}[C]\Big)\{\dot{y}(t)\} \\ &+ \Big([C_d] - [C_a][M]^{-1}[K]\Big)\{y(t)\}\,. \\ &+ \Big([C_a][M]^{-1}[\overline{B}]\Big)\{u(t)\} \end{aligned} \tag{4.26}$$

The *observation equation*:

$$\{y(t)\} = [C_c]\{s(t)\} + [D_c]\{u(t)\} \tag{4.27}$$

provides the vector of the measured outputs as a function of the state and the input; it is obtained from (4.26), taking into account the definition of state vector (4.19), with the following positions:

$$[C_c] = \Big[[C_v] - [C_a][M]^{-1}[C] \quad [C_d] - [C_a][M]^{-1}[K]\Big], \tag{4.28}$$

$$[D_c] = [C_a][M]^{-1}\left[\overline{B}\right]. \tag{4.29}$$

$[C_c]$ is the *output influence matrix*, $[D_c]$ is the *direct transmission matrix*. The direct transmission matrix disappears if no accelerometers are used for output measurements. The physical sense of this matrix is related to the circumstance that a step change in the input $\{u(t)\}$ causes a step change in the acceleration response.

The state equation (4.24) and the observation equation (4.27) define the *continuous-time state-space model*. An important characteristic of this model is the existence of an infinite number of equivalent state-space representations for a given system: each one is referred to as a *realization*. As a consequence, the experimental test allows establishing only one of these infinite realizations. Application of a similarity transformation proves the multiplicity of realizations. In fact, said [T] an arbitrary nonsingular square matrix, substitution of:

$$\{s(t)\} = [T]\{z(t)\} \tag{4.30}$$

into the equations of the continuous-time state-space model yields:

$$\{\dot{z}(t)\} = [T]^{-1}[A_c][T]\{z(t)\} + [T]^{-1}[B_c]\{u(t)\} \tag{4.31}$$

$$\{y(t)\} = [C_c][T]\{z(t)\} + [D_c]\{u(t)\} \tag{4.32}$$

Comparisons of (4.31) with (4.24) and of (4.32) with (4.27) show that the matrices $[T]^{-1}[A_c][T]$, $[T]^{-1}[B_c]$, $[C_c][T]$ and $[D_c]$ describe the same relationships as the matrices $[A_c]$, $[B_c]$, $[C_c]$ and $[D_c]$. Moreover, since the state matrices of any couple of realizations are related by a similarity transformation, the eigenvalues (carrying the information about the modal parameters of the system) are preserved.

Taking into account that experimental tests yield measurements taken at discrete time instants while (4.24) and (4.27) are expressed in continuous time, the continuous-time state-space model has to be converted to discrete time. For a given sampling period Δt, the continuous-time equations can be discretized and solved at all discrete time instants $t_k = k\Delta t$, $k \in N$. An assumption about the behavior of the time-dependent variables between two samples has to be made to this aim. For instance, the Zero Order Hold (ZOH) assumption states that the input is piecewise constant over the sampling period. Under this assumption the continuous-time state-space model can be converted to the *discrete-time state-space model*:

$$\{s_{k+1}\} = [A]\{s_k\} + [B]\{u_k\} \tag{4.33}$$

$$\{y_k\} = [C]\{s_k\} + [D]\{u_k\} \tag{4.34}$$

where $\{s_k\} = \{s(k\Delta t)\}$ is the *discrete-time state vector* yielding the sampled displacements and velocities; $\{u_k\}$ and $\{y_k\}$ are the *sampled input* and *sampled output*, respectively; [A] is the *discrete state matrix*, [B] is the *discrete input*

matrix, [C] is the *discrete output matrix* and [D] is the direct transmission matrix. The relations between continuous-time matrices and the corresponding discrete time matrices are:

$$[A] = e^{[A_c]\,\Delta t} \tag{4.35}$$

$$[B] = ([A] - [I])[A_c]^{-1}[B_c] \tag{4.36}$$

$$[C] = [C_c] \tag{4.37}$$

$$[D] = [D_c] \tag{4.38}$$

Thus, the ZOH sampling does not influence these last two matrices. As an alternative, assuming a piecewise linear behavior between two subsequent samples—First Order Hold (FOH) assumption—different, more complex relations between continuous-time and discrete-time state-space matrices can be derived (see, for instance, Franklin et al. 2006). Mathematical derivation of (4.33) and (4.34) and of the relations between continuous-time and discrete-time matrices is beyond the scope of the present book. The interested reader can refer to the literature (Juang 1994) for more details.

The model expressed by (4.33) and (4.34) is a deterministic model since the system is driven by a deterministic input only. Stochastic components must be necessarily included in order to describe actual measurement data. When stochastic components are included in the model, the following *discrete-time combined deterministic-stochastic state-space model* is obtained:

$$\{s_{k+1}\} = [A]\{s_k\} + [B]\{u_k\} + \{w_k\} \tag{4.39}$$

$$\{y_k\} = [C]\{s_k\} + [D]\{u_k\} + \{v_k\} \tag{4.40}$$

where $\{w_k\}$ is the *process noise* due to disturbances and model inaccuracies, while $\{v_k\}$ is the *measurement noise* due to sensor inaccuracies. The state equation models the dynamic behavior of the system; the observation equation defines that part of the dynamic response of the system that can be observed in the output of the model.

In the context of OMA, structures are excited by immeasurable inputs. Since the information about the input $\{u_k\}$ is not available, the measured system response $\{y_k\}$ is generated only by the two stochastic processes $\{w_k\}$ and $\{v_k\}$, and the following *discrete-time stochastic state-space model* is obtained:

$$\{s_{k+1}\} = [A]\{s_k\} + \{w_k\} \tag{4.41}$$

$$\{y_k\} = [C]\{s_k\} + \{v_k\}. \tag{4.42}$$

In the absence of $\{u_k\}$, its role is implicitly modeled by process noise and measurement noise. In particular, the process noise becomes the input that drives

the dynamics of the system, while the measurement noise accounts for the direct disturbance of the response of the system. Thus, when a stochastic state-space model is adopted, the objective is the determination of the order n of the unknown system and of a realization of the matrices [A] and [C] (up to within a similarity transformation) from a large number of measurements of the output $\{y_k\}$ generated by the system itself. The state matrix [A] transforms the current state of the system $\{s_k\}$ in the next state $\{s_{k+1}\}$, while the product of the observation matrix [C] with the state vector provides the observable part of the dynamics of the system. More precisely, the response vector $\{y_k\}$ is given by the observable part of the state plus the measurement noise. The process noise and the measurement noise are both immeasurable. They are assumed to be zero mean, stationary white noise processes with covariance matrices given by:

$$E\left[\left\{\begin{array}{c}\{w_p\}\\ \{v_p\}\end{array}\right\}\left\langle \{w_q\}^T \quad \{v_q\}^T \right\rangle\right] = \left\{\begin{array}{ll}\left[\begin{array}{cc}[Q^{ww}] & [S^{wv}]\\ [S^{wv}]^T & [R^{vv}]\end{array}\right] & p = q\\ [0] & p \neq q\end{array}\right. \tag{4.43}$$

where p and q are two arbitrary time instants. The estimation of the matrices $[Q^{ww}]$, $[R^{vv}]$ and $[S^{wv}]$ is also part of the identification process. The assumption of white noise for $\{w_k\}$ and $\{v_k\}$ is fundamental in the proof of SSI methods (see Van Overschee and De Moor 1996 for more details). Thus, if the unmeasured input includes some dominant frequency components, they appear as poles of the state matrix [A] together with the eigenvalues of the system. This is equivalent to the identification of the dynamic properties of both the structure under investigation and the excitation system forming the combined system (driven by stationary, zero mean Gaussian white noise as input) that is the generally assumed objective of identification in OMA.

In agreement with the stochastic framework of OMA, the system response in the state-space model is represented by a zero mean Gaussian process. The output covariance matrices are given by:

$$[R_i] = E\left[\{y_{k+i}\}\{y_k\}^T\right] \tag{4.44}$$

and they carry all the information to describe the process. A *covariance equivalent model* can be then defined as the estimated state-space model characterized by correct covariance and, therefore, able to describe the statistical properties of the system response. The estimator producing this model is referred to as an optimal estimator.

The state $\{s_k\}$ is also a zero mean Gaussian process described by its covariance (which is independent of the time instant k):

$$[\Sigma] = E\left[\{s_k\}\{s_k\}^T\right] \tag{4.45}$$

and it is uncorrelated with the process noise and the measurement noise:

$$E\left[\{s_k\}\{w_k\}^T\right] = [0] \tag{4.46}$$

$$E\left[\{s_k\}\{v_k\}^T\right] = [0]. \tag{4.47}$$

Taking into account the previous assumptions about the noise terms, the system response and the state, mathematical manipulations of the state-space equations ((4.41) and (4.42)) lead to the following fundamental relations:

$$[\Sigma] = [A][\Sigma][A]^T + [Q^{ww}] \tag{4.48}$$

$$[R_0] = [C][\Sigma][C]^T + [R^{vv}] \tag{4.49}$$

$$[G] = [A][\Sigma][C]^T + [S^{wv}] \tag{4.50}$$

$$[R_i] = [C][A]^{i-1}[G] \tag{4.51}$$

where:

$$[G] = E\left[\{s_{k+1}\}\{y_k\}^T\right] \tag{4.52}$$

is the *next state-output covariance matrix* (covariance between the response of the system $\{y_k\}$ and the updated state vector $\{s_{k+1}\}$). The last property expressed by (4.51) is very important. In fact, since the output covariance sequence $[R_i]$ can be directly estimated from the measured data (4.44), its decomposition according to (4.51) permits the estimation of the state-space matrices and the solution of the system identification problem.

The stochastic state-space model in (4.41) and (4.42) can be expressed in an alternative form through the introduction of the so-called Kalman filter. Without going into the details (the interested reader can refer to Juang 1994 for a more detailed discussion about the Kalman filter and the related mathematical derivations), the so-called forward innovation model is briefly illustrated below.

For a given time instant t_k, suppose that the system matrices $[A]$, $[C]$, $[Q^{ww}]$, $[R^{vv}]$, $[S^{wv}]$ and all previous measurements $[Y^{k-1}]$ are known:

$$\left[Y^{k-1}\right] = [\{y_0\}, \{y_1\}, \ldots, \{y_{k-1}\}]^T. \tag{4.53}$$

A classical estimation problem concerns the ability to optimally predict the response measurements. Thus, an *optimal predictor* can be defined as the one minimizing the error between the predicted and measured response. The system response can be optimally predicted if an optimal predictor of the states is available. The quality of the predictor of the states is quantified by the *state prediction error*:

$$\{\varepsilon_k\} = \{s_k\} - \{\hat{s}_k\}, \tag{4.54}$$

which represents the part of $\{s_k\}$ that cannot be predicted by the one-step-ahead predictor of the state vector $\{\hat{s}_k\}$. This is defined as the conditional mean of $\{s_k\}$ given all previous measurements:

$$\{\hat{s}_k\} = E\left[\{s_k\}|\left[Y^{k-1}\right]\right]. \tag{4.55}$$

In a similar way it is possible to define the *innovation*:

$$\{e_k\} = \{y_k\} - \{\hat{y}_k\} \tag{4.56}$$

as the part of the measured response $\{y_k\}$ that cannot be predicted by the one-step-ahead predictor $\{\hat{y}_k\}$. This is defined as the conditional mean of $\{y_k\}$ given all previous measurements:

$$\{\hat{y}_k\} = E\left[\{y_k\}|\left[Y^{k-1}\right]\right] = E\left[([C]\{s_k\} + \{v_k\})|\left[Y^{k-1}\right]\right] = [C]\{\hat{s}_k\} \tag{4.57}$$

The last part of (4.57) is obtained by taking into account (4.42) and assuming no correlation between the measurement noise $\{v_k\}$ at instant t_k and the previous measurements $[Y^{k-1}]$. Since $\{y_k\}$ is assumed zero mean and Gaussian distributed, $\{e_k\}$ is a zero mean Gaussian white noise process.

The Kalman filter for linear and time-invariant systems relates the predictors given by (4.55) and (4.57) as follows:

$$\{\hat{s}_{k+1}\} = [A]\{\hat{s}_k\} + [K_k]\{e_k\} \tag{4.58}$$

$$\{e_k\} = \{y_k\} - [C]\{\hat{s}_k\}. \tag{4.59}$$

The matrix $[K_k]$ is referred to as *nonsteady state Kalman gain*. Given the initial state estimate $\{\hat{s}_0\} = \{0\}$, the initial covariance of the state estimate $[P_0] = E\left[\{\hat{s}_0\}\{\hat{s}_0\}^T\right] = [0]$ and the output measurements $[Y^{k-1}]$, the nonsteady-state Kalman state estimate at time t_k can be obtained from the following recursive formulas providing the Kalman state estimate, the Kalman gain, and the Kalman state covariance, respectively:

$$\{\hat{s}_k\} = [A]\{\hat{s}_{k-1}\} + [K_{k-1}](\{y_{k-1}\} - [C]\{\hat{s}_{k-1}\}) \tag{4.60}$$

$$[K_{k-1}] = \left([G] - [A][P_{k-1}][C]^T\right)\left([R_0] - [C][P_{k-1}][C]^T\right)^{-1} \tag{4.61}$$

$$[P_k] = [A][P_{k-1}][A]^T + \left([G] - [A][P_{k-1}][C]^T\right)\left([R_0] - [C][P_{k-1}][C]^T\right)^{-1}\left([G] - [A][P_{k-1}][C]^T\right)^T \tag{4.62}$$

Equation (4.62) is also known as the *Ricatti equation*. The Kalman filter provides the state estimate $\{\hat{s}_k\}$ at instant t_k given the previous state estimate $\{\hat{s}_{k-1}\}$ and the measurements $\{y_{k-1}\}$. Obtained the Kalman state covariance matrix $[P_k]$ as a solution of the Ricatti equation:

$$[P_k] = E\left[\{\hat{s}_k\}\{\hat{s}_k\}^T\right] \tag{4.63}$$

the covariance of the innovation can be computed, taking into account (4.59), as:

$$E\left[\{e_k\}\{e_k\}^T\right] = [R_0] - [C][P_k][C]^T. \tag{4.64}$$

When the measurements are Gaussian distributed, the Kalman filter provides an optimal prediction of the states. It is worth pointing out that the Kalman state covariance is not steady at startup, since the Kalman filter experiences a transient phase. However, under certain assumptions about the state matrix ([A] is stable, that is to say the real parts of all its eigenvalues are negative), the steady state is quickly reached and the state covariance matrix and the Kalman gain become constant (independent of time: $[P_k] = [P]$ and $[K_k] = [K]$). In steady-state:

$$\{\hat{s}_{k+1}\} = [A]\{\hat{s}_k\} + [K]\{e_k\} \tag{4.65}$$

$$\{e_k\} = \{y_k\} - [C]\{\hat{s}_k\}. \tag{4.66}$$

The steady-state Kalman gain [K] is obtained by finding the solution [P] of the algebraic Ricatti equation:

$$[P] = [A][P][A]^T + \left([G] - [A][P][C]^T\right)\left([R_0] - [C][P][C]^T\right)^{-1}\left([G] - [A][P][C]^T\right)^T \tag{4.67}$$

and substituting it into the following equation:

$$[K] = \left([G] - [A][P][C]^T\right)\left([R_0] - [C][P][C]^T\right)^{-1}. \tag{4.68}$$

Then, the covariance matrix of the innovation can be computed:

$$E\left[\{e_k\}\{e_k\}^T\right] = [R_0] - [C][P][C]^T. \tag{4.69}$$

Rearranging (4.66), the *forward innovation model* is obtained:

$$\{\hat{s}_{k+1}\} = [A]\{\hat{s}_k\} + [K]\{e_k\} \tag{4.70}$$

$$\{y_k\} = [C]\{\hat{s}_k\} + \{e_k\}. \tag{4.71}$$

Comparison of the forward innovation model with the state-space model given by (4.41) and (4.42) shows that in the forward innovation model the prediction of the state replaces the state vector and the two processes $\{w_k\}$ and $\{v_k\}$ are converted into a single process, the innovation.

The closed form solution for the Kalman gain given by the Ricatti equation makes the Kalman filter very attractive. However, in the context of dynamic identification the system matrices $[A]$, $[C]$, $[Q^{ww}]$, $[R^{vv}]$, $[S^{wv}]$ are not known.

Thus, the state sequence has to be determined directly from the output data through geometric manipulations without solving the Ricatti equation. The Data-Driven Stochastic Subspace Identification (DD-SSI) method allows the estimation of the states directly from the experimental data by applying robust numerical techniques, such as SVD and QR decomposition (see Sect. 4.5.3.2 for more details).

4.2.3 ARMA Models

The equation of motion of a randomly excited linear time-invariant system can be also written as follows:

$$[M]\{\ddot{y}(t)\} + [C]\{\dot{y}(t)\} + [K]\{y(t)\} = \{w(t)\} \tag{4.72}$$

where $\{w(t)\}$ is a continuous-time, zero mean Gaussian white noise. It is possible to show (Andersen et al. 1996, Andersen 1997) that this system can be also described by a discrete-time Auto-Regressive Moving Average Vector (ARMAV) model (the ARMA model is referred to as an ARMA vector model to point out its multivariate character) by approximating the differential operator with finite differences over a finite time step Δt.

Historically, ARMAV models have been used for the estimation of the modal parameters of civil structures. Due to a number of shortcomings (in particular for systems with many outputs and many modes, where the large set of parameters to be estimated leads to large computational burden and convergence problems), stochastic state-space models have progressively replaced them in the context of modal identification. However, the basics of ARMA models and their relation with state-space models are herein briefly illustrated for the sake of completeness.

In order to explain how modal parameters can be extracted from an ARMA model, assume that a continuous-time system is observed at discrete time instants k with a sampling interval Δt. The discretization is based on the covariance equivalence technique (Bartlett 1946, Pandit and Wu 1983). Since the input on the structure is not available (it is immeasurable), the equivalent discrete-time system can be obtained only by requiring that the covariance function of its response to a Gaussian white noise input is coincident at all discrete time lags with that of the continuous-time system. This implies that the first and second order moments of the response of the discretized model are equal to the first and second order moments of the response of the continuous-time system at all the considered discrete time instants. Under the assumption that the response of the system is Gaussian distributed, the covariance equivalent model is the most accurate approximated model, since it is exact at all discrete time lags. The generalization of this approach to multivariate second order systems is illustrated elsewhere (Andersen et al. 1996). When the dynamic response of the system is driven by the Gaussian white noise $\{w(t)\}$ but there are also some disturbances (process and measurement noise), the latter have also to be taken into account by the equivalent

discrete-time model. In the presence of such disturbances, an ARMAV(n_α, n_γ) model has the form:

$$\begin{aligned}&\{y_k\} + [\alpha_1]\{y_{k-1}\} + \ldots + [\alpha_{n_\alpha}]\{y_{k-n_\alpha}\} \\ &\quad = \{e_k\} + [\gamma_1]\{e_{k-1}\} + \ldots + \left[\gamma_{n_\gamma}\right]\{e_{k-n_\gamma}\}\end{aligned} \tag{4.73}$$

where, as in the case of the state-space model, $\{y_k\}$ is the vector of the output at the time instant t_k, and $\{e_k\}$ is the innovation and it is a zero mean Gaussian white noise. The left-hand side of (4.73) is the Auto-Regressive (AR) part, while the right-hand side is the Moving Average (MA) part. The matrices $[\alpha_i]$ contain the AR parameters, while the matrices $[\gamma_i]$ contain the MA parameters; n_α and n_γ represent the AR and MA order of the model, respectively.

It is possible to show (see, for instance, Andersen 1997, Andersen and Brincker 1999) that a covariance equivalent ARMAV model can be converted into a forward innovation state space model, and vice versa. Let us consider a minimal realization of the state-space model of (4.70) and (4.71). A *minimal realization* corresponds to the minimal state space dimension ensuring that all modes are appropriately excited and observed in the output. In fact, if the order of the state-space model is too large, the model will contain redundant information; on the contrary, if the state-space dimension is too small, a certain amount of information about the modeled system will be lost. More details about the mathematical conditions to obtain a minimal realization can be found elsewhere (see, for instance, Kailath 1980). Said n the order of the minimal realization of the considered forward innovation model and l the number of outputs, if the ratio $n/l = p$ is an integer value it is possible to show that, independently of the specific realization, an ARMAV(p, p) model is equivalent to the considered forward innovation model (Andersen 1997).

The conversion of an ARMAV model into a state-space representation requires the selection of a specific realization. A realization, which can be easily constructed from the AR and MA matrices and is well conditioned (so that it is numerically efficient when implemented into a system identification software), must be adopted. The so-called *observability canonical state-space realization* is usually adopted in this case (Andersen 1997). It is given by:

$$[A] = \begin{bmatrix} [0] & [I] & [0] & \ldots & [0] \\ [0] & [0] & [I] & \ddots & [0] \\ \vdots & \ddots & \ddots & \ddots & \vdots \\ [0] & [0] & [0] & \ddots & [I] \\ -[\alpha_p] & -[\alpha_{p-1}] & -[\alpha_{p-2}] & \cdots & -[\alpha_1] \end{bmatrix} \tag{4.74}$$

$$[K] = \begin{bmatrix} [I] & [0] & [0] & \dots & [0] \\ [\alpha_1] & [I] & [0] & \ddots & [0] \\ \vdots & \ddots & \ddots & \ddots & \vdots \\ [\alpha_{p-2}] & [\alpha_{p-3}] & [\alpha_{p-4}] & \ddots & [0] \\ [\alpha_{p-1}] & [\alpha_{p-2}] & [\alpha_{p-3}] & \dots & [I] \end{bmatrix} \begin{bmatrix} [\gamma_1] - [\alpha_1] \\ [\gamma_2] - [\alpha_2] \\ \vdots \\ [\gamma_{p-1}] - [\alpha_{p-1}] \\ [\gamma_p] - [\alpha_p] \end{bmatrix} \tag{4.75}$$

$$[C] = \begin{bmatrix} [I] & [0] & [0] & \cdots & [0] \end{bmatrix}. \tag{4.76}$$

When the state matrix [A] is expressed in the form of (4.74), it is also known as the *companion matrix* for the auto-regressive matrix polynomial. The EVD of the companion matrix provides the modal parameters of the system:

$$[A] = [\Psi][\mathrm{M}][\Psi]^{-1} \tag{4.77}$$

where the columns $\{\psi_m\}$ of [Ψ] are the pl eigenvectors of [A], while the corresponding pl eigenvalues μ_m are collected in the diagonal matrix [M]. The eigenvectors are a combination of mode shapes $\{\phi_m\}$ and eigenvalues μ_m:

$$[\Psi] = \begin{bmatrix} \{\phi_1\} & \dots & \{\phi_{pl}\} \\ \mu_1\{\phi_1\} & \dots & \mu_{pl}\{\phi_{pl}\} \\ \vdots & \dots & \vdots \\ \mu_1^{p-1}\{\phi_1\} & \dots & \mu_{pl}^{p-1}\{\phi_{pl}\} \end{bmatrix}. \tag{4.78}$$

Thus, taking into account (4.76), the mode shapes of the system can be obtained as:

$$\{\phi_m\} = [C]\{\psi_m\} \tag{4.79}$$

while natural frequencies and damping ratios of the continuous-time system are obtained from the eigenvalues, after their conversion from discrete-time to continuous-time taking into account (4.35):

$$\lambda_m = \frac{\ln(\mu_m)}{\Delta t}, \quad \lambda_m = -\xi_m\omega_m \pm i\omega_m\sqrt{1-\xi_m^2} \tag{4.80}$$

where m = 1, . . ., pl is the index denoting the generic pole. If the modes are underdamped (this is the case of the structural systems considered in this book), the poles appear in complex conjugate pairs (4.80) and the number of modes N_m is half the order pl of the system. The modal properties of the structure are obtained by the EVD of the companion matrix, holding only the AR coefficient matrices. Thus, the MA coefficient matrices do not influence them, and the possibility to use AR models for modal parameter estimation has been investigated (Pandit 1991). However, an AR model of order p is not an equivalent representation of the previously mentioned minimal realization of the forward innovation model.

The use of AR instead of ARMA models can be justified if the AR model order goes to infinity. In fact, it can be shown that an AR model with infinite order is theoretically equivalent to an ARMA model of finite order. However, for very large values of the order of the AR model many spurious poles are introduced and they have to be separated from the true system poles.

4.2.4 Fraction Polynomial Models

The FRF matrix can be expressed not only in pole-residue form (4.9) but also using a *Matrix Fraction Description* (MFD), that is to say, a ratio of two matrix polynomials. In particular, both a Left MFD (LMFD):

$$[H(\omega)] = [A_L(\omega)]^{-1}[B_L(\omega)] \tag{4.81}$$

and a Right MFD (RMFD):

$$[H(\omega)] = [B_R(\omega)][A_R(\omega)]^{-1} \tag{4.82}$$

can be adopted. The *common-denominator model* (also known as scalar matrix fraction model) of the FRF represents a special case of MFD where the numerator is a matrix polynomial while the denominator is a polynomial characterized by scalar coefficients:

$$[H(\omega)] = \frac{[B(\omega)]}{A(\omega)} = \frac{\sum_{j=0}^{n} [\beta_j(\omega)]\Omega^j(\omega)}{\sum_{j=0}^{n} \alpha_j \Omega^j(\omega)} \tag{4.83}$$

where $\Omega(\omega)$ is the *polynomial basis function*. Comparison of (4.83) and (4.9) leads to recognize that the denominator holds the information about the poles of the structure, while the numerator holds the information about the mode shapes. When a common-denominator model is considered, the poles are obtained as roots of the denominator polynomial; in the case of MFD, the poles are obtained as solutions of a generalized eigenvalue problem (Sect. 4.4.3).

When an MFD is adopted, the size ($N_c \times N_c$) of the matrix coefficients [A_j] (with N_c depending on the number of inputs or outputs according to the selected description) and the order n of the matrix polynomial determine the number of modes that can be identified in accordance with the following relation:

$$N_c \cdot n = 2N_m. \tag{4.84}$$

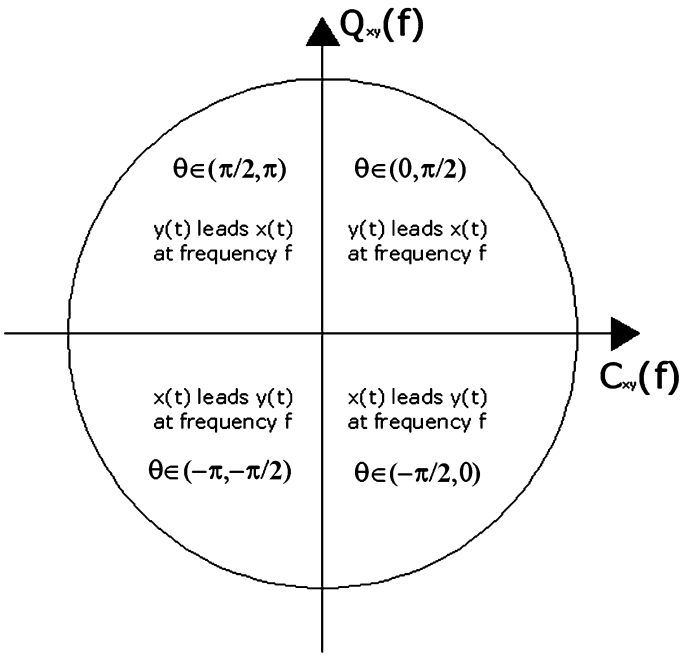

Fig. 4.2 4-quadrant symmetry of cross-power spectra

Based on this relation, a low order model with large matrix coefficients can be expanded to a high order matrix polynomial with smaller matrix coefficients in order to identify N_m modes in the presence of a reduced number of inputs or outputs (low N_c). A polynomial of order $2N_m$ with scalar coefficients represents the limit of this expansion.

In the OMA framework, MFD is applied to power spectra instead of FRFs. As mentioned in Sect. 4.2.1, positive power spectra are also sometimes adopted to improve numerical conditioning (see also Sects. 4.4.3.2 and 4.9). In fact, power spectra show a 4-quadrant symmetry and, therefore, they provide four poles in complex conjugate pairs for each mode. Poles characterized by negative real part are denoted as *stable poles*, while *unstable poles* are characterized by positive real part. The 4-quadrant symmetry (Fig. 4.2) requires doubling the order with respect to FRFs to identify a certain number of modes N_m, and this may result in worse numerical conditioning. Thus, the estimation of positive power spectra, resulting in a prior separation of stable and unstable poles, improves the numerical conditioning and this simplifies the identification of the structural modes by the p-LSCF estimator (Sect. 4.9). Processing positive power spectra could have a detrimental effect on the accuracy and reliability of mode shape estimates. However, the procedure for their computation is illustrated below for the sake of completeness.

The computation of positive power spectra (see also Cauberghe 2004) is based on the procedure for the estimation of unbiased correlation functions via FFT

(Bendat and Piersol 2000). The Wiener-Khinchin relations between correlation and spectral density functions have been introduced in Chap. 2. Those relations make possible the computation of correlation functions as inverse Fourier transforms of spectral density functions, and the computation of spectral density functions as Fourier transforms of correlation functions. However, as a consequence of the periodic assumption of the finite Fourier transform, the correlation functions obtained by this procedure appear as if they were computed from periodic functions. As a result, the value of the correlation function at the generic time lag τ is a combination of two terms, $\hat{R}_{yy}(\tau)$ and $\hat{R}_{yy}(T-\tau)$. In particular, it is possible to show that the following equation holds (Bendat and Piersol 2000):

$$\begin{aligned}\hat{S}_{YY}(f) &= \frac{1}{T}\int_0^T \tau \hat{R}_{yy}(T-\tau)e^{-i2\pi f\tau}d\tau + \frac{1}{T}\int_0^T (T-\tau)\hat{R}_{yy}(\tau)e^{-i2\pi f\tau}d\tau \\ &= \int_0^T \hat{R}_c(\tau)e^{-i2\pi f\tau}d\tau \end{aligned} \tag{4.85}$$

where:

$$\hat{R}_c(\tau) = \frac{(T-\tau)}{T}\hat{R}_{yy}(\tau) + \frac{\tau}{T}\hat{R}_{yy}(T-\tau) \tag{4.86}$$

is the *circular correlation function*, whose expression in discrete time becomes:

$$\hat{R}_c(r\Delta t) = \frac{(N-r)}{N}\hat{R}_{yy}(r\Delta t) + \frac{r}{N}\hat{R}_{yy}[(N-r)\Delta t]. \tag{4.87}$$

A procedure to separate the two contributions consists in adding N zeroes to the original N data values so that the first half of the correlation function estimate shows the correlation function values for the positive lags (the causal part of the correlation function which contains the stable poles) and the second half of the estimate shows the correlation function values for the negative lags (the noncausal part of the correlation function which contains the unstable poles). Equation (4.88) gives the two portions of the correlation function obtained by adding N zeroes:

$$\hat{R}_s(r\Delta t) = \begin{cases} \dfrac{(N-r)}{N}\hat{R}_{yy}(r\Delta t) & r = 0, \ldots, N-1 \\ \dfrac{(r-N)}{N}\hat{R}_{yy}[(2N-r)\Delta t] & r = N, \ldots, 2N-1 \end{cases} \tag{4.88}$$

where the subscript s is referred to the separation of the two contributions. Thus, the causal part of the unbiased correlation function estimate is:

$$\hat{R}_{yy}(r\Delta t) = \frac{N}{N-r}\hat{R}_s(r\Delta t) \qquad r = 0, \ldots, N-1. \tag{4.89}$$

The above discussion leads to the following procedure for the computation of positive power spectra:

- Divide the record of the structural response into n_b independent (no overlap) blocks of N samples, where the number of samples N in each block has to be larger than the maximum lag number of interest m: $N \geq m$;
- Extend each block with additional N zeroes;
- Use the extended blocks to compute the power spectra according to the Welch procedure;
- Compute the inverse Fourier transform and consider only the first m samples for $m < N$, or discard the second half of the obtained correlation function if $m = N$; rescale the values of the obtained correlation function by $N/(N-r)$. For $m = N$, since the tail of the correlation function is affected by high noise levels, an exponential window can be applied to reduce the effect of leakage and the influence of the higher lags characterized by larger variance; however, this requires a correction of the damping values obtained from modal identification: said β the factor determining the ratio between the amplitude at the last time lag and the initial amplitude of the exponential window, the damping associated to the r-th pole λ_r can be corrected taking into account that $\lambda_r^{corrected} = \lambda_r^{estimated} + \beta$ (Verboven 2002, Heylen et al. 1998); a suggested value for β is such that the amplitude at the last time lag of the window is 0.1 % of its initial amplitude (Verboven 2002);
- The positive power spectra are finally obtained by Fourier transform of the retained portion of the causal part of the correlation function.

The positive power spectra show a 2-quadrant symmetry and, therefore, the same order $n = 2N_m$ of FRFs. As a consequence, only one pair of complex conjugate poles is present in the data for each mode. The relation between power spectra and positive power spectra is (Peeters and Van der Auweraer 2005):

$$[S_{YY}(\omega)] = \left[S^{+}_{YY}(\omega)\right] + \left[S^{+}_{YY}(\omega)\right]^{H}. \tag{4.90}$$

4.2.5 The Unified Matrix Polynomial Approach to Modal Analysis

A number of input–output modal identification techniques have been developed over the years according to the theoretical expressions of FRF or IRF. Different physically based models and different mathematical manipulations produced a number of different methods. However, it has been shown (Allemang and Brown 1998) that those apparently unrelated procedures could be treated according to a unified approach. Such an approach is herein summarized because it can be easily extended to OMA. It is useful to highlight the similarities and differences among the various modal identification methods, whose correlation is stronger than it appears at a first insight.

The original approach starts from the polynomial model historically used for the FRF; assuming that the response to the input applied at location q is measured at location p, the related FRF can be expressed as follows:

$$H_{pq}(\omega) = \frac{Y_p(\omega)}{F_q(\omega)} = \frac{\beta_n(i\omega)^n + \beta_{n-1}(i\omega)^{n-1} + \ldots + \beta_1(i\omega)^1 + \beta_0(i\omega)^0}{\alpha_m(i\omega)^m + \alpha_{m-1}(i\omega)^{m-1} + \ldots + \alpha_1(i\omega)^1 + \alpha_0(i\omega)^0} \quad (4.91)$$

or:

$$H_{pq}(\omega) = \frac{Y_p(\omega)}{F_q(\omega)} = \frac{\sum_{k=0}^{n} \beta_k(i\omega)^k}{\sum_{h=0}^{m} \alpha_h(i\omega)^h}. \quad (4.92)$$

Equation (4.92) can be rewritten in order to obtain the following linear equation in the unknown α_h and β_k terms:

$$\sum_{h=0}^{m} \alpha_h(i\omega)^h Y_p(\omega) = \sum_{k=0}^{n} \beta_k(i\omega)^k F_q(\omega). \quad (4.93)$$

For a general MIMO case, (4.93) is expressed in matrix form as follows:

$$\sum_{h=0}^{m} \left([\alpha_h](i\omega)^h\right)\{Y(\omega)\} = \sum_{k=0}^{n} \left([\beta_k](i\omega)^k\right)\{F(\omega)\} \quad (4.94)$$

or:

$$\sum_{h=0}^{m} \left([\alpha_h](i\omega)^h\right)[H(\omega)] = \sum_{k=0}^{n} \left([\beta_k](i\omega)^k\right). \quad (4.95)$$

A similar expression can be derived in the time domain where, in terms of sampled data, the time domain matrix polynomial results from a set of finite difference equations (Allemang and Brown 1998):

$$\sum_{h=0}^{m} [\alpha_h]\{y_{i-h}\} = \sum_{k=0}^{n} [\beta_k]\{f_{i-k}\} \quad (4.96)$$

This model corresponds to an ARMA(m, n) model (compare (4.96) with (4.73)). If only free decay or IRF data are considered, (4.96) can be further simplified since the forcing function can be set equal to zero and the $[\beta_k]$ coefficients can be eliminated (Allemang and Brown 1998):

$$\sum_{h=0}^{m} [\alpha_h]\{y_{i-h}\} = \{0\}. \quad (4.97)$$

The number of roots is given by the product of the order of the polynomial by the number of measurement locations, as for the classical ARMA models.

Comparison of (4.94) and (4.96) leads to recognize that the time and frequency domain models can be expressed in terms of functionally similar matrix polynomial models. Since the ARMA terminology is traditionally related to the time domain, the Unified Matrix Polynomial Approach (UMPA) terminology has been proposed (Allemang and Brown 1998) in order to describe the common polynomial structure characterizing the various modal identification methods in either time or frequency domain. Following the original discussion, the same nomenclature for the coefficient matrices has been used in both time and frequency domain in order to point out the similarities. However, the coefficient matrices in the frequency domain are different from those in the time domain. Moreover, while the characteristic matrix polynomial equation in frequency domain can be expressed in the same domain, for time domain methods it is expressed in the z-domain and the roots z_r in this domain have to be converted in the continuous-time domain (4.80). Once the matrices $[\alpha_h]$ have been found, the modal parameters can be estimated according to the previously described approach (Sect. 4.2.3) based on the construction of the companion matrix.

The extension of UMPA to the output-only case is immediate if FRFs and IRFs are replaced by spectral density functions and correlation functions into (4.95) and (4.97), respectively. Thus, the development of UMPA allowed gathering a number of time domain and frequency domain algorithms in a unified framework, pointing out the relations among different modal identification algorithms beyond their mathematical model (time domain, frequency domain, state-space, AR, ARMA). Nonparametric methods can be seen as zero order models where only the spatial information related to the sensor position is used and data are processed at a single frequency line at a time.

Even if the unifying characteristic of different OMA methods, represented by the matrix polynomial structure, has been remarked, for historical reasons OMA methods are illustrated in the next sections according to the usual classification based on the adopted model and domain of implementation. For instance, the methods based on the analysis of correlation functions, such as Least Squares Complex Exponential (LSCE), Ibrahim Time Domain (ITD), Eigensystem Realization Algorithm (ERA), and Instrumental Variable (IV), will be discussed in different contexts in spite of the previously described common formulation. Similarly, time domain methods based on the analysis of raw data, such as DD-SSI and Prediction Error Method (PEM), will be separately analyzed according to the state-space and ARMA formulation, respectively. The separate discussion follows the historical development of the methods and it is helpful to point out the main differences among them that are mainly related to the role played by noise. Moreover, the separate discussion allows pointing out a specific difference between state-space and ARMA models. In fact, in the state-space representation the internal structure of the system is described, while ARMA models simply map the input–output behavior of the system. For this reason, a state-space model is also referred to as an internal representation of a system, while the ARMA model as an external representation.

4.3 Classification of OMA Techniques

Most OMA techniques are derived from traditional input–output modal identification procedures, but refer to a different mathematical framework. In fact, OMA is developed in a stochastic framework and it is based on the analysis of random signals (Chap. 2). OMA techniques are always of the multiple input type. Thus, classification of OMA methods according to the number of inputs (single input, multiple input), as in the case of input–output modal analysis, is not applicable.

Different criteria may apply for the classification of OMA methods. Each criterion points out a specific aspect common to different analysis methods and it is helpful to guide the user towards the choice of the favorite or most appropriate analysis method, depending on the advantages and limitations related to specific assumptions and data processing procedures.

A first distinction is between *parametric* and *nonparametric methods*. If a model is fitted to data, the technique is referred to as parametric. These procedures are more complex and computational demanding with respect to the nonparametric ones. However, they usually show better performance with respect to the faster and easy-to-use nonparametric techniques. Nonparametric techniques, on the other hand, are particularly useful during field tests to get a quick insight about effectiveness of measurements and results of dynamic identification. In the class of parametric models, a further distinction is made between low order and high order models. A *low order model* is used for those cases where the number of physical coordinates is greater than the number of measurable eigenvalues. On the contrary, a *high order model* is usually adopted when the system is under-sampled in the spatial domain.

Another distinction is between *SDOF* and *MDOF methods*, depending on the assumption about the number of modes determining the structural response in a given bandwidth. If only one mode is dominant, it is possible to assume that the structural response in that frequency range depends only on that mode and its parameters can be separately determined. SDOF methods are based on this assumption. They are very fast and characterized by low computational burden, but the SDOF assumption is a reasonable approximation only if the modes of the structure are well separated. In the presence of closely spaced or even coincident modes, MDOF methods have to be adopted in order to properly identify the different modes contributing to the overall structural response.

Modal frequencies and damping ratios are independent of the output location and they can be estimated on a local basis, that is to say, from the separate analysis of the individual response time histories. In this case, each analyzed time history can provide a slightly different estimate of the same modal parameter: as a result, a set of *local estimates* is obtained. On the contrary, if data processing affects all response measurements at the same time, *global estimates* for the modal parameters are obtained. A further distinction is between *one-stage* and *two-stage methods*. In the first case, natural frequencies, damping ratios, and mode shapes are estimated at the same time; in the second case, instead, selected parameters (for instance, natural frequencies and damping ratios) are estimated first, while the remaining

parameters (for instance, the mode shapes) are estimated in a second data processing step based on the modal estimates obtained in the first stage of analysis.

A classical distinction is based on the domain of implementation. OMA methods based on the analysis of response time histories or correlation functions are referred to as *time domain methods*. Methods based on spectral density functions are, instead, referred to as *frequency domain methods*. This distinction may look like artificial, since they simply consider different representations of the same signal (in fact, it is always possible to transform the signal from one domain to the other). However, when parametric methods are considered, the selection between time and frequency domain can be relevant in practical applications since different mechanisms of noise rejection and quality of numerical conditioning characterize the two classes of methods.

Time domain methods are usually better conditioned than the frequency domain counterparts. This is mainly related to the effect of the powers of frequencies in frequency domain equations; numerical conditioning has been recently improved through the adoption of polynomial basis functions formulated in the z-domain (see also Sect. 4.4.3 for more details).

The adopted strategy to deal with noisy measurements represents another discriminating aspect between time domain and frequency domain methods. Time domain methods are usually more suitable to handle noisy data, and they can avoid some signal processing errors, such as leakage. Time domain methods take advantage of the SVD to reject noise or, as in the case of ARMA models, they try to model also the noise. However, in this latter case a higher model order is required to fit noise effects and, as a consequence, a lot of additional spurious poles appear. Averaging is, instead, the strategy adopted by frequency domain methods to deal with noisy measurements (see also Chap. 2).

Among the parametric time domain methods a further distinction is between *covariance-driven* and *data-driven methods*. The former require a preprocessing step to estimate the correlation functions from response measurements; the latter, instead, directly process the raw data.

4.4 Frequency Domain Methods

4.4.1 The Basic Frequency Domain (Peak-Picking) Method

The most undemanding method for output-only modal parameter identification is the Basic Frequency Domain (BFD) method, also known as the Peak-Picking method. It is based on the computation of auto- and cross-spectra and it has been widely used in the past for modal identification purposes (see, for instance, Felber 1993 for its application in civil engineering). The name of the method comes from the fact that the modes are identified by picking the peaks in the PSD plots.

The BFD technique can be classified as a SDOF method for OMA. In fact, it is based on the assumption that, around a resonance, only one mode is dominant. As a consequence, the pole-residue form of the output PSD matrix (4.13) can be

approximated by the contribution of the dominant mode only. For instance, if only the r-th mode is dominant, the structural response is approximately equal to the modal response:

$$\{y(t)\} \approx \{\phi_r\} p_r(t) \tag{4.98}$$

where $p_r(t)$ is the modal coordinate related to the r-th mode. As a consequence, the correlation functions are approximately given by:

$$\left[R_{yy}(\tau)\right] = E\left[\{y(t+\tau)\}\{y(t)\}^T\right] = R_{p_r p_r}(\tau)\{\phi_r\}\{\phi_r\}^T \tag{4.99}$$

where:

$$R_{p_r p_r}(\tau) = E[p_r(t+\tau)p_r(t)] \tag{4.100}$$

is the modal auto-correlation function, and the spectral density matrix is given by:

$$[G_{YY}(\omega)] = G_{P_r P_r}(\omega)\{\phi_r\}\{\phi_r\}^H \tag{4.101}$$

where $G_{P_r P_r}(\omega)$ is the auto-spectral density function of the modal coordinate. It is clear from (4.101) that in this case the PSD matrix is of rank one. Thus, at resonance any column of the PSD matrix can be considered as an estimate of the corresponding mode shape, up to a scaling factor (the input being unmeasured).

From a practical point of view, the trace of the PSD matrix (the sum of the auto-spectra) at each discrete frequency value is computed first to identify the peaks corresponding to structural resonances. Then, the mode shapes associated to the identified frequencies are obtained from one of the columns of the PSD matrix. A reference sensor for the computation of the cross-spectral densities with all other measurement channels has to be selected. The reference sensor has to be selected so that most of the modes can be observed. As a consequence, sensors close to nodes of the mode shapes cannot be adopted as reference sensors. The ideal choice for the reference sensor makes possible the identification of all the modes through the computation a single column of the PSD matrix (the column made by the cross-spectral densities between the selected reference sensor and all other sensors). However, depending on the geometry of the structure and the adopted sensor layout, a single reference sensor could be insufficient to identify all the modes and at least a couple of reference sensors with different orientation have to be adopted. For instance, in the case of a building-like structure characterized by two bending modes in two orthogonal directions—x and y—and sensors parallel to these directions, the selection of a sensor measuring along x as reference permits the identification of the bending modes in the x direction and eventually torsional modes, but it is inadequate to identify the bending modes in the y direction. These can be observed only through the selection of an additional reference sensor measuring along y.

The inspection of the coherence functions (Chap. 2) between couples of channels also supports the identification of the actual modes of the structure (Fig. 4.3).

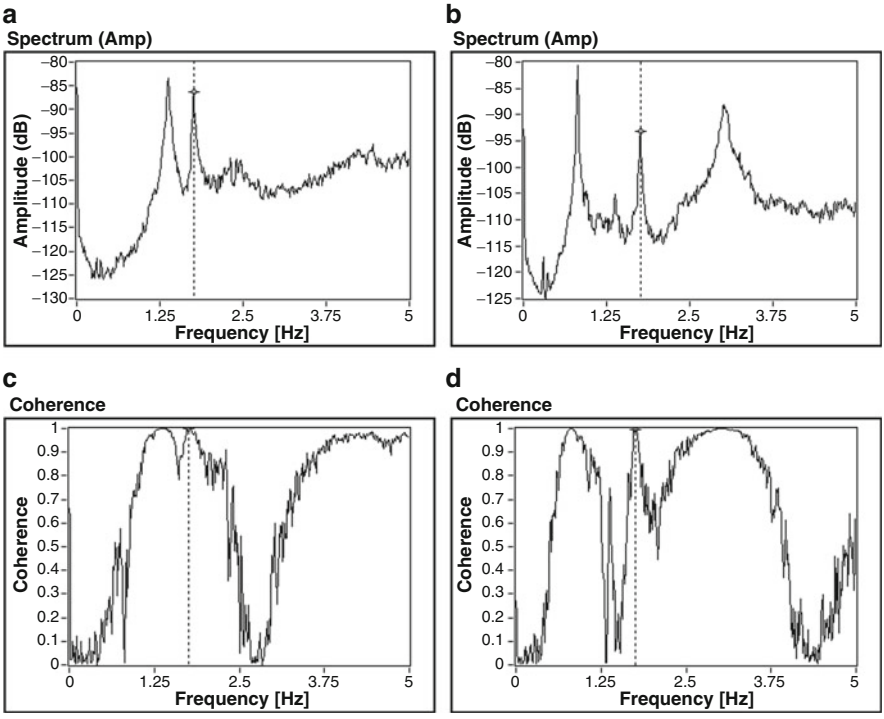

Fig. 4.3 Auto-power spectra of two reference channels in orthogonal directions (**a**, **b**) and coherence functions with channels in the same directions of the references (**c**, **d**); note that the torsional mode (marked in the plots) yields high coherence with both the reference channels

In fact, in correspondence of a resonant frequency, the coherence function is close to 1 because of the high signal-to-noise ratio at that frequency. This characteristic is helpful in the discrimination between real eigenfrequencies and peaks due to disturbances. Moreover, the coherence function can support the identification of the nature of a mode. For instance, assume that the structure under investigation shows two bending modes in two orthogonal directions—x and y—and a torsional mode in a certain frequency range. When the torsional mode is considered, the coherence function shows a value close to 1 if either the two channels are in the same direction or in two orthogonal directions. On the contrary, bending modes are associated to low values of the coherence when it is computed for two orthogonal sensors. The combination of information from spectra and coherence functions, therefore, makes possible the identification of structural modes. This procedure sometimes makes possible the identification even of closely spaced modes. However, the success of the identification process heavily depends on the geometry of the structure and the skill of the analyst. The results of modal identification suffer a certain degree of subjectivity also in the case of noisy measurements, when the peaks in the spectra are not clear.

The BFD method provides local estimates of the modal properties. Moreover, the accuracy of the estimated eigenfrequencies depends on the frequency resolution of the spectra. A fine frequency resolution is fundamental to obtain good natural frequency estimates.

In principle, the BFD should be applied to evaluate natural frequencies and mode shapes only. The half-power bandwidth method is sometimes applied to get damping estimates from the spectra. However, a number of studies have shown that they are not accurate (see, for instance, Peeters 2000, Rainieri et al. 2010).

In summary, the BFD technique is effective when damping is low and modes are well separated. If these conditions are violated it may lead to erroneous results. In fact, the method identifies ODSs instead of the actual mode shapes, and they are generally a combination of all mode shapes; they are good approximations of the actual mode shapes if only one mode is dominant at the considered frequencies. In the case of closely spaced modes, the respective contributions are significant and the ODS is the superposition of multiple modes. Despite of these drawbacks, the method is very simple and undemanding from a computational point of view. Thus, it is a basic but useful analysis tool for the analyst, in particular during field tests, to get a quick insight about effectiveness of measurements and results of dynamic identification.

4.4.2 The Frequency Domain Decomposition Method

The introduction of the FDD technique (Brincker et al. 2001) has overcome the previously discussed drawbacks of the BFD method concerning the identification of closely spaced modes. This method was originally applied to FRFs and known as Complex Mode Indicator Function (CMIF) to point out its ability to detect multiple roots and, therefore, the possibility to count the number of dominant modes at a certain frequency (Shih et al. 1988). The method has been then systematized for the use with response spectrum data.

A theoretical proof of the method is based on the modal expansion of the structural response:

$$\{y(t)\} = [\Phi]\{p(t)\} \tag{4.102}$$

where [Φ] is the modal matrix and {p(t)} the vector of modal coordinates. From (4.102) the correlation matrix of the responses can be computed:

$$\left[R_{yy}(\tau)\right] = E\left[\{y(t+\tau)\}\{y(t)\}^T\right] = [\Phi]\left[R_{pp}(\tau)\right][\Phi]^T \tag{4.103}$$

The PSD matrix can be obtained from (4.103) by taking the Fourier transform:

$$[G_{YY}(\omega)] = [\Phi][G_{PP}(\omega)][\Phi]^H \tag{4.104}$$

The PSD matrix of the modal coordinates is diagonal if they are uncorrelated. A similar decomposition is obtained in the case of uncorrelated excitation forces characterized by a flat spectral density function (Brincker and Zhang 2009).

Taking into account that the SVD of the PSD matrix at a certain frequency ω leads to the following factorization:

$$[G_{YY}(\omega)] = [U][\Sigma][V]^H \tag{4.105}$$

where [U] and [V] are the unitary matrices holding the left and right singular vectors and [Σ] is the matrix of singular values (arranged in descending order), for a Hermitian and positive definite matrix, such as the PSD matrix, it follows that [U] = [V] and the decomposition of (4.105) can be rewritten as:

$$[G_{YY}(\omega)] = [U][\Sigma][U]^H. \tag{4.106}$$

The comparison between (4.104) and (4.106) suggests that it is possible to identify a one-to-one relationship between singular vectors and mode shapes; moreover, the singular values are related to the modal responses and they can be used to define the spectra of equivalent SDOF systems characterized by the same modal parameters as the modes contributing to the response of the MDOF system under investigation. Since the SVD provides the singular values arranged in descending order, near a resonance the first singular value contains the information about the dominant mode at that frequency. Moreover, since the number of nonzero elements in [Σ] equals the rank of the PSD matrix at the considered frequency, this property can be used to identify closely spaced or even coincident modes. In fact, the number of dominant singular values (defining the rank of the output PSD matrix) at a certain frequency equals the number of modes that give a significant contribution to the structural response at that particular frequency. Assuming that only one mode is dominant at the frequency ω, and that the selected frequency is associated to the peak of resonance of the k-th mode, the PSD matrix approximates to a rank one matrix with only one term on the right side of (4.106):

$$[G_{YY}(\omega)] = \sigma_1\{u_1\}\{u_1\}^H, \qquad \omega \to \omega_k. \tag{4.107}$$

In such a case, the first singular vector $\{u_1\}$ represents an estimate of the mode shape of the k-th mode:

$$\{\hat{\phi}_k\} = \{u_1(\omega_k)\} \tag{4.108}$$

and the corresponding singular value σ_1 belongs to the auto PSD function of the equivalent SDOF system corresponding to the mode of interest. The equivalent SDOF PSD function is identified as the set of singular values around a peak of the singular value plots (Fig. 4.4) that are characterized by similar singular vectors. In the enhanced version of the method, the so-called Enhanced Frequency Domain Decomposition (EFDD) (Brincker et al. 2001, Gade et al. 2005), this SDOF PSD function is used to estimate also the modal damping ratio. The comparison of the

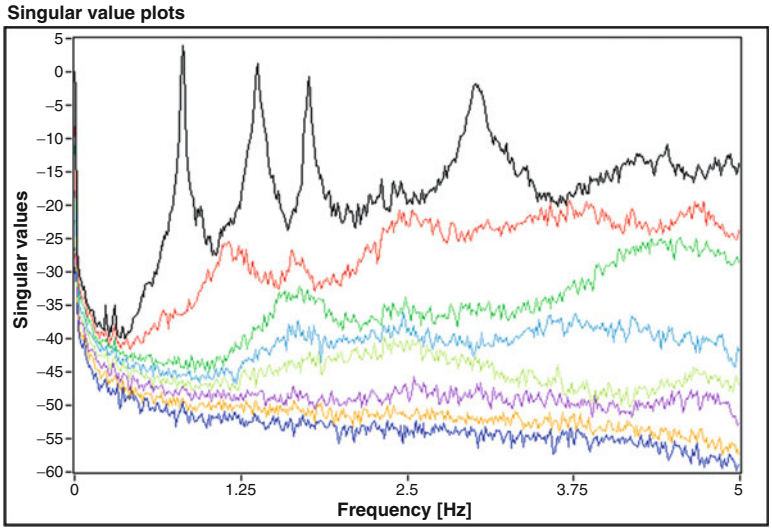

Fig. 4.4 Sample singular value plots

mode shape estimate $\{\hat{\phi}_k\}$ at the peak with the singular vectors associated to the frequency lines around the peak leads to the identification of the singular values whose singular vectors show a correlation with $\{\hat{\phi}_k\}$ higher than a user-defined threshold, the so-called *MAC Rejection Level*. Such singular values define the equivalent SDOF PSD function. The *Modal Assurance Criterion* (MAC) is used as a measure of the correlation between two modal vectors (see also Sect. 4.8.2.2 for more details about the MAC index); it is given by (Allemang and Brown 1982):

$$MAC\left(\{u_j\},\{\hat{\phi}_k\}\right) = \frac{\left|\{u_j\}^H\{\hat{\phi}_k\}\right|^2}{\left(\{u_j\}^H\{u_j\}\right)\left(\{\hat{\phi}_k\}^H\{\hat{\phi}_k\}\right)} \tag{4.109}$$

where $\{u_j\}$ is the generic singular vector in the vicinity of the peak in the singular value plots corresponding to the k-th mode.

By definition, the MAC is a number in the range [0, 1]; it is equal to zero when the vectors under comparison are orthogonal, and equal to 1 when the vectors differ by a scale factor only. A typically adopted value of the MAC Rejection Level is about 0.8. The identified equivalent SDOF PSD function is used to evaluate the modal damping ratio, and to get estimates of the natural frequency independent of the frequency resolution of the spectra. The inverse Fourier transform of the equivalent SDOF PSD function yields an approximated correlation function of the equivalent SDOF system. Thus, an estimate of the modal damping ratio is obtained in the time domain through a linear regression on the logarithmic decrement. In a similar way, an estimate of the natural frequency independent of the frequency resolution can be obtained through a linear regression on the zero crossing times of the equivalent SDOF system correlation function, eventually taking into account that damped $f_{d,k}$ and undamped

natural frequency f_k (which are very similar at low values of the modal damping ratio ξ_k) are related as follows:

$$f_{d,k} = f_k \sqrt{1 - \xi_k^2}. \tag{4.110}$$

The FDD method permits the identification of closely spaced modes. However, it is worth pointing out that in this case the mode shape estimates could be biased. In fact, since the SVD forces the singular vectors to be orthogonal, if the experimental mode shapes are also orthogonal the obtained estimates are unbiased. On the contrary, if the mode shapes are not orthogonal, the mode shape estimates for the closely spaced modes are biased and the bias mainly affects the weak mode, while the mode shape estimate for the dominant mode is still good. The bias depends on the difference between the first and second singular value: the larger this difference, the smaller the error. Thus, the mode shape estimates should be obtained from singular vectors at frequencies characterized by the largest difference between the first and second singular value. In the presence of closely spaced modes, this frequency might be different from the frequency of the peak.

In the literature it is possible to find variants to the above-described classical implementation of the FDD/EFDD method (Jacobsen et al. 2008, Rodrigues et al. 2004). In particular, an alternative implementation of FDD based on EVD instead of SVD is also available (Brincker and Zhang 2009). Among the FDD variants, it is worth mentioning the so-called Frequency-Spatial Domain Decomposition (FSDD), where spatial filtering is adopted to enhance the estimation of modal frequencies and damping ratios. The *spatial filtering*, also known as coherent averaging, is a method for data condensation based on a dot product of the data with a weighting vector. Information in the data that is not coherent with the weighting vectors is averaged out of the data. Typical spatial filtering procedures are based on the use of data coming from sensors located in a local area of the system in order to enhance local modes, or on the use of mode shape estimates as weighting functions to enhance particular modes. The spatial filtering belongs to the class of the so-called condensation algorithms together with least squares and transformations (such as SVD). The FSDD makes use of mode shape estimates computed via SVD of the output PSD matrix to enhance PSDs. The use of a mode shape estimate (provided by FDD) as weighting vector leads to an enhanced PSD, which approximates the PSD of a SDOF system. As a consequence, a SDOF curve fitter may be profitably used to estimate the natural frequency and the damping ratio of the considered mode. More details about FSDD can be found elsewhere (Zhang et al. 2005a).

4.4.3 Frequency Domain Parametric Methods for OMA

Frequency domain parametric modal identification methods are based on either fraction polynomial models or the modal (pole-residue) model. Modal identification methods based on the modal model, such as the Least Squares Frequency

Domain (LSFD) estimator, have an historical relevance but they are not in wide use. In fact, when an estimate of the pole is not available, the LSFD method leads to a nonlinear least squares problem that needs for an optimization algorithm to be solved and good starting values to reduce the iterations. As a consequence, the LSFD estimator is used only to obtain global estimates of the mode shapes in combination with other methods providing the poles.

The methods based on MFD are basically curve-fitting techniques based on the minimization of an equation error between the measured and the predicted PSD matrix. For instance, the equation error for a common-denominator model is given by:

$$\varepsilon_{YY}(\omega_f) = \hat{G}_{YY}(\omega_f) - \frac{B_{YY}(\omega_f, \{\theta\})}{A(\omega_f, \{\theta\})} \tag{4.111}$$

where $\hat{G}_{YY}(\omega_f)$ is the measured value of the spectrum at the frequency line f for a generic couple of measurement channels; B_{YY} and A are the numerator and denominator polynomials, respectively; the polynomial coefficients $\{\theta\}$ are the parameters to be estimated. In order to identify the parameters $\{\theta\}$, a cost function is defined as the sum of squares of the Frobenius norms of the errors at all frequency lines:

$$\ell(\{\theta\}) = \sum_{f=1}^{N_f} \left\| [\varepsilon(\omega_f)] \right\|_F^2 \tag{4.112}$$

where $\varepsilon_{YY}(\omega_f)$ is the generic element of $[\varepsilon(\omega_f)]$.

The cost function has a nonlinear expression in the unknown parameters. Thus, iterative algorithms, such as the Gauss-Newton approach, have to be applied. However, they typically suffer problems of convergence, local minima, and computational burden. Moreover, since the solution is sensitive to the initial value, good starting values are required. Maximum Likelihood Estimators (MLEs) are based on this approach. In order to find good initial values for the application of the MLE, some approaches to linearize the cost function have been introduced. As a consequence, sub-optimal initial values of the parameters are obtained as a solution of a linear least squares problem.

The Least Squares Complex Frequency (LSCF) method is a parametric frequency domain modal identification method originally developed to provide good initial values of the parameters to the MLE with low computational efforts. However, it has been found that it is also able to provide fairly accurate modal parameter estimates and, as a consequence, it can be confidently applied as modal identification technique (Verboven 2002, Zhang et al. 2005b).

For this reason and the previously mentioned drawbacks related to the solution of an optimization problem by iterative algorithms, the MLE is not widely used in practical applications. The interested reader can refer to the literature on this topic for more details (Schoukens and Pintelon 1991, Pintelon et al. 1994). In the following, attention is focused on the LSCF estimator. The main advantage with

its use is in the possibility to get very clear stabilization diagrams (see Sect. 4.9 for more details). This simplifies the identification of the structural modes and provides interesting opportunities for the automation of the modal identification process. However, the LSCF method shows some limitations in the identification of closely spaced modes. Thus, a poly-reference version of the method, the Poly-reference LSCF estimator (also known under the commercial name of PolyMAX), has been introduced to deal with the identification of closely spaced poles. Both the LSCF method and its poly-reference version can be classified as two stage modal identification methods. In fact, the identification of the mode shapes is based on previous estimates of natural frequencies and damping ratios. In particular, as explained next, the identification of the mode shapes is usually carried out according to the LSFD approach once the poles associated to structural modes have been identified in the first stage of analysis.

4.4.3.1 The Least Squares Complex Frequency Method

The LSCF estimator takes advantage of the global character of the structural poles and the common-denominator model to identify the modal parameters. It can be classified as a parametric, frequency domain modal identification procedure. The analysis parameter is represented by the order of the polynomial in the model.

Assume that the numerator polynomial and the common-denominator polynomial are characterized by the same order n. For a generic couple k of output channels ($k = 1, \ldots, l \cdot l$), the cross-power spectrum at frequency line f ($f = 1, \ldots, N_f$) is modeled as:

$$G_k(\omega_f) = \frac{N_k(\Omega_f, \{\theta\})}{d(\Omega_f, \{\theta\})} \tag{4.113}$$

where:

$$N_k(\Omega_f, \{\theta\}) = \sum_{j=0}^{n} N_{k,j} \Omega_f^j \tag{4.114}$$

$$d(\Omega_f, \{\theta\}) = \sum_{j=0}^{n} d_j \Omega_f^j \tag{4.115}$$

are the numerator polynomial and the common-denominator polynomial, respectively. The coefficients d_j and $N_{k,j}$ are the unknown, complex-valued parameters $\{\theta\}$ to be estimated. Ω_f is the *generalized transform variable*, evaluated at the frequency line f. Different choices for Ω_f are possible.

In its classical implementation, the LSCF estimator was based on a continuous-time domain model with real-valued coefficients. In that case the generalized transform variable was $\Omega_f = i\omega_f$.

Nevertheless, the problem was numerically ill-conditioned, in particular for high order systems, and even the normalization of the frequency axis led to moderate

improvements of the numerical conditioning. A significant improvement of numerical conditioning of continuous-time domain models was obtained through the introduction of orthogonal polynomials—Forsythe and Chebyshev polynomials—(Verboven et al. 2005) as generalized transform variable. Nevertheless, numerical conditioning problems were still present to a certain extent and the coefficients estimated according to the polynomial basis had to be transformed back to the original power polynomial basis in order to extract the modal parameters. In order to overcome these drawbacks, the LSCF estimator is currently based on a common-denominator model in the discrete-time domain, and the generalized transform variable has the following formulation in the z-domain:

$$\Omega_f = e^{i\omega_f \Delta t} = z_f. \tag{4.116}$$

This complex polynomial basis function ensures good numerical conditioning. As a consequence, only the z-domain formulation is considered in the following. From (4.116) it follows that:

$$\Omega_f^j = e^{(i\omega_f \Delta t)j} = z_f^j \tag{4.117}$$

The estimation of the coefficients $\{\theta\}$ requires the application of a constraint in the solution of the least squares problem. In fact, multiplication of numerator and denominator by a scalar $a \neq 0$ yields an equivalent scalar matrix fraction description:

$$G_k(\omega_f) = \frac{N_k(\Omega_f, \{\theta\})}{d(\Omega_f, \{\theta\})} = \frac{a \cdot N_k(\Omega_f, \{\theta\})}{a \cdot d(\Omega_f, \{\theta\})}. \tag{4.118}$$

Possible strategies to remove the parameter redundancy consist in setting one of the denominator coefficients equals to 1 (the effect of different choices for the restrained coefficient is discussed in Sect. 4.9) or in imposing that the vector of the parameters $\{\theta\}$ (or eventually the vector holding only the denominator coefficients) has norm 1.

In the following derivations the highest order coefficient of the denominator is constrained to be equal to 1:

$$d_n = 1 \tag{4.119}$$

since this choice simplifies the identification of the structural poles (Sect. 4.9).

The polynomial coefficients are obtained as a solution of a linear least squares problem. In order to obtain equations that are linear in the parameters, the following approximation is considered:

$$\varepsilon_k(\omega_f, \{\theta\}) = N_k(\Omega_f, \{\theta\}) - \hat{G}_k(\omega_f) d(\Omega_f, \{\theta\}) \approx 0 \tag{4.120}$$

where $\hat{G}_k(\omega_f)$ is the measured spectrum for the k-th couple of output channels, evaluated at the frequency line f. The unknown polynomial coefficients are obtained through the minimization of the following equation error:

$$\ell(\{\theta\})_{LS} = \sum_{k=1}^{l \cdot l} \sum_{f=1}^{N_f} \left| N_k(\Omega_f, \{\theta\}) - \hat{G}_k(\omega_f) d(\Omega_f, \{\theta\}) \right|^2. \tag{4.121}$$

Since (4.120) is linear in the unknown parameters {θ}, it can be rewritten as follows, taking into account that a common-denominator model has been adopted:

$$\{\varepsilon\} = [J]\{\theta\} = \begin{bmatrix} [\Gamma_1] & [0] & \dots & [0] & [\Upsilon_1] \\ [0] & [\Gamma_2] & \ddots & [0] & [\Upsilon_2] \\ \vdots & \vdots & \ddots & \vdots & \vdots \\ [0] & [0] & \dots & [\Gamma_{l \cdot l}] & [\Upsilon_{l \cdot l}] \end{bmatrix} \begin{Bmatrix} \{\theta_{N_1}\} \\ \{\theta_{N_2}\} \\ \vdots \\ \{\theta_{N_{l \cdot l}}\} \\ \{\theta_d\} \end{Bmatrix} \approx \{0\} \tag{4.122}$$

where:

$$\{\varepsilon\} = \begin{Bmatrix} \{\varepsilon_1\} \\ \vdots \\ \{\varepsilon_k\} \\ \vdots \\ \{\varepsilon_{l \cdot l}\} \end{Bmatrix}, \qquad \{\varepsilon_k\} = \begin{Bmatrix} \varepsilon_k(\omega_1) \\ \varepsilon_k(\omega_2) \\ \vdots \\ \varepsilon_k(\omega_{N_f}) \end{Bmatrix} \tag{4.123}$$

$$\{\theta_{N_k}\} = \begin{Bmatrix} N_{k,0} \\ N_{k,1} \\ \dots \\ N_{k,n} \end{Bmatrix} \tag{4.124}$$

$$\{\theta_d\} = \begin{Bmatrix} d_0 \\ d_1 \\ \dots \\ d_n \end{Bmatrix} \tag{4.125}$$

$$[\Gamma_k] = \begin{Bmatrix} \{\Gamma_k(\omega_1)\}^T \\ \{\Gamma_k(\omega_2)\}^T \\ \dots \\ \{\Gamma_k(\omega_{N_f})\}^T \end{Bmatrix} = \begin{bmatrix} z^0(\omega_1) & z^1(\omega_1) & \dots & z^n(\omega_1) \\ z^0(\omega_2) & z^1(\omega_2) & \dots & z^n(\omega_2) \\ \dots & \dots & \dots & \dots \\ z^0(\omega_{N_f}) & z^1(\omega_{N_f}) & \dots & z^n(\omega_{N_f}) \end{bmatrix} \tag{4.126}$$

$$[\Upsilon_k] = \begin{Bmatrix} \{\Upsilon_k(\omega_1)\}^T \\ \{\Upsilon_k(\omega_2)\}^T \\ \vdots \\ \{\Upsilon_k(\omega_{N_f})\}^T \end{Bmatrix} = \begin{bmatrix} -\hat{G}_k(\omega_1)z^0(\omega_1) & \dots & -\hat{G}_k(\omega_1)z^n(\omega_1) \\ \vdots & \dots & \vdots \\ -\hat{G}_k(\omega_{N_f})z^0(\omega_{N_f}) & \dots & -\hat{G}_k(\omega_{N_f})z^n(\omega_{N_f}) \end{bmatrix} \tag{4.127}$$

The unknown parameters can be estimated directly from the Jacobian matrix [J]. However, a significant reduction in computational time and memory requirements can be achieved through the formulation of normal equations. The normal matrix:

$$[J]^H[J] = \begin{bmatrix} [\Gamma_1]^H[\Gamma_1] & [0] & \dots & [\Gamma_1]^H[\Upsilon_1] \\ [0] & [\Gamma_2]^H[\Gamma_2] & \dots & [\Gamma_2]^H[\Upsilon_2] \\ \vdots & \vdots & \ddots & \vdots \\ [\Upsilon_1]^H[\Gamma_1] & [\Upsilon_2]^H[\Gamma_2] & \dots & \sum_{k=1}^{l \cdot l}[\Upsilon_k]^H[\Upsilon_k] \end{bmatrix} \tag{4.128}$$

consists of submatrices that are structured (Toeplitz) matrices (a *Toeplitz matrix* is a matrix in which each diagonal is characterized by the repetition of the same element). If the following submatrices are defined:

$$[R_k] = [\Gamma_k]^H[\Gamma_k] \tag{4.129}$$

$$[S_k] = [\Gamma_k]^H[\Upsilon_k] \tag{4.130}$$

$$[T_k] = [\Upsilon_k]^H[\Upsilon_k] \tag{4.131}$$

the normal equations can be written in this form:

$$[J]^H[J]\{\theta\} = \begin{bmatrix} [R_1] & [0] & \dots & [S_1] \\ [0] & [R_2] & \dots & [S_2] \\ \vdots & \vdots & \ddots & \vdots \\ [S_1]^H & [S_2]^H & \dots & \sum_{k=1}^{l \cdot l}[T_k] \end{bmatrix} \begin{Bmatrix} \{\theta_{N_1}\} \\ \{\theta_{N_2}\} \\ \vdots \\ \{\theta_{N_{l \cdot l}}\} \\ \{\theta_d\} \end{Bmatrix} \approx \{0\}. \tag{4.132}$$

Since the parameter constraint has been applied to the denominator coefficients $\{\theta_d\}$ only, the numerator coefficients can be eliminated from the normal equations by substitution of:

$$\{\theta_{N_k}\} = -[R_k]^{-1}[S_k]\{\theta_d\} \tag{4.133}$$

into (4.132); this results in the so-called *reduced normal equations*:

$$\left[\sum_{k=1}^{l\cdot l}\left([T_k]-[S_k]^H[R_k]^{-1}[S_k]\right)\right]\{\theta_d\}=[M]\{\theta_d\}\approx\{0\}. \tag{4.134}$$

A significant reduction in the dimension of the problem has been obtained, since the square $(n+1)\times(n+1)$ matrix [M] is much smaller than the normal matrix $[J]^H[J]$. Under the constraint given by (4.119), the least squares solution is obtained as:

$$\{\theta_d\}=\begin{bmatrix}-\left[M_{(1:n,\,1:n)}\right]^{-1}\left[M_{(1:n,\,n+1)}\right]\\ 1\end{bmatrix} \tag{4.135}$$

where $[M_{(1:n,1:n)}]$ is the submatrix made by the first n rows and n columns of $[M]$, while $[M_{(1:n,n+1)}]$ is the submatrix made by the first n rows and the last column of $[M]$. Once the coefficients $\{\theta_d\}$ have been computed, the poles in the z-domain are obtained as the roots of the denominator polynomial. Taking into account the relation between the poles in the z-domain and those in the Laplace domain:

$$z_r=e^{\lambda_r\Delta t}\Rightarrow\lambda_r=\frac{\ln(z_r)}{\Delta t} \tag{4.136}$$

the natural frequency, the damped modal frequency, and the damping ratio of the r-th mode can be computed as follows:

$$f_r=\frac{|\lambda_r|}{2\pi} \tag{4.137}$$

$$f_{d,r}=\frac{\mathrm{Im}\,(\lambda_r)}{2\pi} \tag{4.138}$$

$$\xi_r=-\frac{Re(\lambda_r)}{|\lambda_r|}. \tag{4.139}$$

Once the denominator coefficients $\{\theta_d\}$ are known, the numerator coefficients can be obtained from (4.133); the mode shapes can be theoretically estimated from those polynomial coefficients. However, the numerator coefficients are actually computed only if the LSCF estimator is used to determine the starting value for the MLE. In practical applications mode shapes are, instead, obtained from the modal model as a solution of a second least squares problem. The reason under this two-stage approach is that the common-denominator model does not force rank-one residue matrices on the measurements, while it is known from modal analysis theory that the residue matrix is of rank one.

Once the structural modes are identified, the corresponding poles are passed to the LSFD estimator for the identification of the residue matrices and, as a consequence, the mode shapes associated to the selected physical poles. Since the poles are known from the previous stage, the modal model is linear in the parameters (the residues), which can be obtained as a solution of a linear least squares problem.

The residue matrices can be computed by minimizing the following functions:

$$g_k(R_{k,j}) = \sum_{f=1}^{N_f} \left(\hat{G}_k(\omega_f) - \sum_{j=1}^{N_m} \left(\frac{R_{k,j}}{i\omega_f - \lambda_j} + \frac{R_{k,j}^*}{i\omega_f - \lambda_j^*} \right) \right)^2 \tag{4.140}$$

with respect to $R_{k,j}$ ($k = 1, \ldots, l \cdot l$) in a least squares sense. In general, two additional terms, the upper (UR) and lower (LR) residual terms, can be considered (Peeters and Van der Auweraer 2005). They are introduced to approximate the effects of out-of-band modes (below the lower bound and above the upper bound of the analyzed frequency range). However, their use is restricted to continuous-time fraction polynomial models (Verboven 2002).

The minimization of g_k implies that its partial derivatives with respect to the unknown residual coefficients $R_{k,j}$ are zero:

$$\frac{\partial g_k}{\partial R_{k,j}} = 2 \sum_{f=1}^{N_f} \left(\hat{G}_k(\omega_f) - \sum_{j=1}^{N_m} \left(\frac{R_{k,j}}{i\omega_f - \lambda_j} + \frac{R_{k,j}^*}{i\omega_f - \lambda_j^*} \right) \right) \left(-\frac{1}{i\omega_f - \lambda_j} \right) = 0 \tag{4.141}$$

with $k = 1, \ldots, l \cdot l$ and $j = 1, \ldots, 2N_m$, where N_m denotes the number of identified physical modes. The obtained equations can be expressed in matrix form as follows:

$$[\Lambda_\Lambda]\{R_k\} = \{G_\Lambda\} \tag{4.142}$$

where:

$$[\Lambda_\Lambda] = \sum_{f=1}^{N_f} \{\Lambda(\omega_f)\}\{\Lambda(\omega_f)\}^T \tag{4.143}$$

$$\{G_\Lambda\} = \sum_{f=1}^{N_f} \hat{G}_k(\omega_f)\{\Lambda(\omega_f)\} \tag{4.144}$$

$$\{\Lambda(\omega_f)\} = \begin{Bmatrix} \frac{1}{i\omega_f - \lambda_1} \\ \vdots \\ \frac{1}{i\omega_f - \lambda_j} \\ \vdots \\ \frac{1}{i\omega_f - \lambda_{N_m}} \\ \frac{1}{i\omega_f - \lambda_1^*} \\ \vdots \\ \frac{1}{i\omega_f - \lambda_j^*} \\ \vdots \\ \frac{1}{i\omega_f - \lambda_{N_m}^*} \end{Bmatrix} \tag{4.145}$$

$$\{R_k\} = \begin{Bmatrix} R_{k,1} \\ \vdots \\ R_{k,j} \\ \vdots \\ R_{k,N_m} \\ R_{k,1}^* \\ \vdots \\ R_{k,j}^* \\ \vdots \\ R_{k,N_m}^* \end{Bmatrix}. \tag{4.146}$$

As a consequence, since the physical poles are known, the residues can be determined as follows:

$$\{R_k\} = [\Lambda_\Lambda]^{-1}\{G_\Lambda\}, \qquad k = 1, \ldots, l \cdot l. \tag{4.147}$$

The $l \times l$ residue matrix $[R_j]$ corresponding to the j-th mode is easily constructed by taking the elements of the $\{R_k\}$ vectors corresponding to λ_j for k = 1,. . ., $l{\cdot}l$. Once the $[R_j]$ matrices ($j = 1, \ldots, N_m$) have been determined, the mode shapes $\{\phi_j\}$ are obtained by SVD of the residue matrices:

$$[R_j] = [U][\Sigma][V]^T \tag{4.148}$$

In fact, assuming that $rank([R_j]) = 1$, the first column of $[U]$ is an estimate of the mode shape $\{\phi_j\}$ of the j-th mode.

4.4.3.2 The Poly-Reference Least Squares Complex Frequency Method

The poly-reference version of the LSCF estimator is based on an RMFD. The development of the p-LSCF method was motivated by some inherent limitations of the LSCF estimator based on the common-denominator model. In particular, they concern the identification of closely spaced modes and the reduction of the quality of fit when the polynomial model is converted to a modal model (Peeters and Van der Auweraer 2005). In fact, closely spaced poles might erroneously show up as a single pole in LSCF, in particular at low values of the model order. The reduction of the quality of fit is instead related to the fact that the common-denominator model does not force the residue matrices to be rank-one. This extra freedom leads to an "artificial" enhancement of the quality of fit, since the model does not fulfill the modal analysis theory in terms of rank of the residue matrices.

The p-LSCF method is herein illustrated with reference to one-sided spectra, but positive power spectra are analyzed in the same way by replacing $[G_{YY}(\omega_f)]$ with $[S^+_{YY}(\omega_f)]$ (or their respective estimates), and $\langle \hat{G}_o(\omega_f) \rangle$ with $\langle \hat{S}^+_o(\omega_f) \rangle$. A comparison between the results obtained from the application of the method to positive power spectra and one-sided spectra is reported in Sect. 4.9. In p-LSCF the PSD matrix at each frequency line f (f = 1, …, N_f) is modeled by the RMFD (Cauberghe 2004):

$$\left[G_{YY}(\omega_f)\right] = \left[B(\Omega_f, [\theta])\right]\left[A(\Omega_f, [\theta])\right]^{-1} \tag{4.149}$$

where $[\theta]$ is the matrix of the unknown parameters. For every output channel o (o = 1, …, l), $\langle B_o(\Omega_f, [\theta]) \rangle$ is the numerator matrix polynomial:

$$\langle B_o(\Omega_f, [\theta]) \rangle = \sum_{j=1}^{n} \langle B_{o,j} \rangle \Omega_f^j \tag{4.150}$$

and $[A(\Omega_f, [\theta])]$ is the denominator matrix polynomial:

$$\left[A(\Omega_f, [\theta])\right] = \sum_{j=0}^{n} [A_j] \Omega_f^j. \tag{4.151}$$

The $1 \times l$ matrices $\langle B_{o,j} \rangle$ and the $l \times l$ matrices $[A_j]$ are the unknown parameters to be estimated. The polynomial coefficients can be collected in a single complex-valued matrix as follows:

$$[\theta] = \begin{bmatrix} [\beta_1] \\ \vdots \\ [\beta_l] \\ [\alpha] \end{bmatrix} \tag{4.152}$$

where:

$$[\beta_o] = \begin{bmatrix} \langle B_{o,0} \rangle \\ \vdots \\ \langle B_{o,n} \rangle \end{bmatrix} \tag{4.153}$$

$$[\alpha] = \begin{bmatrix} [A_0] \\ \dots \\ [A_n] \end{bmatrix} \tag{4.154}$$

and n is the model order. As in the case of the common-denominator model, the polynomial basis function can be expressed in the continuous Laplace domain ($\Omega_f = i\omega_f$) or in the discrete z-domain. As already mentioned in the illustration of the LSCF method, the z-domain formulation (4.116) is recommended to improve numerical conditioning.

The following error formulation:

$$\langle E_o(\omega_f, [\theta]) \rangle = \langle B_o(\Omega_f, [\theta]) \rangle - \langle \hat{G}_o(\omega_f) \rangle [A(\Omega_f, [\theta])] \tag{4.155}$$

is introduced to obtain a linear least squares problem. This is defined by minimizing the following cost function:

$$\ell([\theta]) = \sum_{o=1}^{l} \sum_{f=1}^{N_f} tr\left(\langle E_o(\omega_f, [\theta]) \rangle^H \langle E_o(\omega_f, [\theta]) \rangle \right). \tag{4.156}$$

The minimization of the cost function given by (4.156) corresponds to the solution of the following matrix equation:

$$[J][\theta] = [0] \tag{4.157}$$

where the Jacobian matrix [J] is given by:

$$[J] = \begin{bmatrix} [\Gamma_1] & [0] & \dots & [0] & [\Upsilon_1] \\ [0] & [\Gamma_2] & \dots & [0] & [\Upsilon_2] \\ \vdots & \vdots & \ddots & \vdots & \vdots \\ [0] & [0] & \dots & [\Gamma_l] & [\Upsilon_l] \end{bmatrix} \tag{4.158}$$

with:

$$[\Gamma_o] = \begin{bmatrix} \langle 1 & z_1 & \dots & z_1^n \rangle \\ \langle 1 & z_2 & \dots & z_2^n \rangle \\ & & \dots & \\ \langle 1 & z_{N_f} & \dots & z_{N_f}^n \rangle \end{bmatrix} \tag{4.159}$$

$$[\Upsilon_o] = \begin{bmatrix} -\langle 1 & z_1 & \dots & z_1^n \rangle \otimes \langle \hat{G}_o(\omega_1) \rangle \\ -\langle 1 & z_2 & \dots & z_2^n \rangle \otimes \langle \hat{G}_o(\omega_2) \rangle \\ & & & \\ -\langle 1 & z_{N_f} & \dots & z_{N_f}^n \rangle \otimes \langle \hat{G}_o(\omega_{N_f}) \rangle \end{bmatrix}. \tag{4.160}$$

$\otimes$ denotes the Kronecker product. The matrices $[\Gamma_o]$ and $[\Upsilon_o]$ have dimensions $N_f \times (n+1)$ and $N_f \times (n+1) \cdot l$, respectively.

It is possible to show that (Cauberghe 2004):

$$\ell([\theta]) = \sum_{o=1}^{l} \sum_{f=1}^{N_f} tr\left(\langle E_o(\omega_f, [\theta]) \rangle^H \langle E_o(\omega_f, [\theta]) \rangle \right) = tr\left([\theta]^H [J]^H [J] [\theta] \right) \tag{4.161}$$

and, on the analogy with the LSCF estimator, it is possible to reduce the dimensions of the matrix equation through the definition of the normal equations:

$$[J]^H [J] [\theta] = \begin{bmatrix} [R_1] & \dots & [0] & [S_1] \\ \vdots & \ddots & \vdots & \vdots \\ [0] & \dots & [R_l] & [S_l] \\ [S_1]^H & \dots & [S_l]^H & \sum_{o=1}^{l} [T_o] \end{bmatrix} \begin{bmatrix} [\beta_1] \\ \vdots \\ [\beta_l] \\ [\alpha] \end{bmatrix} = [0] \tag{4.162}$$

with:

$$[R_o] = [\Gamma_o]^H [\Gamma_o] \tag{4.163}$$

$$[S_o] = [\Gamma_o]^H [\Upsilon_o] \tag{4.164}$$

$$[T_o] = [\Upsilon_o]^H [\Upsilon_o]. \tag{4.165}$$

$[R_o]$, $[S_o]$ and $[T_o]$ have dimensions $(n+1) \times (n+1)$, $(n+1) \times (n+1) \cdot l$ and $(n+1) \cdot l \times (n+1) \cdot l$, respectively. The $[\beta_o]$ coefficients can be eliminated from (4.162) taking into account that:

$$[\beta_o] = -[R_o]^{-1} [S_o] [\alpha]. \tag{4.166}$$

As a final result, the reduced normal equations are obtained:

$$\sum_{o=1}^{l} \left([T_o] - [S_o]^H [R_o]^{-1} [S_o] \right) [\alpha] = [M] [\alpha] = [0] \tag{4.167}$$

where [M] is a square $(n+1) \cdot l \times (n+1) \cdot l$ matrix.

On the analogy with the LSCF method, the parameter redundancy is removed by setting one of the denominator coefficients equal to the identity matrix. If the

highest order coefficient is constrained to be equal to the identity matrix of dimensions $l \times l$:

$$[A_n] = [I_l] \tag{4.168}$$

the least squares solution is given by:

$$[\alpha] = \begin{bmatrix} -\left[M_{(1:nl,\,1:nl)}\right]^{-1}\left[M_{(1:nl,\,(nl+1):(n+1)l)}\right] \\ [I_l] \end{bmatrix}. \tag{4.169}$$

The matrix $[M_{(1:nl,1:nl)}]$ is the submatrix of $[M]$ made by its first n·l rows and columns; the matrix $[M_{(1:nl,(nl+1):(n+1)l)}]$ is the submatrix of $[M]$ made by its first n·l rows and its last n·l columns. Once the $[\alpha]$ coefficients have been determined, the $[\beta_o]$ coefficients can be computed by substitution of $[\alpha]$ into (4.166).

The roots of the denominator polynomial $[A(\Omega_f, [\theta])]$ are the eigenvalues of the following companion matrix:

$$[A] = \begin{bmatrix} -[A_0]^{-1}[A_n] & -[A_0]^{-1}[A_{n-1}] & \dots & -[A_0]^{-1}[A_2] & -[A_0]^{-1}[A_1] \\ [I] & [0] & \dots & [0] & [0] \\ \vdots & \vdots & \ddots & \vdots & \vdots \\ [0] & [0] & \dots & [I] & [0] \end{bmatrix} \tag{4.170}$$

The companion matrix is a square n·l × n·l matrix and it models a dynamic system with (n·l)/2 modes. Its eigenvalues z_r have to be converted into the poles expressed in the Laplace domain as per (4.136). Equations (4.137)–(4.139) provide the natural frequency, the damped modal frequency, and the damping ratio of the r-th mode, respectively.

Once the poles associated to physical modes have been selected, the LSFD estimator is used to get the corresponding mode shapes. The residue matrices can be computed by minimizing the scatter between the experimentally estimated PSD matrix and the modeled one (De Troyer et al. 2009a):

$$\left[g\left(\left[R_j\right]\right)\right] = \sum_{f=1}^{N_f}\left(\left[\hat{G}_{YY}(\omega_f)\right] - \sum_{j=1}^{N_m}\left(\frac{\left[R_j\right]}{i\omega_f - \lambda_j} + \frac{\left[R_j\right]^*}{i\omega_f - \lambda_j^*}\right)\right)^2. \tag{4.171}$$

The minimization of $[g([R_j])]$ implies that its partial derivatives with respect to the unknown residues are zero. The obtained equations can be expressed in matrix form as follows:

$$[\Lambda_\Lambda][R] = [G_\Lambda] \tag{4.172}$$

where:

$$[\Lambda_\Lambda] = \sum_{f=1}^{N_f} \left(\begin{bmatrix} \frac{[I_l]}{(i\omega_f - \lambda_1)(i\omega_f - \lambda_1)} & \frac{[I_l]}{(i\omega_f - \lambda_1^*)(i\omega_f - \lambda_1)} & \cdots & \frac{[I_l]}{(i\omega_f - \lambda_{N_m})(i\omega_f - \lambda_1)} & \frac{[I_l]}{\left(i\omega_f - \lambda_{N_m}^*\right)(i\omega_f - \lambda_1)} \\ \vdots & \vdots & \ddots & \vdots & \vdots \\ \frac{[I_l]}{(i\omega_f - \lambda_1)\left(i\omega_f - \lambda_{N_m}^*\right)} & \frac{[I_l]}{(i\omega_f - \lambda_1^*)\left(i\omega_f - \lambda_{N_m}^*\right)} & \cdots & \frac{[I_l]}{(i\omega_f - \lambda_{N_m})\left(i\omega_f - \lambda_{N_m}^*\right)} & \frac{[I_l]}{\left(i\omega_f - \lambda_{N_m}^*\right)\left(i\omega_f - \lambda_{N_m}^*\right)} \end{bmatrix} \right) \tag{4.173}$$

$$[R] = \begin{bmatrix} [R_1] \\ [R_1]^* \\ \vdots \\ [R_{N_m}] \\ [R_{N_m}]^* \end{bmatrix} \tag{4.174}$$

$$[G_\Lambda] = \sum_{f=1}^{N_f} \left(\begin{bmatrix} \frac{\left[\hat{G}_{YY}(\omega_f)\right]}{(i\omega_f - \lambda_1)} \\ \frac{\left[\hat{G}_{YY}(\omega_f)\right]}{(i\omega_f - \lambda_1^*)} \\ \vdots \\ \frac{\left[\hat{G}_{YY}(\omega_f)\right]}{(i\omega_f - \lambda_{N_m})} \\ \frac{\left[\hat{G}_{YY}(\omega_f)\right]}{\left(i\omega_f - \lambda_{N_m}^*\right)} \end{bmatrix} \right). \tag{4.175}$$

The mode shape of the j-th mode can be finally estimated once the corresponding $l \times l$ residue matrix $[R_j]$ has been computed from (4.172) (Sect. 4.4.3.1).

4.5 Time Domain Methods

4.5.1 NExT-Type Procedures

A number of modal identification techniques, initially developed in the deterministic framework of traditional input–output modal analysis, have been extended to output-only modal analysis recognizing that the correlation functions of random responses can be expressed as a sum of decaying sinusoids (4.15) holding the information about the modal parameters. As a consequence, correlation functions of the random responses of the structure under natural excitation have replaced the experimental estimates of IRFs in the application of such modal analysis techniques in the output-only case. For this reason, this class of OMA methods is traditionally referred to as NExT.

The three main methods in this class are:

- The LSCE method,
- The ITD method,
- The ERA method (Juang and Pappa 1985, Juang 1994).

In this section, only the LSCE and the ITD methods are presented. In fact, ERA relies on the system realization theory and it is not herein illustrated because of its similarities with subspace methods. The reader can refer to Sect. 4.5.3.1 for output-only modal identification based on correlation functions and state-space model.

NExT-type methods were very popular at the beginning of OMA. LSCE and ITD have also experienced some enhancements over the years, for instance in order to deal with closely spaced modes (Olsen and Brincker 2013) and spurious harmonics (Mohanty 2005). Due to their historical relevance, they are herein illustrated in their most relevant aspects. However, these methods have been progressively abandoned in favor of the more robust subspace methods. The interested reader can refer to the literature for more details (Allemang and Brown 1998, Vold et al. 1982, Ibrahim and Mikulcik 1977, Mohanty 2005, Olsen and Brincker 2013).

The LSCE method is the time-domain counterpart of the LSCF estimator. Thus, it is basically a curve-fitting algorithm aimed at the extraction of the modal parameters from correlation functions. From (4.15) the generic correlation function can be rewritten as follows in discrete-time and for $k \geq 0$:

$$R_{ij}(k\Delta t) = \sum_{r=1}^{N_m} \left(C_{ij,r} e^{\lambda_r k\Delta t} + C^*_{ij,r} e^{\lambda^*_r k\Delta t} \right) \tag{4.176}$$

where $C_{ij,r}$ is the element ij of the residue matrix associated to the r-th mode (the notation for the residues has been slightly modified in this section with respect to the rest of the chapter for the sake of clarity). Taking into account that the poles appear in complex conjugate pairs and considering all the poles in sequence, (4.176) can be rewritten as:

$$R_{ij}(k\Delta t) = \sum_{r=1}^{n} \overline{C}_{ij,r} e^{\overline{\lambda}_r k\Delta t} \tag{4.177}$$

where $\overline{C}_{ij,r}$ is the constant associated to the r-th pole $\overline{\lambda}_r$ and the sum is extended to $n = 2N_m$ terms. Moreover, since the poles are in complex conjugate pairs, there exists a polynomial of order n of which $z_r = e^{\lambda_r \Delta t}$ ($r = 1, \ldots, n$) are roots:

$$\beta_0 z_r^0 + \beta_1 z_r^1 + \ldots + \beta_{n-1} z_r^{n-1} + z_r^n = 0 \tag{4.178}$$

Equation (4.178) is also known as *Prony's equation*. The highest order coefficient β_n is set equal to 1.

In order to determine the polynomial coefficients β_k, assuming that a number of samples q larger than 2n are available, (4.177) can be written for the full dataset as follows:

$$\begin{aligned} R_{ij}(k\Delta t)|_{k=0} &= \overline{C}_{ij,1} + \overline{C}_{ij,2} + \ldots + \overline{C}_{ij,n} \\ R_{ij}(k\Delta t)|_{k=1} &= \overline{C}_{ij,1} z_1^1 + \overline{C}_{ij,2} z_2^1 + \ldots + \overline{C}_{ij,n} z_n^1 \\ &\vdots \\ R_{ij}(k\Delta t)|_{k=q} &= \overline{C}_{ij,1} z_1^q + \overline{C}_{ij,2} z_2^q + \ldots + \overline{C}_{ij,n} z_n^q \end{aligned} . \tag{4.179}$$

Multiplying the correlation at time instant k by the coefficient β_k:

$$\begin{aligned} \beta_0 R_{ij}(k\Delta t)|_{k=0} &= \beta_0 \overline{C}_{ij,1} + \beta_0 \overline{C}_{ij,2} + \ldots + \beta_0 \overline{C}_{ij,n} \\ \beta_1 R_{ij}(k\Delta t)|_{k=1} &= \beta_1 \overline{C}_{ij,1} z_1^1 + \beta_1 \overline{C}_{ij,2} z_2^1 + \ldots + \beta_1 \overline{C}_{ij,n} z_n^1 \\ &\vdots \\ \beta_q R_{ij}(k\Delta t)|_{k=q} &= \beta_q \overline{C}_{ij,1} z_1^q + \beta_q \overline{C}_{ij,2} z_2^q + \ldots + \beta_q \overline{C}_{ij,n} z_n^q \end{aligned} . \tag{4.180}$$

and summing up these values, the following equation is obtained:

$$\sum_{k=0}^{q} \beta_k R_{ij}(k\Delta t) = \sum_{r=1}^{n} \left(\overline{C}_{ij,r} \sum_{k=0}^{q} \beta_k z_r^k \right). \tag{4.181}$$

It is convenient to set $q = n = 2N_m$. Taking into account (4.178) and that $\beta_n = 1$, the following equation is obtained:

$$\sum_{k=0}^{n-1} \beta_k R_{ij}(k\Delta t) = -R_{ij}(n\Delta t). \tag{4.182}$$

Repeating this process for different sets of samples (for instance, the next set can be made by the samples $k = 1, \ldots, n+1$), a set of n equations in the n unknown β_k coefficients is obtained:

$$[R_{ij}]\{\beta\} = -\left\{\widetilde{R}_{ij}\right\} \tag{4.183}$$

where:

$$[R_{ij}] = \begin{bmatrix} R_{ij}(k\Delta t)|_{k=0} & R_{ij}(k\Delta t)|_{k=1} & \ldots & R_{ij}(k\Delta t)|_{k=n-1} \\ R_{ij}(k\Delta t)|_{k=1} & \iddots & \iddots & R_{ij}(k\Delta t)|_{k=n} \\ \vdots & \iddots & \iddots & \vdots \\ R_{ij}(k\Delta t)|_{k=n-1} & R_{ij}(k\Delta t)|_{k=n} & \ldots & R_{ij}(k\Delta t)|_{k=2n-2} \end{bmatrix} \tag{4.184}$$

is the Hankel matrix (a *Hankel matrix* is a matrix that is constant along its anti-diagonals) holding the values of the correlation function,

$$\{\beta\} = \begin{Bmatrix} \beta_0 \\ \beta_1 \\ \vdots \\ \beta_{n-1} \end{Bmatrix} \tag{4.185}$$

is the vector of the unknown β_k coefficients, and:

$$\left\{\widetilde{R}_{ij}\right\} = \begin{Bmatrix} R_{ij}(n\Delta t) \\ R_{ij}((n+1)\Delta t) \\ \vdots \\ R_{ij}((2n-1)\Delta t) \end{Bmatrix}. \tag{4.186}$$

$[R_{ij}]$, $\{\beta\}$ and $\left\{\widetilde{R}_{ij}\right\}$ have dimensions $\mathrm{n} \times \mathrm{n}$, $\mathrm{n} \times 1$ and $\mathrm{n} \times 1$, respectively. The unknown coefficients are given by:

$$\{\beta\} = -\left[R_{ij}\right]^{-1}\left\{\widetilde{R}_{ij}\right\}. \tag{4.187}$$

They are also the coefficients of the Prony's equation (4.178), whose roots $z_r = e^{\lambda_r \Delta t}$ provide the natural frequency, the damped modal frequency, and the damping ratio ((4.137)–(4.139)) after the conversion into the continuous Laplace domain (4.136).

The above procedure uses a single correlation function. However, since the $\{\beta\}$ coefficients are global quantities related to the modal parameters, the correlation between any couple of response time series has to provide the same polynomial coefficients (Mohanty 2005). As a consequence, repeating the above procedure for any couple of response time histories leads to the following overdetermined set of equations:

$$\begin{bmatrix} [R_{11}] \\ [R_{12}] \\ \vdots \\ [R_{ll}] \end{bmatrix} \{\beta\} = -\begin{Bmatrix} \left\{\widetilde{R}_{11}\right\} \\ \left\{\widetilde{R}_{12}\right\} \\ \vdots \\ \left\{\widetilde{R}_{ll}\right\} \end{Bmatrix} \tag{4.188}$$

which can be solved in a least squares sense by pseudo-inverse techniques (Chap. 2).

Once the physical poles have been identified, they can be inserted into (4.177) to determine the constants $\overline{C}_{ij,r}$ from the following set of equations:

$$\begin{bmatrix} z_1^0 & z_2^0 & \dots & z_n^0 \\ z_1^1 & z_2^1 & \dots & z_n^1 \\ \vdots & \vdots & \dots & \vdots \\ z_1^{n-1} & z_2^{n-1} & \dots & z_n^{n-1} \end{bmatrix} \begin{Bmatrix} \overline{C}_{ij,1} \\ \overline{C}_{ij,2} \\ \vdots \\ \overline{C}_{ij,n} \end{Bmatrix} = \begin{Bmatrix} R_{ij}(k\Delta t)\big|_{k=0} \\ R_{ij}(k\Delta t)\big|_{k=1} \\ \vdots \\ R_{ij}(k\Delta t)\big|_{k=n-1} \end{Bmatrix}. \tag{4.189}$$

Thus, the LSCE method is a two-stage method for OMA, where mode shapes are estimated only in a second stage of analysis following the identification of the physical poles. On the analogy with the LSCF estimator, there exists also a poly-reference version of the algorithm, which considers all the measurement channels as references, computes the matrix coefficients $[\beta_1], \ldots, [\beta_n]$ by least squares, and extracts the poles as a solution of a generalized eigenvalue problem. The interested reader can refer to the literature (Heylen et al. 1998, Vold et al. 1982) for more details.

The ITD method is a global modal identification procedure based on processing of all the measured correlation functions at once. Taking into account that the generic correlation function can be decomposed as a sum of complex exponentials and arranging the measured correlation functions in a block Hankel matrix:

$$\left[H_{0|n-1}\right] = \begin{bmatrix} \left[\hat{R}_{yy}(0)\right] & \left[\hat{R}_{yy}(1)\right] & \ldots & \left[\hat{R}_{yy}(n-1)\right] \\ \left[\hat{R}_{yy}(1)\right] & \iddots & \iddots & \left[\hat{R}_{yy}(n)\right] \\ \vdots & \iddots & \iddots & \vdots \\ \left[\hat{R}_{yy}(n-1)\right] & \left[\hat{R}_{yy}(n)\right] & \ldots & \left[\hat{R}_{yy}(2n-2)\right] \end{bmatrix} \tag{4.190}$$

the following decomposition can be considered:

$$\left[H_{0|n-1}\right] = [\Psi][\Lambda] \tag{4.191}$$

where $[\Psi]$ contains the information about the mode shapes, and $[\Lambda]$ holds the information about the poles.

A second set of equations is obtained by a time-shift Δt of all the entries in the $[H_{0|n-1}]$ matrix. The second block Hankel matrix is related to $[\Lambda]$ as follows:

$$\left[H_{1|n}\right] = \left[\overline{\Psi}\right][\Lambda]. \tag{4.192}$$

The relation between the matrices $[\Psi]$ and $\left[\overline{\Psi}\right]$ is expressed by the *system matrix* $[A]$ as:

$$[A][\Psi] = \left[\overline{\Psi}\right]. \tag{4.193}$$

Substitution of (4.193) into (4.192) yields:

$$\left[H_{1|n}\right] = [A][\Psi][\Lambda] \tag{4.194}$$

and, taking into account (4.191), the following equation is obtained:

$$[A]\left[H_{0|n-1}\right] = \left[H_{1|n}\right] \tag{4.195}$$

which provides the system matrix $[A]$ from the measured data contained in the matrices $[H_{0|n-1}]$ and $[H_{1|n}]$:

$$[A] = \left[H_{1|n}\right]\left[H_{0|n-1}\right]^{+}. \tag{4.196}$$

The modal parameters are finally estimated by the eigenvalue decomposition of the system matrix. Its eigenvalues are the system poles in the z-domain. The natural frequency, the damped modal frequency, and the damping ratio are obtained from (4.137), (4.138), and (4.139), respectively, once the eigenvalues have been converted into the continuous Laplace domain (4.136). The eigenvector of the system matrix corresponding to a certain eigenvalue is finally used to obtain an estimate of the mode shape for that mode. It is worth pointing out that the ITD method is a low order method. As a consequence, the number of measurement channels l limits the number of identifiable poles (and therefore modes).

4.5.2 AR- and ARMA-Type Methods

The use of ARMA models for output-only modal identification has been attempted in the past, but they never became popular in this field due to a number of drawbacks (convergence problems, excessive computational time). Nevertheless, for their historical relevance, the main concepts under the application of AR and ARMA models to OMA are herein briefly summarized.

In Sect. 4.2.3 it has been mentioned that an ARMAV(p, p) model:

$$\{y_k\} + [\alpha_1]\{y_{k-1}\} + \ldots + [\alpha_p]\{y_{k-p}\} = \{e_k\} + [\gamma_1]\{e_{k-1}\} + \ldots + [\gamma_p]\{e_{k-p}\}. \tag{4.197}$$

is an equivalent representation of a dynamic system with $\mathrm{n} = \mathrm{p} \cdot l$ poles in the presence of noise (namely, low signal-to-noise ratio; in the absence of noise, a covariance equivalent model is an ARMAV(p, p − 1) model; Andersen 1997, Andersen et al. 1996). It can be used to describe a linear, time-invariant structure vibrating under unknown input forces, which can be modeled as a zero-mean Gaussian white noise process. Since the order p of the ARMA model is related to the order n of the system, the poles of the structure are included in the model only if $pl \geq n$. Thus, a preliminary estimate of the model order and, therefore, of the number of modes in the investigated frequency range is needed. In the case $pl > n$, additional nonphysical poles appear next to the physical poles and have to be distinguished (Peeters 2000). The poles are extracted from the AR matrix coefficients, while the MA parameters ensure that the statistical description of the data is optimal.

PEM is a data-driven method for the estimation of an ARMA model. A detailed description of the method and an extensive discussion about its application for the identification of the modal parameters of civil engineering structures can be found elsewhere (Ljung 1999, Andersen 1997). The ARMAV model is fitted to the measured time signals by minimizing the *output prediction error*:

$$\{e(t_k, [\alpha_i], [\gamma_i])\} = \{y(t_k)\} - \left\{\hat{y}\left(t_k | \left[Y^{k-1}\right], [\alpha_i], [\gamma_i]\right)\right\} \tag{4.198}$$

given by the difference between the measured time signals and the predicted output of the ARMAV model, which depends on the model parameters $[\alpha_i]$ and $[\gamma_i]$ and on

the past data $[Y^{k-1}]$ up to t_{k-1}. Unfortunately, the minimization of the prediction error requires a nonlinear optimization procedure. Since in practical applications a large number of parameters have to be estimated, this may lead to problems with computational time and convergence. An optimization scheme able to reduce the set of parameters to be estimated has been therefore proposed (Brincker and Andersen 1999a). It basically carries out a translation of the ARMA model in state-space form, defines a reduced set of parameters in the modal domain and then goes back to the ARMA domain to perform the optimization according to PEM. However, in the presence of good quality data this optimization scheme does not significantly improve the modal parameter estimates with respect to the stochastic state-space model (Brincker and Andersen 1999b). Thus, even if ARMA models can be potentially applied in the field of OMA, limited applications of PEM can be found in the literature as a result of the highly nonlinear parameter estimation problem. Since the nonlinearity is associated to the MA terms and the information about the poles is in the AR coefficients, alternative strategies have been developed where the MA coefficients are not estimated.

A first strategy completely omits the MA part, and the application of PEM to the following AR model:

$$\{y_k\} + [\alpha_1]\{y_{k-1}\} + \ldots + [\alpha_p]\{y_{k-p}\} = \{e_k\} \tag{4.199}$$

leads to a linear least squares problem, which can be easily solved. However, as mentioned in Sect. 4.2.3, an AR model of order p is not an equivalent representation of a vibrating structure with p/ poles, and the use of the AR model is justified only if its order goes to infinity. Unfortunately, this causes the introduction of a lot of spurious poles that have to be distinguished from the physical ones.

The IV method represents an attempt to overcome the limitations associated to the estimation of the AR terms only. This result is obtained through the formulation of a linear problem for the identification of the AR parameters, but an ARMA model is retained as underlying structure. The method starts recognizing that the ARMAV(p, p) model of (4.197) is adequate for modal parameter estimation if, when fitting the measured data $\{y_k\}$, it extracts the maximum of information from them and returns residuals $\{e_k\}$ uncorrelated with the past data:

$$E\left[\{e_k\}\{y_{k-i}\}^T\right] = [0] \qquad \forall i > 0. \tag{4.200}$$

Since $\{e_{k-p}\}$ is the oldest term in the MA part of (4.197), post-multiplying both sides of (4.197) by $\{y_{k-p-i}\}^T$ (i > 0) and taking the expectation yield the following equation:

$$\begin{aligned} &E\left[\{y_k\}\{y_{k-p-i}\}^T\right] + [\alpha_1]E\left[\{y_{k-1}\}\{y_{k-p-i}\}^T\right] \\ &\quad + \ldots + [\alpha_p]E\left[\{y_{k-p}\}\{y_{k-p-i}\}^T\right] = [0] \qquad \forall i > 0 \end{aligned} \tag{4.201}$$

where the equality follows from (4.200). The assumption of stationarity implies:

$$E\left[\{y_k\}\{y_{k-i}\}^T\right] = E\left[\{y_{k+i}\}\{y_k\}^T\right] = [R_i] \qquad \forall i > 0 \tag{4.202}$$

so that the fundamental equation of the IV method can be expressed in terms of the output correlations $[R_i]$ as:

$$\left[R_{p+i}\right] + [\alpha_1]\left[R_{p+i-1}\right] + \ldots + \left[\alpha_p\right][R_i] = [0] \qquad \forall i > 0. \tag{4.203}$$

Equation (4.203) can be rewritten as:

$$[\alpha_1]\left[R_{p+i-1}\right] + \ldots + \left[\alpha_p\right][R_i] = -\left[R_{p+i}\right] \qquad \forall i > 0 \tag{4.204}$$

pointing out the similarity with the (poly-reference) LSCE method. This is a further example of how different algorithms can be traced back to a common mathematical background, as discussed in Sect. 4.2.5.

If the output correlations are replaced by their estimates $\left[\hat{R}_i\right]$ and (4.204) is written for all the available time lags i, the AR parameters $[\alpha_1], \ldots, [\alpha_p]$ can be obtained as a least squares solution of an overdetermined set of equations. Natural frequencies, damping ratios, and mode shapes are finally computed from the results of the eigenvalue decomposition of the companion matrix of the AR coefficients, as described in Sect. 4.2.3.

4.5.3 Stochastic Subspace Identification

4.5.3.1 Covariance-Driven Stochastic Subspace Identification

The Covariance-driven Stochastic Subspace Identification (Cov-SSI) method addresses the stochastic realization problem, that is to say the problem of identifying a stochastic state-space model from output-only data. The origin of the method can be traced back to the system realization theory for deterministic (input–output) cases and the concept of minimal realization developed by Ho and Kalman (Ho and Kalman 1966).

An extensive discussion about the system realization theory can be found elsewhere (Juang 1994). Here just some basic concepts are reported. As mentioned in Sect. 4.2.3, a minimal realization is the state-space model with the smallest state-space dimension among all the realizable systems characterized by the same input–output relation. To construct such a model, it is important to check whether or not all the system states of interest can be excited (controlled) and/or observed (Juang 1994).

By definition, a state of a system is controllable if it can be reached from any initial state of the system in a finite time interval by some control actions; in a similar way, a state of the system is observable if the knowledge of input and output over a finite time interval completely determines the state.

It is possible to show (Juang 1994) that, if a certain condition about the rank of two specific matrices is fulfilled, the system is observable and controllable.

Such matrices are the so-called observability and controllability matrices and they will be introduced next in this section.

A system of order n is observable/controllable if and only if the observability/controllability matrix is of rank n. The solution of the realization problem consists in determining a minimal realization of order n of the state-space matrices from the measured data. As clarified next in this chapter, in practical applications the actual order of the system is unknown and its determination is always affected by a certain degree of uncertainty due to noise effects. As a consequence, even if a minimal realization of a system of order n can be theoretically identified from the measured data and used to extract the modal parameters, the determination of the correct order of the system is usually a very complex task. A conservative approach to identify all the structural modes in the data consists in the overestimation of the order of the system. This causes the appearance of additional nonphysical poles next to the physical poles, and specific criteria and tools to sort the structural poles are needed (refer to Sect. 4.9 for more details).

The Cov-SSI method can be classified as a time-domain, parametric, covariance-driven procedure for OMA. It starts from the computation of output correlations:

$$\left[\hat{R}_i\right] = \frac{1}{N-i}\left[Y_{(1:N-i)}\right]\left[Y_{(i:N)}\right]^T \tag{4.205}$$

where $[Y_{(1:N-i)}]$ is obtained from the $l \times$ N data matrix $[Y]$ by removal of the last i samples, while $[Y_{(i:N)}]$ is obtained from $[Y]$ by removal of the first i samples; $\left[\hat{R}_i\right]$ denotes the unbiased estimate of the correlation matrix at time lag i based on a finite number of data. The estimated correlations at different time lags are gathered into the following block Toeplitz matrix:

$$\left[T_{1|i}\right] = \begin{bmatrix} \left[\hat{R}_i\right] & \left[\hat{R}_{i-1}\right] & \dots & \left[\hat{R}_1\right] \\ \left[\hat{R}_{i+1}\right] & \left[\hat{R}_i\right] & \ddots & \left[\hat{R}_2\right] \\ \vdots & \vdots & \ddots & \vdots \\ \left[\hat{R}_{2i-1}\right] & \left[\hat{R}_{2i-2}\right] & \dots & \left[\hat{R}_i\right] \end{bmatrix} \tag{4.206}$$

Each correlation matrix has dimensions $l \times l$; thus, the block Toeplitz matrix has dimensions $li \times li$. For the identification of a system of order n, the number of block rows i has to fulfill the following condition:

$$li \geq n \tag{4.207}$$

In practical applications the actual order of the system is obviously unknown. However, an estimate of the number of modes in the frequency range of interest can be obtained in a number of ways, for instance as the number of peaks in the trace of the PSD matrix or in the singular value plots given by the SVD of the PSD matrix (see Sects. 4.4.1 and 4.4.2).

Assuming that the order of the system has been estimated and taking into account that the number of outputs l is a constant of the identification problem, a value for i larger than or equal to n/l can be set. The adopted value for i is basically a user's choice and it is definitely based on a physically insight of the problem.

Applying the factorization property given by (4.51) to the block Toeplitz matrix:

$$\left[T_{1|i}\right] = \begin{bmatrix} [C] \\ [C][A] \\ \vdots \\ [C][A]^{i-1} \end{bmatrix} \begin{bmatrix} [A]^{i-1}[G] & \cdots & [A][G] & [G] \end{bmatrix} = [O_i][\Gamma_i] \tag{4.208}$$

the *observability matrix*:

$$[O_i] = \begin{bmatrix} [C] \\ [C][A] \\ \vdots \\ [C][A]^{i-1} \end{bmatrix} \tag{4.209}$$

and the *reversed controllability matrix*:

$$[\Gamma_i] = \begin{bmatrix} [A]^{i-1}[G] & \cdots & [A][G] & [G] \end{bmatrix} \tag{4.210}$$

are obtained. $[O_i]$ and $[\Gamma_i]$ have dimensions li × n and n × li, respectively. If the condition of (4.207) is fulfilled and the system is observable and controllable, the rank of the block Toeplitz matrix equals n. In fact, it is a product of a matrix with n columns—$[O_i]$—and a matrix with n rows—$[\Gamma_i]$—.

The SVD of the block Toeplitz matrix:

$$\left[T_{1|i}\right] = [U][\Sigma][V]^T = \begin{bmatrix} [U_1] & [U_2] \end{bmatrix} \begin{bmatrix} [\Sigma_1] & [0] \\ [0] & [0] \end{bmatrix} \begin{bmatrix} [V_1]^T \\ [V_2]^T \end{bmatrix} \tag{4.211}$$

provides its rank, which equals the number of nonzero singular values (Sect. 2.3.1). If the zero singular values and the corresponding singular vectors are omitted, (4.208) and (4.211) yield:

$$\left[T_{1|i}\right] = [O_i][\Gamma_i] = [U_1][\Sigma_1][V_1]^T \tag{4.212}$$

where the matrices $[U_1]$ and $[V_1]^T$ have dimensions li × n and n × li, respectively, and the n × n diagonal matrix $[\Sigma_1]$ holds the positive singular values arranged in descending order. The matrices $[O_i]$ and $[\Gamma_i]$ can be computed by splitting the SVD in two parts as follows:

$$[O_i] = [U_1][\Sigma_1]^{1/2}[T] \tag{4.213}$$

$$[\Gamma_i] = [T]^{-1}[\Sigma_1]^{1/2}[V_1]^T \tag{4.214}$$

where $[T]$ is a nonsingular matrix which plays the role of a similarity transformation applied to the state-space model (Sect. 4.2.2); since the choice of $[T]$ simply determines one of the infinite equivalent realizations of the state-space model, it can be set equal to the identity matrix:

$$[T] = [I] \tag{4.215}$$

Taking into account the definitions of observability matrix (4.209) and controllability matrix (4.210), the output influence matrix $[C]$ and the next state-output covariance matrix $[G]$ can be easily obtained as the first l rows of $[O_i]$ and the last l columns of $[\Gamma_i]$, respectively.

The state matrix $[A]$ can be computed according to different approaches. The first is based on the decomposition property of the one-lag shifted Toeplitz matrix:

$$\left[T_{2|i+1}\right] = \begin{bmatrix} \left[\hat{R}_{i+1}\right] & \left[\hat{R}_{i}\right] & \dots & \left[\hat{R}_{2}\right] \\ \left[\hat{R}_{i+2}\right] & \left[\hat{R}_{i+1}\right] & \ddots & \left[\hat{R}_{3}\right] \\ \vdots & \vdots & \ddots & \vdots \\ \left[\hat{R}_{2i}\right] & \left[\hat{R}_{2i-1}\right] & \dots & \left[\hat{R}_{i+1}\right] \end{bmatrix} = [O_i][A][\Gamma_i] \tag{4.216}$$

Introducing (4.213) and (4.214) into (4.216), taking into account (4.215) and solving for $[A]$, the following expression for the state matrix is obtained:

$$[A] = [O_i]^{+}\left[T_{2|i+1}\right][\Gamma_i]^{+} = [\Sigma_1]^{-1/2}[U_1]^{T}\left[T_{2|i+1}\right][V_1][\Sigma_1]^{-1/2}. \tag{4.217}$$

This variant of the Cov-SSI algorithm is basically equivalent to the NExT-ERA method.

As an alternative, the state matrix $[A]$ can be estimated by exploiting the shift structure of the observability matrix. Pre- and post-multiplying the matrix $[T_{1|i}]$ by the invertible weighting matrices $[W_1]$ and $[W_2]$, computing the SVD of the weighted Toeplitz matrix and omitting the zero singular values yield the following expression for the observability matrix (Yi and Yun 2004):

$$[O_i] = [W_1]^{-1}[U_1][\Sigma_1]^{1/2} \tag{4.218}$$

and the state matrix is given by:

$$[A] = \left[O_i^{\uparrow}\right]^{+}\left[O_i^{\downarrow}\right] \tag{4.219}$$

where $[O_i^{\uparrow}]$ and $[O_i^{\downarrow}]$ are obtained from the matrix $[O_i]$ by removal of the last and the first l rows, respectively.

Depending on the adopted weighting matrices, the following two variants of Cov-SSI can be considered: Balanced Realization (BR) and Canonical Variate Analysis (CVA).

The BR Cov-SSI uses identity matrices as weights:

$$[W_1] = [W_2] = [I] \tag{4.220}$$

In a balanced realization the controllability grammian—$[\Gamma_i]\ [\Gamma_i]^T$—and the observability grammian—$[O_i]^T[O_i]$—are equal and diagonal (taking into account that $[U_1]$ and $[V_1]$ are orthonormal matrices):

$$\begin{aligned}[O_i]^T[O_i] &= [\Sigma_1]^{1/2}[U_1]^T[U_1][\Sigma_1]^{1/2} = [\Sigma_1] = [\Sigma_1]^{1/2}[V_1]^T[V_1][\Sigma_1]^{1/2} \\ &= [\Gamma_i][\Gamma_i]^T \end{aligned} \tag{4.221}$$

and this implies that the realized system is controllable as well as observable (Juang 1994). A balanced realization means that the signal transfers from the input to the state and from the state to the output are similar and balanced (Juang 1994).

In the CVA variant of Cov-SSI the Cholesky factorization (Chap. 2) of the following matrices:

$$\left[T^+_{0|i-1}\right] = \begin{bmatrix} [\hat{R}_0] & [\hat{R}_1]^T & \dots & [\hat{R}_{i-1}]^T \\ [\hat{R}_1] & [\hat{R}_0] & \ddots & [\hat{R}_{i-2}]^T \\ \vdots & \ddots & \ddots & \vdots \\ [\hat{R}_{i-1}] & [\hat{R}_{i-2}] & \dots & [\hat{R}_0] \end{bmatrix} = [L^+][L^+]^T \tag{4.222}$$

$$\left[T^-_{0|i-1}\right] = \begin{bmatrix} [\hat{R}_0] & [\hat{R}_1] & \dots & [\hat{R}_{i-1}] \\ [\hat{R}_1]^T & [\hat{R}_0] & \ddots & [\hat{R}_{i-2}] \\ \vdots & \ddots & \ddots & \vdots \\ [\hat{R}_{i-1}]^T & [\hat{R}_{i-2}]^T & \dots & [\hat{R}_0] \end{bmatrix} = [L^-][L^-]^T \tag{4.223}$$

provides the weights (Hermans and Van Der Auweraer 1999):

$$[W_1] = [L^+]^{-1}, \quad [W_2] = [L^-]^{-1} \tag{4.224}$$

In CVA Cov-SSI the singular values of the weighted Toeplitz matrix $[W_1][T_{1|i}][W_2]$ can be interpreted as the cosines of the angles, the so-called canonical angles, between two subspaces (Hermans and Van Der Auweraer 1999). The CVA weighting can be physically interpreted as a weighting that leads to balanced modes in terms of energy. As a consequence, it enhances the possibility to identify those modes that are less excited in operational conditions.

Once the matrices $[A]$ and $[C]$ have been estimated, the modal parameters can be extracted. The (complex conjugate pairs of) poles in discrete-time are in the diagonal matrix $[M]$ obtained from the eigenvalue decomposition of the state matrix (4.77). After the conversion of the poles corresponding to physical modes from discrete-time to continuous-time (4.136), the natural frequencies, the damped modal frequencies,

and the damping ratios can be estimated according to (4.137), (4.138), and (4.139), respectively. The mode shape of the r-th mode is estimated from the eigenvector $\{\psi_r\}$ of $[A]$ corresponding to the selected pole z_r according to (4.79).

About the transformation from continuous-time to discrete-time and vice versa, it is worth noting that the restriction of the Laplace variable to purely imaginary values corresponds to a restriction to values on the unit circle in discrete-time (Verboven 2002). Moreover, the transformation from discrete-time to continuous-time is not unique (Juang 1994). Any couple of frequencies differing by a multiple of $2\pi/\Delta t$ is indistinguishable when observed at the sampled times. As a consequence, Δt must be sufficiently short or a filter has to be adopted in order to prevent that the frequencies beyond the Nyquist frequency are mirrored at a lower frequency in the realization (aliasing).

The output correlations and the identified state-space matrices are estimates of the corresponding true quantities based on a finite number of samples (for this reason, they should be denoted with ^: $[\hat{A}]$, $[\hat{C}]$, $[\hat{G}]\ldots$). The presence of noise can determine some errors in the estimates. Typical noise sources are:

- modeling inaccuracies (for example, the system that generated the data cannot be exactly modeled as a stochastic state-space model),
- measurement noise (due to sensors and measurement hardware),
- computational noise (due to the finite precision),
- the finite number of data points (leading to estimates of the output correlations).

As a consequence of noise and the finite number of samples, also the factorization property of the Toeplitz matrix (4.208) does not hold exactly. If, in principle, the order n of the system can be obtained as the number of nonzero singular values of the block Toeplitz matrix $[T_{1|i}]$, the presence of noise makes all singular values different from zero. Thus, the rank of $[T_{1|i}]$ is "approximately" n, and the truncation of the smallest singular values leads to a certain error in the estimation of the state-space matrices. A rule of thumbs for the evaluation of the order n of the system suggests to look at the gap between two subsequent singular values. The model order is identified in correspondence of the maximum value of this gap. However, this criterion cannot be slavishly applied, since clear gaps are often absent in the case of real records of the structural response. As a consequence, as previously mentioned, a usual practice consists in overestimating the model order to a certain extent and in sorting out the physical poles by appropriate tools and criteria. They are illustrated in Sect. 4.9.

An assessment of the quality of the identified state-space model is possible through the comparison of the synthesized spectra with those directly estimated from the measurements. A closed-form expression for the spectrum of a discrete-time stochastic state-space model is as follows (Peeters 2000):

$$[S_{YY}(z)] = [C](z[I] - [A])^{-1}[G] + [R_0] + [G]^T\left(z^{-1}[I] - [A]^T\right)^{-1}[C]^T\Big|_{z=e^{i\omega\Delta t}}. \tag{4.225}$$

4.5.3.2 Data-Driven Stochastic Subspace Identification

DD-SSI algorithms have become very popular in the system identification community in recent years. Such techniques are very attractive for a number of reasons. They rely on an elegant mathematical framework and robust linear algebra tools to identify the state-space matrices from the raw data. As a result, in comparison with other data driven algorithms such as PEM, nonlinear optimization problems are avoided. In fact, the identification problem is linearized, that is to say it is reduced to a simple least squares problem. Moreover, the use of well-known tools from numerical linear algebra, such as SVD and LQ decomposition, leads to a numerically very efficient implementation.

An innovative aspect of DD-SSI consists in the identification of the state sequence before the estimation of the state-space matrices. A number of theorems show that the states can directly be calculated from measurements through some geometric operations (Van Overschee and De Moor 1996). These are the so-called orthogonal and oblique projections. In the context of OMA, only orthogonal projections are used. The concept of projection can be easily understood if the rows of a matrix are interpreted as a basis for a vector space. Therefore, it is possible to define the operator $[\Pi_E]$, which projects the row space of a matrix on the row space of a reference matrix [E]:

$$[\Pi_E] = [E]^T \left([E][E]^T \right)^+ [E]. \tag{4.226}$$

The orthogonal projection of the row space of a generic matrix [F] on the row space of [E] is:

$$[F]/[E] = [F][\Pi_E] = [F][E]^T \left([E][E]^T \right)^+ [E]. \tag{4.227}$$

More details about projections and their role in DD-SSI can be found elsewhere (Van Overschee and De Moor 1996). The key idea, which has to be remarked here, is that the Kalman filter state estimates can be obtained as a linear combination of the rows of certain block Hankel matrices holding the raw data. As discussed in Sect. 4.2.2, the role of the Kalman filter is to produce an optimal prediction of the state vector $\{s_k\}$ from observations of the outputs up to the time instant $k-1$. The Kalman filter state sequence $\left[\hat{S}_i\right]$, therefore, collects all the state estimates obtained from the output data at the previous i time instants. Each column of $\left[\hat{S}_i\right]$ represents one of these state estimates. For instance, assuming that the filter is started at j different time instants, so that the Kalman filter state sequence is:

$$\left[\hat{S}_i\right] = \left[\{\hat{s}_i\} \quad \{\hat{s}_{i+1}\} \quad \dots \quad \{\hat{s}_{i+j-1}\} \right] \tag{4.228}$$

the $(q+1)$-th column $\{\hat{s}_{i+q}\}$ of $\left[\hat{S}_i\right]$ represents the state estimate based on the following i output values: $\{y_q\}, \dots, \{y_{i+q-1}\}$ (Van Overschee and De Moor 1996).

The DD-SSI algorithm starts from a block Hankel matrix constructed directly from the measurement data. It has 2i block rows and j columns (for the statistical proof of the method, the following assumption is made: $j \to \infty$; thus, j must be rather large). The value of i is determined in agreement with (4.207). The block Hankel matrix has dimension $2li \times j$ and it can be partitioned into the two sub-matrices of the past—$[Y_p]$—and future—$[Y_f]$—outputs as follows:

$$\left[H_{0|2i-1}\right] = \frac{1}{\sqrt{j}} \left[\begin{array}{cccc} \{y_0\} & \{y_1\} & \cdots & \{y_{j-1}\} \\ \{y_1\} & \iddots & \iddots & \{y_j\} \\ \vdots & \iddots & \iddots & \vdots \\ \{y_{i-1}\} & \{y_i\} & \cdots & \{y_{i+j-2}\} \\ \hline \{y_i\} & \{y_{i+1}\} & \cdots & \{y_{i+j-1}\} \\ \{y_{i+1}\} & \iddots & \iddots & \{y_{i+j}\} \\ \vdots & \iddots & \iddots & \vdots \\ \{y_{2i-1}\} & \{y_{2i}\} & \cdots & \{y_{2i+j-2}\} \end{array}\right] = \left[\begin{array}{c} [Y_{0|i-1}] \\ \hline [Y_{i|2i-1}] \end{array}\right] = \left[\begin{array}{c} [Y_p] \\ \hline [Y_f] \end{array}\right]. \tag{4.229}$$

The sub-matrices $[Y_p]$ and $[Y_f]$ have dimensions $li \times j$. The output data are scaled by the factor $1/\sqrt{j}$ to be consistent with the definition of correlation (Chap. 2). In fact, it is possible to show that, under the assumptions of ergodicity and $j \to \infty$, the block Toeplitz matrix of correlations can be computed from the block Hankel matrices of output data as follows:

$$\left[T_{1|i}\right] \approx \frac{1}{j} \left[Y_f\right] \left[Y_p\right]^T. \tag{4.230}$$

In practical applications the number of columns j is taken equal to $N - 2i + 1$, so all given data samples are used. Adding one block row to the past outputs and omitting the first block row of the future outputs yield another division of the Hankel matrix:

$$\left[H_{0|2i-1}\right] = \left[\begin{array}{c} [Y_{0|i-1}] \\ \hline [Y_{i|i}] \\ \hline [Y_{i+1|2i-1}] \end{array}\right] = \left[\begin{array}{c} [Y_{0|i}] \\ \hline [Y_{i+1|2i-1}] \end{array}\right] = \left[\begin{array}{c} [Y_p^+] \\ \hline [Y_f^-] \end{array}\right]. \tag{4.231}$$

where $[Y_p{}^+]$ is the block Hankel matrix of the past outputs with one block row added, and $[Y_f{}^-]$ is the block Hankel matrix of the future outputs with the first block row removed. The identification of the Kalman filter state sequences and, as a consequence, of the state-space matrices is based on the orthogonal projection of the row space of the future outputs on the row space of the past outputs. The definition of this projection:

$$[P_i] = [Y_f] \Big/ [Y_p] = [Y_f] [Y_p]^T \left([Y_p] [Y_p]^T\right)^+ [Y_p]. \tag{4.232}$$

points out that correlations and projections are closely related. In fact, $[Y_f][Y_p]^T$ and $[Y_p][Y_p]^T$ are basically block Toeplitz matrices holding output correlations. The orthogonal projection of (4.232) can be efficiently computed by the LQ factorization of the block Hankel matrix of the outputs $[H_{0|2i-1}]$:

$$\left[H_{0|2i-1}\right] = [L][Q] \tag{4.233}$$

so that the Hankel matrix is expressed as the product of a lower triangular matrix $[L]$:

$$[L] = \begin{array}{c} \\ li \\ l \\ l(i-1) \end{array} \begin{array}{c} \\ \updownarrow \\ \updownarrow \\ \updownarrow \end{array} \begin{array}{c} \begin{array}{ccc} li & l & l(i-1) \\ \leftrightarrow & \leftrightarrow & \leftrightarrow \end{array} \\ \begin{bmatrix} [L_{11}] & [0] & [0] \\ [L_{21}] & [L_{22}] & [0] \\ [L_{31}] & [L_{32}] & [L_{33}] \end{bmatrix} \end{array} \tag{4.234}$$

and an orthonormal matrix $[Q]$:

$$[Q] = \begin{array}{c} j \\ \leftrightarrow \end{array} \begin{bmatrix} [Q_1]^T \\ [Q_2]^T \\ [Q_3]^T \end{bmatrix}. \tag{4.235}$$

The projections $[P_i]$ and $[P_{i-1}]$ of the row space of the future outputs on the row space of the past outputs can be obtained from the LQ decomposition as follows:

$$[P_i] = \left[Y_f\right] \Big/ \left[Y_p\right] = \begin{bmatrix} [L_{21}] \\ [L_{31}] \end{bmatrix} [Q_1]^T \tag{4.236}$$

$$[P_{i-1}] = \left[Y_f^-\right] \Big/ \left[Y_p^+\right] = \begin{bmatrix} [L_{31}] & [L_{32}] \end{bmatrix} \begin{bmatrix} [Q_1]^T \\ [Q_2]^T \end{bmatrix}. \tag{4.237}$$

Moreover, the output sequence $[Y_{i|i}]$ (4.231) can be expressed as:

$$\left[Y_{i|i}\right] = \begin{bmatrix} [L_{21}] & [L_{22}] \end{bmatrix} \begin{bmatrix} [Q_1]^T \\ [Q_2]^T \end{bmatrix}. \tag{4.238}$$

Assuming that the system is controllable and observable (so that all its modes are excited by the process noise and can be identified) and the condition expressed by (4.207) is satisfied, the main theorem of DD-SSI states that the projection matrix $[P_i]$ can be factorized into the product of the observability matrix $[O_i]$ and the Kalman filter state sequence $\left[\hat{S}_i\right]$ (Van Overschee and De Moor 1996):

$$[P_i] = [O_i]\left[\hat{S}_i\right] = \begin{bmatrix} [C] \\ [C][A] \\ \vdots \\ [C][A]^{i-1} \end{bmatrix} \left[\{\hat{s}_i\} \quad \{\hat{s}_{i+1}\} \quad \cdots \quad \{\hat{s}_{i+j-1}\} \right]. \tag{4.239}$$

The factorization of the projection matrix into the product of a matrix with n columns—$[O_i]$—and a matrix with n rows—$\left[\hat{S}_i\right]$—implies that $rank([P_i]) = n$. Estimating the rank of $[P_i]$ by SVD and retaining only the nonzero singular values:

$$[P_i] = [[U_1][U_2]] \begin{bmatrix} [\Sigma_1] & [0] \\ [0] & [0] \end{bmatrix} \begin{bmatrix} [V_1]^T \\ [V_2]^T \end{bmatrix} = [U_1][\Sigma_1][V_1]^T \tag{4.240}$$

the observability matrix and the Kalman filter state sequence can be computed as:

$$[O_i] = [U_1][\Sigma_1]^{1/2}[T] \tag{4.241}$$

$$\left[\hat{S}_i\right] = [O_i]^+[P_i] \tag{4.242}$$

where the similarity transformation $[T]$ can be set equal to the identity matrix.

A factorization similar to (4.239) can be applied to $[P_{i-1}]$, obtaining:

$$[P_{i-1}] = \left[O_i^{\uparrow}\right]\left[\hat{S}_{i+1}\right]. \tag{4.243}$$

Since $\left[O_i^{\uparrow}\right]$ can be directly obtained from $[O_i]$ by deleting the last l rows, while $[P_{i-1}]$ has been obtained from the LQ decomposition of the Hankel matrix of the output data, the Kalman state sequence $\left[\hat{S}_{i+1}\right]$ can be computed from (4.243) as follows:

$$\left[\hat{S}_{i+1}\right] = \left[O_i^{\uparrow}\right]^+[P_{i-1}]. \tag{4.244}$$

The state-space matrices can be now derived according to three different approaches. They differ for the capability to ensure the positive realness of covariance sequences. In simple words, the first two algorithms that are going to be illustrated provide asymptotically unbiased estimates (if $i \to \infty$) of the noise covariances $[Q^{ww}]$, $[R^{vv}]$ and $[S^{wv}]$ (4.43) and of the matrices $[G]$ and $[R_0]$ but they do not ensure the positive realness. This can lead to a synthesized spectrum matrix which is not positive definite at all frequencies. Since for a positive definite matrix all its diagonal entries are positive (Golub and Van Loan 1996), the synthesized spectrum might become negative at certain frequencies and this is obviously meaningless. Moreover, when the covariance sequence is not positive real, an innovation model cannot be computed. When the positive realness of covariance sequences is of interest, the third algorithm has to be adopted which, however, is not asymptotically unbiased. More details about positive realness and its implications can be found elsewhere (Van Overschee and De Moor 1996). It is

worth pointing out that also the Cov-SSI algorithm does not ensure the positive realness of the identified covariance sequence and, as a consequence, a forward innovation model cannot be obtained.

The first algorithm uses the state sequences to estimate the state-space matrices. In fact, once the Kalman filter state sequences $\left[\hat{S}_i\right]$ and $\left[\hat{S}_{i+1}\right]$ have been estimated according to (4.242) and (4.244), the matrices $[A]$ and $[C]$ can be computed from the following overdetermined set of linear equations, obtained by stacking the state-space models for the time instants from i up to $\mathrm{i}+\mathrm{j}-1$:

$$\begin{bmatrix} \left[\hat{S}_{i+1}\right] \\ \left[Y_{i|i}\right] \end{bmatrix} = \begin{bmatrix} [A] \\ [C] \end{bmatrix} \left[\hat{S}_i\right] + \begin{bmatrix} [\rho_w] \\ [\rho_v] \end{bmatrix}. \tag{4.245}$$

Since the Kalman filter residuals $[\rho_w]$ and $[\rho_v]$ are uncorrelated with the states $\left[\hat{S}_i\right]$ (see also (4.46) and (4.47)), this set of equations can be solved in a least squares sense. In fact, taking into account that the least squares residuals are orthogonal and, therefore, uncorrelated with the regressors $\left[\hat{S}_i\right]$, asymptotically unbiased least squares estimate of $[A]$ and $[C]$ are obtained as follows (Van Overschee and De Moor 1993):

$$\begin{bmatrix} [A] \\ [C] \end{bmatrix} = \begin{bmatrix} \left[\hat{S}_{i+1}\right] \\ \left[Y_{i|i}\right] \end{bmatrix} \left[\hat{S}_i\right]^{+}. \tag{4.246}$$

It is worth noting that all quantities on the right side of (4.246) can be expressed in terms of the LQ factors. As a result of their orthonormality, the Q factors cancel out in (4.246). A significant data reduction can be therefore obtained by expressing the right-side quantities in (4.246) in terms of the L factors only.

The matrix $[G]$ corresponds to the last l columns of the reversed controllability matrix, which can be computed as follows:

$$[\Gamma_i] = [O_i]^{+} \left[T_{1|i}\right] \tag{4.247}$$

while $[R_0]$ is obtained as the autocorrelation of $[Y_{i|i}]$:

$$[R_0] = \frac{1}{j} \left[Y_{i|i}\right] \left[Y_{i|i}\right]^{T}. \tag{4.248}$$

The second algorithm takes advantage of the shift structure of the observability matrix, which implies that:

$$\left[O_i^{\uparrow}\right] [A] = \left[O_i^{\downarrow}\right]. \tag{4.249}$$

As a consequence, the discrete state matrix can be computed in agreement with (4.219). Alternatively, it can be computed by SVD of the concatenated matrix $\left[\left[O_i^{\downarrow}\right] \quad -\left[O_i^{\uparrow}\right]\right]$:

$$\left[\left[O_i^{\downarrow}\right] \quad -\left[O_i^{\uparrow}\right]\right] = [U][\Sigma][V]^T \tag{4.250}$$

where the matrix $[V]$ can be then partitioned as follows:

$$[V] = \begin{matrix} \\ n \updownarrow \\ n \updownarrow \end{matrix} \begin{matrix} \overset{n}{\leftrightarrow} & \overset{n}{\leftrightarrow} \\ \end{matrix} \begin{bmatrix} [V_{11}] & [V_{12}] \\ [V_{21}] & [V_{22}] \end{bmatrix}. \tag{4.251}$$

The matrix $[A]$ is finally given by (Van Overschee and De Moor 1996):

$$[A] = [V_{22}][V_{12}]^{-1} \tag{4.252}$$

while the matrix $[C]$ is directly obtained from the first l rows of $[O_i]$. The matrices $[G]$ and $[R_0]$ are obtained as for the previous algorithm.

The third algorithm computes $[A]$ and $[C]$ by least squares in agreement with (4.245) and (4.246), as in the case of the first algorithm, but the matrices $[G]$ and $[R_0]$ are obtained by a different procedure. The covariances of the process and measurement noise are obtained from the residuals as follows:

$$\frac{1}{j}\begin{bmatrix}[\rho_w]\\ [\rho_v]\end{bmatrix}\begin{bmatrix}[\rho_w]^T & [\rho_v]^T\end{bmatrix} = \begin{bmatrix}\left[Q_i^{ww}\right] & \left[S_i^{wv}\right] \\ \left[S_i^{wv}\right]^T & \left[R_i^{vv}\right]\end{bmatrix} \tag{4.253}$$

where the subscript $_i$ indicates that they are nonsteady state covariance matrices of the nonsteady state Kalman filter equation (see also Sect. 4.2.2):

$$[\Sigma_{i+1}] = [A][\Sigma_i][A]^T + \left[Q_i^{ww}\right] \tag{4.254}$$

$$[G] = [A][\Sigma_i][C]^T + \left[S_i^{wv}\right] \tag{4.255}$$

$$[R_0] = [C][\Sigma_i][C]^T + \left[R_i^{vv}\right]. \tag{4.256}$$

Since the Kalman filter converges when $i \to \infty$, the following approximations:

$$[Q^{ww}] = \left[Q_i^{ww}\right], \quad [S^{wv}] = \left[S_i^{wv}\right], \quad [R^{vv}] = \left[R_i^{vv}\right]. \tag{4.257}$$

introduce a bias when i is finite but they ensure the positive realness of the covariance sequences, since the matrix $\begin{bmatrix} [Q^{ww}] & [S^{wv}] \\ [S^{wv}]^T & [R^{vv}] \end{bmatrix}$ is positive definite by construction and this condition leads to positive real covariance sequences (Van Overschee and De Moor 1996). Once the matrices $[A]$, $[C]$, $[Q^{ww}]$, $[R^{vv}]$ and $[S^{wv}]$ are known, the matrices $[G]$ and $[R_0]$ can be obtained from (4.48)–(4.50). Solution of the Ricatti equation (4.67), together with (4.68), provides the Kalman gain and, as a consequence, the forward innovation model is finally obtained (Van Overschee and De Moor 1996).

Once the matrices $[A]$ and $[C]$ have been determined according to one of the previous algorithms, the modal parameters can be obtained from the eigenvalue decomposition of the discrete state matrix as discussed in the previous sections ((4.77), (4.79), (4.137), (4.138), (4.139)), after the conversion of the eigenvalues from discrete-time to continuous time (4.136). Since the modal parameter estimates depend on $[A]$ and $[C]$ only, they are not affected by eventual bias on the matrices $[G]$ and $[R_0]$. When also these last two matrices are estimated, the spectrum matrix of the model can be computed from (4.225).

It is worth emphasizing that, due to the finite data length, the identified state-space model (and therefore the matrices $[A]$, $[C]$, $[G]$ and $[R_0]$) is just an estimate of the model that actually generated the data. On the analogy with the Cov-SSI method, the order of the system can be obtained as the rank of the projection matrix $[P_i]$, if the number of block rows has been set in agreement with (4.207). Since none of the singular values will exactly be zero as a result of the presence of noise, the rank of the matrix can only approximately be determined in correspondence with the maximum gap between two subsequent singular values (which are arranged in descending order). In practical applications, since a clear drop in the sequence of singular values is often not detectable, the order of the system is overestimated to a certain extent and specific tools and criteria are used to identify the physical poles (Sect. 4.9).

On the analogy with Cov-SSI, some variants of DD-SSI can be obtained through the application of some weights to the projection matrix $[P_i]$ before SVD. The weighting matrices $[W_1]$ and $[W_2]$ have dimensions $li \times li$ and $j \times j$, respectively, and they obey some conditions. In particular, $[W_1]$ is of full rank, while $[W_2]$ is such that:

$$rank\left(\left[Y_p\right]\right) = rank\left(\left[Y_p\right]\left[W_2\right]\right). \tag{4.258}$$

The variants of DD-SSI and the corresponding weighting matrices are:

- the Unweighted Principal Component (UPC) algorithm: $[W_1] = [I_{li}]$, $[W_2] = [I_j]$ (where the subscripts $_{li}$ and $_j$ denote the dimensions of the identity matrix);
- the principal component (PC) algorithm: $[W_1] = [I_{li}]$, $[W_2] = \left[Y_p\right]^T \left(\frac{1}{j}\left[Y_p\right]\left[Y_p\right]^T\right)^{-1/2}\left[Y_p\right]$;
- the CVA: $[W_1] = \left(\frac{1}{j}\left[Y_f\right]\left[Y_f\right]^T\right)^{-1/2}$, $[W_2] = [I_j]$.

In the case of CVA DD-SSI the singular values of the weighted projection matrix $[W_1][P_i][W_2]$ can be interpreted as the cosines of the principal angles between two subspaces, the row space of the past outputs $[Y_p]$ and the row space of the future outputs $[Y_f]$ (see Van Overschee and De Moor 1996 for more details).

As a practical rule, UPC DD-SSI should be used in the presence of modes of equal strength and data with a good signal-to-noise ratio; on the contrary, CVA DD-SSI should be used in the presence of noisy data and modes characterized by widely different strength. The PC variant can be considered as a compromise between UPC and CVA. Even if these three variants have different physical explanations, a number of computer simulations and practical applications have demonstrated that there are no significant accuracy differences among them in the field of OMA (Zhang et al. 2005b).

The above discussion about Cov-SSI and DD-SSI is certainly not comprehensive, but, in agreement with the objectives of this book, it provides the main concepts for the implementation of those algorithms for OMA applications. The interested reader can refer to the literature for an extensive discussion about SSI methods and their variants (Van Overschee and De Moor 1996, Aoki 1987, Katayama 2005).

4.5.4 Second Order Blind Identification

A recent proposal in the field of OMA concerns the possibility to apply Blind Source Separation (BSS) techniques to identify the modal parameters. BSS techniques allow extracting a set of signals, the so-called *sources*, from observations of their mixtures (Ans et al. 1985), based on fairly general assumptions about the sources and the mixing process.

Applicability of BSS techniques to OMA has been investigated in detail in a number of fairly recent publications (Kerschen et al. 2007, Poncelet et al. 2007, Zhou and Chelidze 2007, McNeill and Zimmerman 2008). In the context of OMA, such techniques can be referred to as time domain methods. Moreover, since no model is fitted to the data, they can be classified as nonparametric methods. Even if BSS techniques, which are based only on a statistical treatment of data, show promising performance in the field of output-only modal identification of civil structures, some limitations can be identified. They are related to the basic assumptions under different BSS techniques and their compatibility with the dynamic systems of interest. These aspects are discussed in this section right after a short introduction about BSS.

BSS techniques can be classified as linear or nonlinear, depending on the type of combination of the sources. Moreover, linear simultaneous (static) mixing and convolutive mixing can be considered. Even if the convolution product of the IRF of a structure with the external forcing vector gives the dynamic response of the structure itself, the problem of extraction of the sources from convolutive mixtures is not completely solved yet. For this reason, the possibility to interpret

the dynamic response of a structure as a static mixture of sources has been investigated for modal identification purposes (Kerschen et al. 2007).

Assuming that the dynamic response of a structure can be modeled as a linear and static mixture of sources, it can be expressed in matrix form as follows (Poncelet et al. 2007):

$$\{y(t)\} = [A]\{s(t)\} \tag{4.259}$$

where $\{s(t)\}$ are the source signals and $[A]$ is now referred to as the *mixing matrix*. BSS techniques aim at recovering the mixing matrix $[A]$ and the sources $\{s(t)\}$ from their observed mixtures $\{y(t)\}$, based on general assumptions about the sources themselves.

The applicability of BSS to vibration data is obvious if the modal expansion of the dynamic response of the structure (4.102) is compared to (4.259). Such a comparison shows that there is a one-to-one relationship between mixing matrix and sources on one hand and modal matrix and modal coordinates on the other hand. Thus, under given assumptions, the modal coordinates may act as virtual sources regardless of the number and type of the physical excitation forces (Kerschen et al. 2007, Poncelet et al. 2007). No mathematical model is assumed to describe the process that produced the measured data. The mixing model is the only assumption, confirming that BSS techniques can be referred to as nonparametric procedures for modal identification.

The above-mentioned concepts and the moderate complexity of BSS justify the increasing application of these statistical signal-processing techniques in the field of OMA. In the case of static mixing, two approaches can be identified: the first is based on higher-order statistics, if the sources are statistically independent and no more than one source is Gaussian (Comon 1994); the second relies on second-order statistics, if the sources are uncorrelated (Belouchrani et al. 1997). In both cases separation is affected by some indeterminacies related to the order of the sources (any permutation of the sources is also a solution of the blind identification problem) and their amplitude.

Early use of BSS for modal identification can be found in a number of publications (Feeny and Kappagantu 1998, Kerschen and Golinval 2002) focused on the relation between proper orthogonal modes provided by a Principal Component Analysis (PCA) and normal modes. Applicability of PCA to real case studies has been limited by the need for information about the mass matrix (Kerschen et al. 2007). Chelidze and Zhou (Chelidze and Zhou 2006) investigated this issue, developing a new multivariate data analysis method (the so-called smooth orthogonal decomposition). Additional details about applicability of PCA in structural dynamics can be found in the literature (Kerschen et al. 2005).

Independent Component Analysis (ICA) appears much more suitable than PCA to vibration data processing for modal identification purposes (Kerschen et al. 2007). The main assumptions of ICA for the solution of the blind identification problem are the mutual independence (so that the joint probability density of the sources can be factorized into the product of their marginal densities) and non-Gaussianity of the sources (only one source with Gaussian distribution can

be tolerated; Even and Moisan 2005). Under these assumptions, the solution of an optimization problem based on a given cost function provides the sources. In particular, ICA is based on the maximization of non-Gaussianity of the sources. Moreover, as many other BSS algorithms, it includes some preprocessing steps. In particular, centering (removal of mean values from measurements) and whitening (basically, a PCA) are carried out in order to reduce the noise level and improve convergence.

The main drawbacks of ICA are related to the use of high-order statistics, whose estimation is computational demanding and difficult in the presence of a scarcity of data, and to some limitations strictly related to modal identification. In fact, ICA works well only in the case of weakly damped systems, characterized by damping ratios lower than 1 % (Kerschen et al. 2007). These reasons make ICA unattractive for modal identification purposes.

Methods based on second-order statistics of the observed signals assume that the sources are uncorrelated for all delays and have different spectra. Among these, the Algorithm for Multiple Unknown Signal Extraction (AMUSE) (Tong et al. 1991) and the Second Order Blind Identification (SOBI) algorithm are based on a similar theoretical background. In fact, they exploit the information contained in covariance matrices. However, while SOBI jointly diagonalizes several time-shifted covariance matrices, AMUSE relies on the EVD of the covariance matrix eventually at one time lag only. Thus, SOBI overcomes the shortcoming of AMUSE related to an eventually inappropriate choice of the time lag. This can result in two similar eigenvalues and makes unfeasible the identification of the corresponding sources. It has been shown that SOBI is also much more robust to noise than AMUSE (Zhou and Chelidze 2007).

When SOBI is applied to vibration data, the real-valued mixing matrix implies real-valued mode shape estimates. This can be a drawback of the method in the presence of complex modes. An evolution of SOBI able to deal with complex modes is the Blind Modal Identification (BMID) algorithm (McNeill and Zimmerman 2008).

In this section attention is focused on SOBI, with an illustration of the main steps of the algorithm and its theoretical assumptions in agreement with relevant publications available in the literature (Belouchrani et al. 1997, Poncelet et al. 2007, Zhou and Chelidze 2007). In fact, normal modes are typically identified from modal identification tests of civil structures, so SOBI can be profitably applied in most cases.

On the analogy with other BSS techniques, the measured response is assumed to be a linear mixture of the sources (the modal coordinates), as expressed by (4.259). If some (additive) noise $\{n(t)\}$ is present in the measured response, (4.259) can be rewritten as follows:

$$\{y(t)\} = [A]\{s(t)\} + \{n(t)\}. \tag{4.260}$$

The l recorded time histories are, therefore, modeled as a linear combination of N_m sources plus noise. As a consequence, if there are N_m modes in the frequency

range under investigation, they can be identified only if $rank([A]) = N_m$. Since the mixing matrix has dimensions $l \times \mathrm{N_m}$, this implies that the number of measurement channels has to be equal or larger than the number of active modes: $l \geq N_m$. Moreover, since the columns of the mixing matrix represent estimates of the mode shapes of the structure under test, a careful selection of sensor locations is needed so that the observed mode shape vectors are linearly independent and the rank of $[A]$ is preserved. Taking into account the previously mentioned limitations, SOBI can be classified as a low order method for OMA. The issues related to the identifiability of a limited number of modes can be mitigated through the repeated application of band-pass filtering until the entire frequency range of interest is investigated. However, this procedure leads to a major increase in the time of analysis.

Assuming that the sources are stationary, uncorrelated, and scaled to have unit variance, their covariance matrix is the identity matrix:

$$[R_{ss}(0)] = E\left\{\{s(t)\}\{s(t)\}^T\right\} = [I]. \tag{4.261}$$

The additive noise is assumed to be a temporally and spatially white stationary random process, with:

$$E[\{n(t)\}] = \{0\} \tag{4.262}$$

$$E\left[\{n(t)\}\{n(t)\}^T\right] = \sigma^2[I] \tag{4.263}$$

If the added noise is also independent of the source signals, this implies:

$$E\left[\{n(t)\}\{s(t)\}^T\right] = [0]. \tag{4.264}$$

The first step of the algorithm consists of whitening the signal part $\{x(t)\} = [A]\{s(t)\}$ of the observed data. This is achieved by applying a linear transformation to $\{x(t)\}$ such that the whitened data $\{z(t)\}$ are uncorrelated and have unit variance:

$$\{z(t)\} = [W]\{x(t)\} \Rightarrow [R_{zz}(0)] = E\left[\{z(t)\}\{z(t)^T\}\right] = [I]. \tag{4.265}$$

The matrix $[W]$ defining this transformation is referred to as the *whitening matrix*. From (4.265) and (4.261) it is easy to recognize that:

$$[R_{zz}(0)] = [W][A]E\left[\{s(t)\}\{s(t)^T\}\right][A]^T[W]^T = [W][A][A]^T[W]^T = [I]. \tag{4.266}$$

Thus, if $[W]$ is a whitening matrix, $[A'] = [W][A]$ is an $\mathrm{N_m} \times \mathrm{N_m}$ unitary matrix. As a consequence, the mixing matrix can be factored as the product of the inverse of the whitening matrix and a unitary matrix (to be determined).

Whitening of the measured response $\{y(t)\}$ also obeys a linear model:

$$[W]\{y(t)\} = [W]([A]\{s(t)\} + \{n(t)\}) = [A']\{s(t)\} + [W]\{n(t)\}. \tag{4.267}$$

From the covariance matrix of the observed mixture:

$$\left[R_{yy}(0)\right] = E\left[\{y(t)\}\{y(t)\}^T\right] = [A][A]^T + \sigma^2[I] \tag{4.268}$$

the following equation is obtained:

$$[A][A]^T = \left[R_{yy}(0)\right] - \sigma^2[I]. \tag{4.269}$$

Combining (4.267) with (4.269) and taking into account (4.261), (4.263), and (4.264), it is possible to show that the whitening matrix $[W]$ can be derived from the covariance matrix $[R_{yy}(0)]$, provided that the noise covariance is known or can be estimated:

$$[W]\left[R_{yy}(0)\right][W]^T = [W][A][A]^T[W]^T + [W]\sigma^2[W]^T. \tag{4.270}$$

From a practical point of view, once the measured data have been centralized by removal of the mean value from each component of $\{y(t)\}$, whitening is obtained via PCA as follows.

First of all, the eigenvalue decomposition of $[R_{yy}(0)]$ is computed:

$$\left[R_{yy}(0)\right] = E\left[\{y(t)\}\{y(t)\}^T\right] = [E][D][E]^T \tag{4.271}$$

where $[E]$ is the orthogonal matrix of eigenvectors and $[D]$ is the diagonal matrix of eigenvalues. If only the N_m largest eigenvalues $d_1, \ldots, d_{N_m}$ and the corresponding eigenvectors $\{e_1\}, \ldots, \{e_{N_m}\}$ of $[R_{yy}(0)]$ are retained, the average of the remaining $l - N_m$ eigenvalues provide an estimate $\hat{\sigma}^2$ of the noise variance, under the assumption of white noise (Belouchrani et al. 1997). The whitened signals are then computed from the largest eigenvalues and the corresponding eigenvectors as:

$$\{z(t)\} = \left([D_{N_m}] - \hat{\sigma}^2[I_{N_m}]\right)^{-1/2}[E_{N_m}]^T\{y(t)\} = [W]\{y(t)\} \tag{4.272}$$

where $[D_{N_m}]$ is the submatrix of $[D]$ holding only the N_m largest eigenvalues, $[E_{N_m}]$ is the submatrix of $[E]$ collecting the eigenvectors corresponding to the N_m largest eigenvalues of $[R_{yy}(0)]$ and the whitening matrix is given by:

$$[W] = \left([D_{N_m}] - \hat{\sigma}^2[I_{N_m}]\right)^{-1/2}[E_{N_m}]^T. \tag{4.273}$$

Taking into account (4.272), p time-shifted covariance matrices have to be computed:

$$[R_{zz}(\tau_k)] \qquad k = 1, \ldots, p. \tag{4.274}$$

In order to estimate the sources and the mixing matrix, an approximate joint diagonalization of those p time-shifted covariance matrices is carried out according to the Joint Approximate Diagonalization (JAD) technique (Belouchrani et al. 1997). The objective of JAD is to find the unitary matrix $\left[\widetilde{A}'\right]$ that approximately diagonalizes the time-shifted covariance matrices. An optimization problem is defined with respect to the matrix $\left[\widetilde{A}'\right]$ which minimizes the sum of the off-diagonal terms of $\left[\widetilde{A}'\right]^T [R_{zz}(\tau_k)] \left[\widetilde{A}'\right]$ (k = 1, . . ., p) for the p time-shifted covariance matrices:

$$\min_{\left[\widetilde{A}'\right]} \sum_{k=1}^{p} off\left(\left[\widetilde{A}'\right]^T [R_{zz}(\tau_k)] \left[\widetilde{A}'\right]\right) \tag{4.275}$$

The solution to the minimization problem is pursued by means of a numerical algorithm based on the Jacobi rotation technique (Cardoso and Souloumiac 1996). Two parameters have to be set: the number p of time-shifted covariance matrices to be jointly diagonalized, and the threshold t used to stop JAD. About the threshold t, the problem of its setting has been analyzed by Cardoso and Souloumiac (Cardoso and Souloumiac 1996), showing that very small values for t have no sense because the diagonality criterion is approximate itself. Thus, it is usually unnecessary to push the accuracy of the rotation matrix to the machine precision. A value equal to its square root can be recommended. About the number p of time-shifted covariance matrices, the diagonalization performance improves when p increases and it seems to rapidly converge (Belouchrani et al. 1997). Once the matrix $\left[\widetilde{A}'\right]$ has been obtained, the de-mixing matrix $[U]$ and the mixing matrix $[A]$ can be computed:

$$[U] = \left[\widetilde{A}'\right]^T [W] \tag{4.276}$$

$$[A] = [W]^+ \left[\widetilde{A}'\right] \tag{4.277}$$

The resulting sources are shift-uncorrelated because the matrices $[R_{ss}(\tau_k)]$ are nearly diagonal. They are obtained as follows:

$$\{s(t)\} = [U]\{y(t)\}. \tag{4.278}$$

The mode shapes of the structure are obtained from the columns of the mixing matrix. The technique for the estimation of natural frequencies and damping ratios depends on the type of data used for modal identification. In the literature SOBI has been applied to free responses, impulse responses, and responses to random excitation (Zhou and Chelidze 2007, McNeill and Zimmerman 2008, Poncelet et al. 2007). In the first two cases, the estimation of natural frequencies and damping

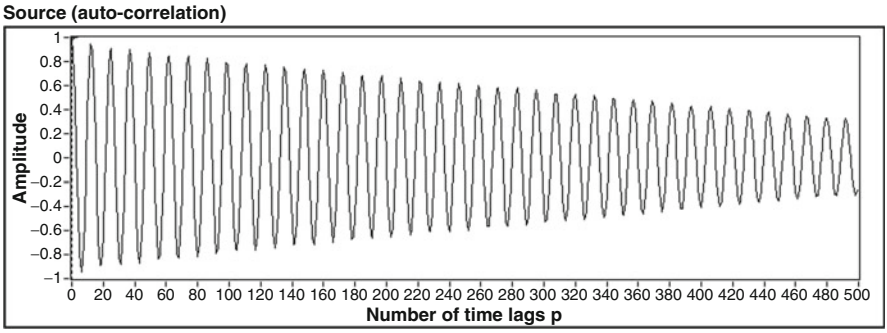

Fig. 4.5 Sample auto-correlation of a source

ratios from the obtained sources is straightforward. In fact, taking into account that the free vibration response can be expressed as a sum of exponentially decaying sinusoids, fitting this expression to the data permits the estimation of the modal parameters (refer to McNeill and Zimmerman 2008 for more details). In the case of response to random excitation, if the estimation of natural frequencies from the identified sources is again straightforward, this is not the case of damping ratios, whose estimation requires the knowledge of the applied random excitation (Poncelet et al. 2007). However, the extension of SOBI to the analysis of random responses for the estimation of modal parameters including damping is immediate by taking into account that also the correlations of random responses can be expressed as a sum of decaying sinusoids. This is the same basic assumption of the NExT-type procedures. Thus, for random responses there is no need to recover the sources, since natural frequencies and damping ratios can be directly estimated from their correlations $R_{ss}(\tau_k)$ (Fig. 4.5) as obtained from JAD. A simplified approach to the estimation of the modal properties by SOBI in the case of random response can be outlined as follows:

- Compute the whitening matrix $[W]$ from the centralized dataset according to (4.271) and (4.273); since the number of modes is not known a-priori and the criterion for proper selection of the number N_m of eigenvalues to be retained is still debated, it is possible to set $N_m = l$; since l sources are extracted from the data but the number of modes is likely lower than l, the sources associated to the actual structural modes have to be selected based, for instance, on the error in fitting the correlations $R_{ss}(\tau_k)$ by exponentially damped harmonic functions; this approach has been originally proposed by Poncelet et al. (Poncelet et al. 2007) for the analysis of impulse responses;
- Compute $\{z(t)\} = [W]\{y(t)\}$;
- Compute the time-shifted covariance matrices $[R_{zz}(\tau_k)]$ and select p of them to apply JAD;

- The JAD of the p time-shifted covariance matrices $[R_{zz}(\tau_k)]$ with k = 1,. . .,p provides the unitary matrix $\left[\widetilde{A}'\right]$, which permits the computation of the mixing matrix $[A]$ according to (4.277), and the autocorrelations of the sources $R_{ss}(\tau_k)$;
- Natural frequencies and damping ratios are estimated from the correlations of the sources $R_{ss}(\tau_k)$; regression on zero-crossing times and logarithmic decrement (as with EFDD) or other SDOF estimators can be used; the use of SDOF curve fitting estimators permits the computation of the fitting error and, as a result, a quantitative selection of the correlations associated to actual structural modes in the case noise rejection has not been previously carried out in the computation of the whitening matrix; the selection of the number of time lags p now plays a primary role in the process, since it is not responsible only for the matrix $\left[\widetilde{A}'\right]$ but it also defines the length of the correlation functions $R_{ss}(\tau_k)$; thus, taking into account the physics of the problem, p has to be set as a function of the period of the fundamental mode so that a sufficient number of cycles are present in the auto-correlation of the source associated to the fundamental mode;
- The mode shapes are obtained from the columns of the mixing matrix corresponding to the source correlations selected in the previous step of analysis.

It is interesting to note that, unlike other two-stage modal identification methods, SOBI provides the mixing matrix and, therefore, the mode shapes first, while natural frequencies and damping ratios are estimated in a second stage through post-processing of the obtained sources. Finally, it is worth pointing out that only source signals having different spectral shape can be recovered by JAD (Belouchrani et al. 1997). This means that SOBI can identify distinct modes but it shows serious limitations in the presence of repeated modes.

4.6 Other Methods for OMA

Several different methods for OMA have appeared in the literature over the years. Most of them are just variants of the previously described algorithms, aiming at improving specific aspects or overcoming some drawbacks inherent in those procedures. However, additional original tools and methods for OMA have also been proposed. For instance, examples of wavelet analysis for output-only modal identification of natural frequencies and damping ratios only (Ruzzene et al. 1997, Gouttebroze and Lardies 2001) or also of mode shapes (Lardies and Gouttebroze 2002, Han et al. 2005) are available. Other researchers have instead proposed the use of cepstral analysis for OMA (Hanson et al. 2007). Even if wavelet and cepstral analysis show some advantages, they are not widely used. The interested reader can refer to the literature for more details. Other techniques for OMA that have been systematized over the years and are currently in use are based on transmissibility functions and the RD signature.

4.6.1 Transmissibility Functions

The use of transmissibility functions for OMA was first proposed in 2007 (Devriendt and Guillaume 2007). The method has been progressively refined and improved over the years: the basic concepts are herein reported.

The *transmissibility function* is defined as a sort of FRF and, as such, it can be estimated in a nonparametric preprocessing step. However, transmissibility functions are computed from variables of the same type instead of conjugate variables (i.e.: motion response and force input) as in classical FRFs. The transmissibility function between the output i and a reference output j is given by the ratio of their Fourier transforms:

$$T_{ij}(\omega) = \frac{Y_i(\omega)}{Y_j(\omega)}. \tag{4.279}$$

In the practice it is estimated from the spectra as:

$$T_{ij}(\omega) = \frac{S_{Y_iY_j}(\omega)}{S_{Y_jY_j}(\omega)}. \tag{4.280}$$

Since the reference output is present in all transmissibility functions, it has to be carefully selected so that it carries the maximum amount of information about the structural modes.

Starting from the definition of transmissibility function and taking into account the modal model or, equivalently, the common denominator model, it is possible to show that the transmissibility does not depend on the coloring of the unknown forces, which can be arbitrary, but it only depends on the location and amplitude of the unknown forces. Moreover, the poles of the transmissibility functions are not the system poles, which are canceled out by taking the ratio between the response spectra. Thus, the peaks in the magnitude of transmissibility functions do not coincide with the structural resonances. However, an opportune combination of transmissibility functions obtained under different loading conditions makes possible the identification of the system poles. In fact, the transmissibility functions approach a constant value when converging to a pole of the system (Devriendt and Guillaume 2007):

$$\lim_{\omega \to \omega_n} T_{ij}(\omega) = \frac{\phi_{i,n}}{\phi_{j,n}}. \tag{4.281}$$

As shown by (4.281), such a value is directly related to the mode shape components at the measurement locations i and j. Moreover, since the limit is independent of the input, transmissibility functions pertaining to the same responses but computed from two tests characterized by different loading conditions a and b

exactly cross each other in correspondence with the structural resonances. As a consequence, their difference is zero at a structural resonance:

$$\lim_{\omega \to \omega_n} \left(T_{ij}^a(\omega) - T_{ij}^b(\omega) \right) = \frac{\phi_{i,n}}{\phi_{j,n}} - \frac{\phi_{i,n}}{\phi_{j,n}} = 0. \tag{4.282}$$

This implies that the poles of the system are also poles of the following rational function, given by the inverse of the difference between transmissibility functions associated to the same responses but computed for different loading conditions:

$$\frac{1}{\Delta T_{ij}^{ab}(\omega)} = \frac{1}{T_{ij}^a(\omega) - T_{ij}^b(\omega)}. \tag{4.283}$$

The application of parametric frequency domain estimators based on the common denominator model to (4.283) provides the structural poles. The mode shapes are estimated in a second stage from the residues (Devriendt et al. 2010).

The functions given by (4.283) might contain additional poles not related to the structure. However, the poles of the system can be easily distinguished from the additional mathematical poles by using a SVD (Devriendt and Guillaume 2008).

Even if the method is still under development, the main advantage consists in its robustness even in the presence of spurious harmonics. In fact, the method seems to be able to provide unbiased estimates of the modal parameters even in the case of spurious harmonics close to the structural resonances (Devriendt et al. 2009), thus overcoming a relevant limitation of standard OMA methods (see also Chap. 5). Nor prior knowledge about the frequency of the spurious harmonic neither filtering/interpolation are required. The only requirement affects the loading conditions, which must differ for location, number, or amplitude of the applied forces.

4.6.2 The Random Decrement Technique

The Random Decrement (RD) technique is a simple method for the estimation of functions that can be interpreted as free decays and, therefore, processed by covariance-driven identification methods. Thus, it represents a preliminary signal processing step for OMA rather than an autonomous OMA method. However, it is discussed here because it represents an alternative method for the estimation of correlation functions that is often applied in combination with some of the previously discussed OMA methods.

The RD technique was developed in the late 1960s at NASA (Cole 1968, Cole 1973) as a method to characterize stochastic time series. It was soon extended to modal identification of structures (Ibrahim 1977). The theoretical basis of the method has been later systematized and extended by other researchers (Vandiver et al. 1982, Asmussen et al. 1999).

The RD technique provides an estimate of the so-called RD signature. Under the assumption of ergodic stochastic processes, the cross-RD signature is estimated

from two time series $y_1(t)$ and $y_2(t)$ by averaging N_b segments of the time series $y_1(t)$ associated to the N_b triggering points where the time series $y_2(t)$ satisfies at the time instants t_n the triggering condition $C_{y_2}(t_n)$:

$$\hat{D}_{y_1y_2}(\tau) = \frac{1}{N_b}\sum_{n=1}^{N_b} y_1(t_n+\tau)|C_{y_2}(t_n). \tag{4.284}$$

Up to M data points before and M points after the trig points ($\tau = m\Delta t$, $-M \le m \le M$) are used in the computation of the signature, where M is user-defined. The number N_b of averages depends on the length of the time series and the adopted triggering condition. Different triggering conditions $C_{y_2}(t_n)$ can be applied:

- Level crossing: $y_2(t_n) = \overline{y}_2$,
- Slope crossing: $\dot{y}_2(t_n) = \overline{\dot{y}}_2$,
- Positive value: $y_2(t_n) > 0$,
- Positive slope: $\dot{y}_2(t_n) > 0$,

and any combination of the previous conditions (for instance, zero crossing condition with positive slope: $y_2(t_n) = 0 \wedge \dot{y}_2(t_n) > 0$). When the triggering condition is applied to the same time series, whose data segments are averaged in (4.284), the auto-RD signature is estimated:

$$\hat{D}_{y_1y_1}(\tau) = \frac{1}{N_b}\sum_{n=1}^{N_b} y_1(t_n+\tau)|C_{y_1}(t_n). \tag{4.285}$$

When the condition affects both level and slope, it has been shown (Brincker et al. 1992) that the RD signature estimate is a linear combination of the correlation function and its derivative:

$$D_{y_1y_2}(\tau) = \frac{R_{y_1y_2}(\tau)}{\sigma^2_{y_2}}\overline{y}_2 + \frac{\dot{R}_{y_1y_2}(\tau)}{\sigma^2_{\dot{y}_2}}\overline{\dot{y}}_2 \tag{4.286}$$

where $\sigma^2_{y_2}$ is the variance of the triggering process $y_2(t)$ and $\sigma^2_{\dot{y}_2}$ is the variance of the derivative $\dot{y}_2(t)$ of the triggering process. The triggering condition can be selected in order to obtain an RD-signature, which is proportional only to the correlation function or its derivative. In particular, conditions applied only to the triggering process (i.e. level crossing, positive value) lead to an RD-signature proportional to the correlation function only, while the application of triggering conditions only to the derivative of the triggering process (i.e. slope crossing, positive slope) yields an RD signature proportional to the derivative of the correlation function.

A relevant application of the RD signature concerns the investigations about the amplitude dependence of modal damping ratios by appropriately varying the triggering condition. The interested reader can refer to the literature (Tamura and Suganuma 1996) for more details.

4.7 Some Remarks About OMA Methods

The theoretical background of a number of output-only modal identification procedures has been analyzed in the previous sections, discussing in detail those aspects related to the software implementation of selected algorithms. Far from being a comprehensive discussion about OMA techniques, the analysis of the individual methods in their most relevant aspects provides an overview of the advantages and drawbacks, from a practical point of view, related to the use of different analysis procedures. Relevant results of a comparative analysis of the previously illustrated OMA methods are summarized in this section, also to explain the larger attention devoted to some methods with respect to the others. The following considerations have also guided the selection of the procedures implemented into the software accompanying this book and used for the applications proposed at the end of this chapter. Even if the test engineer typically has a favorite OMA method of his own, selected according to criteria related to the simplicity or accuracy of the method itself, the concurrent use of different OMA techniques is always recommended for successful modal parameter identification. In fact, the comparison of the estimates provided by different OMA methods ensures the reliability of the modal identification results.

Even if developed since a long time and widely applied to civil engineering structures, NExT-type procedures have been progressively abandoned in favor of the more robust subspace methods. When NExT-type procedures appeared, they represented a significant enhancement in the field of output-only modal analysis with respect to the classical Peak Picking technique. In fact, they improved the accuracy of data analysis, especially in the presence of closely spaced modes, and allowed the extraction of actual mode shapes instead of ODSs. Notwithstanding their historical relevance, they show some limitations with respect to the subspace methods. The ITD method, for instance, suffers the lack of noise truncating mechanisms, thus leading to several spurious poles. Moreover, high order modes require filtering procedures to be extracted and this leads to the repeated application of the procedure to the same dataset, resulting in a time consuming process.

ARMA models aim at modeling the dynamics of both the structural system and the noise. Since also noise is modeled, lots of additional spurious poles, not related to the dynamics of the system under test, appear. This makes the selection of the system poles difficult, and the presence of noise can affect the modal parameter estimates as well. For instance, the lack of a noise truncating mechanism in the IV method is reflected in less accurate mode shape estimates with respect to subspace methods; moreover, higher order models are required to obtain good modal parameter estimates (Peeters 2000). When PEM is considered, the advantage of an optimal statistical description of data due to the presence of the MA matrix polynomial is paid by the need to solve a highly nonlinear optimization problem. Since the application of PEM does not improve too

much the modal parameter estimates (Brincker and Andersen 1999b), subspace methods, characterized by lower computational time and no convergence problems, are preferred.

Subspace methods have noise truncating mechanisms based on SVD. Since the identification problem is solved by means of linear algebra tools, nonlinear optimization problems are avoided. This results also in a lower computational burden. In the presence of noise or poorly excited modes, weighting matrices can be applied to improve the performance of the estimators. Both Cov-SSI and DD-SSI perform equally well in terms of quality of the modal parameter estimates; however, DD-SSI can be implemented in a way that positive realness of the covariance sequences is ensured. All the above-mentioned characteristics have made SSI methods very popular in the modal analysis community.

The availability of nonparametric frequency domain OMA procedures in the equipment of the modal analyst is also recommended. They can be profitably used for a quick check and analysis of data in the field. In fact, they are less computational demanding with respect to subspace methods and give reasonable estimates of the modal parameters. The use of FDD is recommended because of its less restrictive assumptions with respect to BFD. Moreover, due to the simplicity of nonparametric frequency domain methods, they can be used to get a first insight into the identification problem and, as a result, to guide the setting of the analysis parameters in subspace algorithms.

Other methods such as LSCF (and its poly-reference version) and SOBI are becoming more and more popular because they simplify the identification of the structural modes and provide interesting opportunities for the automation of the modal identification process (Chap. 6).

Whatever is the adopted OMA method, modal identification tests often require processing of a large amount of data. However, a certain degree of redundancy or overdetermination is always present in the data. As a consequence, techniques for the reduction of the amount of data to processed can profitably be applied in order to keep the computational time within reasonable values. Filtering and decimation are usually used to reject unnecessary information and to limit the frequency band under investigation. Selected reference channels (Peeters 2000) are also sometimes adopted in order to reduce data redundancy. They have to be carefully chosen to avoid that some modes are lost together with the redundant information. The use of reference channels can lead to problems of missing modes mainly in the presence of repeated roots and a too small number of reference channels, or in the case of local modes, which do not appear in the selected reference channels. An approach to the selection of the best reference channels is based on the computation of the correlation coefficients of the measured data:

$$\rho^2_{y_i y_j} = \frac{R^2_{y_i y_j}(0)}{R_{y_i y_i}(0) R_{y_j y_j}(0)} \tag{4.287}$$

and on the construction of the following matrix:

$$\left[\rho_{y_i y_j}\right] = \begin{bmatrix} 1 & \rho_{y_1 y_2} & \rho_{y_1 y_3} & \cdots & \rho_{y_1 y_l} \\ \rho_{y_2 y_1} & 1 & \rho_{y_2 y_3} & \cdots & \vdots \\ \rho_{y_3 y_1} & \rho_{y_3 y_2} & \ddots & \cdots & \vdots \\ \vdots & \cdots & \cdots & \ddots & \vdots \\ \rho_{y_l y_1} & \cdots & \cdots & \cdots & 1 \end{bmatrix}. \tag{4.288}$$

For each channel, the following index can be computed:

$$M_i = \sum_{j=1}^{l} \left|\rho_{y_i y_j}\right| \quad j \neq i, \quad i = 1, \ldots, l \tag{4.289}$$

and the reference channels are finally selected as those characterized by the largest values of the M_i index.

The use of reference channels leads to an appreciable reduction of computational efforts and response time. In the previous sections about OMA methods all measurement channels have been taken as references. When only some channels are selected as references, slight changes to the previously described algorithms are required in order to take into account that the number r of reference channels is lower than the total number of measurement channels. The interested reader can refer to the literature for reference-based versions of some of the OMA procedures discussed in this chapter (see, for instance, Peeters and De Roeck 1999 for the reference-based version of SSI algorithms).

Another interesting aspect, which is beyond the scope of the present book, concerns the possibility to estimate the uncertainty bounds of the modal parameter estimates from a single output-only modal identification test. This information plays a primary role in a variety of applications, ranging from the analysis of the influence of selected parameters on the vibration response to SHM. Moreover, the information about the uncertainty bounds can support the discrimination between physical and spurious poles, since the latter are usually characterized by larger variance. The interested reader can refer to the literature for more details (Reynders et al. 2008, Pintelon et al. 2007, De Troyer et al. 2009a, De Troyer et al. 2009b).

4.8 Post-Processing of Modal Parameter Estimates

4.8.1 Analysis of Mode Shape Estimates

Most of the OMA methods provide their results in the form of complex eigenvalues and complex eigenvectors. Since the mode shape estimates are in the form of complex vectors, a distinction between normal modes, characterized by real-valued mode shape vectors, and complex modes is needed.

In particular, it is worth realizing if complex mode shape estimates actually represent the dynamics of the structure under investigation or they are the result of other factors.

In the case of normal (real) modes, the displacements at the various DOFs reach their maximum at the same time and pass through the equilibrium position at the same time. This is not the case of complex modes, where both the maximum values and the null values of modal displacements are attained at different time instants for the various DOFs (Chopra 2000). As a result, while the phase angles are all 0° or 180° for normal modes, both amplitude and phase characterize the motion of the different DOFs in the case of complex modes.

Complex modes may originate for a number of reasons, such as gyroscopic effects, aerodynamic effects, nonlinearities, and nonproportional damping (Ewins 2000, Chopra 2000).

Close modes sometimes show significant complexity, too (Ewins 2000). In this regard it is worth noting that two modes characterized by some frequency separation (that is to say, the difference between the respective natural frequencies) may be close or not depending on the value of damping: the larger the damping, the closer the modes. As a measure of separation of two modes, the *modal overlap factor* (MOF) (Srikantha Phani and Woodhouse 2007) can be computed:

$$MOF_n = \frac{f_n \xi_n}{f_n - f_{n-1}} \tag{4.290}$$

where f_n and f_{n-1} represent the natural frequencies of the two modes under consideration, while ξ_n is the damping ratio associated to the n-th mode.

Even if in the majority of cases the identified modes are normal, it is important to recognize those situations where complex modes have to be expected and properly estimated.

Complex modes are often obtained from modal tests as a result of measurement noise (poor signal-to-noise ratio). However, the degree of complexity is usually moderate. Even if slight complexities can be encountered in practical applications and a complex-to-real conversion of mode shapes can be carried out with negligible errors, the evaluation of specific indicators can provide a quantitative measure of the degree of complexity of the estimated mode shapes.

The simplest method to assess modal complexity consists in plotting the components of the i-th eigenvector in the complex plane, thus obtaining the so-called *complexity plot* (Fig. 4.6). It permits the evaluation of the degree of complexity by a simple visual inspection. A method based on complexity plots for the quantitative assessment of the degree of complexity of the estimated mode shapes is described elsewhere (Ewins 2000). Other indexes measuring the mode shape complexity are the *Modal Phase Collinearity* (MPC) and the *Mean Phase Deviation* (MPD).

If a structure is proportionally damped, the mode shape components for a certain mode lie on a straight line in the complex plane (Fig. 4.6a).

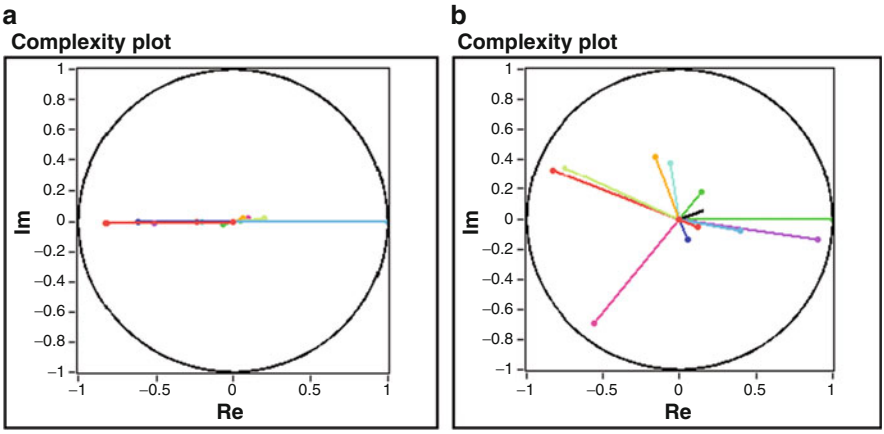

Fig. 4.6 Complexity plots for normal (**a**) and complex (**b**) modes

Deviations from this behavior can be quantified by the MPC for nearly real normal modes (Pappa et al. 1992). It can be computed by subtracting the mean value of the r-th mode shape vector components to each of them:

$$\tilde{\phi}_{i,r} = \phi_{i,r} - \frac{\sum_{k=1}^{l} \phi_{k,r}}{l} \qquad i = 1, \ldots, l. \tag{4.291}$$

The MPC of the r-th mode shape is then given by:

$$MPC_r = \frac{\left\|\mathrm{Re}\left(\left\{\tilde{\phi}_r\right\}\right)\right\|^2 + \left(\mathrm{Re}\left(\left\{\tilde{\phi}_r\right\}^T\right)\mathrm{Im}\left(\left\{\tilde{\phi}_r\right\}\right)\right)\left(2\left(\varepsilon_{MPC}^2 + 1\right)\sin^2(\theta_{MPC}) - 1\right)\Big/\varepsilon_{MPC}}{\left\|\mathrm{Re}\left(\left\{\tilde{\phi}_r\right\}\right)\right\|^2 + \left\|\mathrm{Im}\left(\left\{\tilde{\phi}_r\right\}\right)\right\|^2} \tag{4.292}$$

where:

$$\varepsilon_{MPC} = \frac{\left\|\mathrm{Im}\left(\left\{\tilde{\phi}_r\right\}\right)\right\|^2 - \left\|\mathrm{Re}\left(\left\{\tilde{\phi}_r\right\}\right)\right\|^2}{2\left(\mathrm{Re}\left(\left\{\tilde{\phi}_r\right\}^T\right)\mathrm{Im}\left(\left\{\tilde{\phi}_r\right\}\right)\right)} \tag{4.293}$$

$$\theta_{MPC} = \arctan\left(|\varepsilon_{MPC}| + \mathrm{sgn}(\varepsilon_{MPC})\sqrt{1 + \varepsilon_{MPC}^2}\right) \tag{4.294}$$

$\|\cdot\|$ and $\mathrm{sgn}(\cdot)$ denote the L_2 norm and the signum function, respectively. MPC values are dimensionless and bounded between 0 and 1. For real modes, the index approaches unity, while its value is low in the case of a complex mode.

If normal modes are expected, a low value of MPC may indicate nonstructural modes.

As an alternative, the degree of complexity can be quantified by computing the MPD. A simple expression for MPD (Heylen et al. 1998) starts from the computation of the following index for the r-th mode shape vector:

$$MP_r = \frac{\sum_{k=1}^{l} \varphi_{k,r}}{l} \tag{4.295}$$

with:

$$\begin{aligned} \varphi_{k,r} &= \arctan\left(\frac{\mathrm{Re}(\phi_{k,r})}{\mathrm{Im}(\phi_{k,r})}\right) \quad if \quad \arctan\left(\frac{\mathrm{Re}(\phi_{k,r})}{\mathrm{Im}(\phi_{k,r})}\right) \geq 0 \\ \varphi_{k,r} &= \arctan\left(\frac{\mathrm{Re}(\phi_{k,r})}{\mathrm{Im}(\phi_{k,r})}\right) + \pi \quad if \quad \arctan\left(\frac{\mathrm{Re}(\phi_{k,r})}{\mathrm{Im}(\phi_{k,r})}\right) < 0. \end{aligned} \tag{4.296}$$

Then, the MPD index is computed as follows:

$$MPD_r = \sqrt{\frac{\sum_{k=1}^{l} (\varphi_{k,r} - MP_r)^2}{l}}. \tag{4.297}$$

In the case of normal mode shapes, the value of MPD is zero. An improvement of the MPD index for those cases where there are mode shape components with a large imaginary part but a small real part can be found in the literature (Reynders et al. 2012).

Taking into account the previous discussion and that OMA provides only un-scaled mode shapes, there is the need for simple approaches to scaling and complex-to-real conversion of the estimated mode shape vectors.

The need for complex-to-real conversion of the estimated mode shapes stems from one of the typical applications of modal data, the comparison between the experimental values of the modal properties and those obtained from numerical models. In fact, the latter are usually obtained from undamped models and, as a consequence, the mode shapes are real-valued. Whenever normal modes are expected from the modal test, the simplest approach to carry out the complex-to-real conversion consists in analyzing the phase of each mode shape component and setting it equal to 0° or 180° depending on its initial value. If the phase angle lies in the first or in the fourth quadrant it is set equal to 0°; it is set equal to 180° if it lies in the second or in the third quadrant. To be rigorous, this approach should be applied only in the case of nearly normal modes, when the phase angles differ

no more than $\pm 10^\circ$ from 0° to 180°. However, it is frequently extended to all phase angles (Ewins 2000).

The mode shape vectors obtained from the different OMA methods are often rescaled so that the magnitude of the largest modal displacement is equal to 1. A simple procedure to obtain normalized, real mode shapes starting from the experimental results is the following:

- starting from the complex-valued components of the r-th experimental mode shape, find the component $\phi_{r,max}$ characterized by the largest modulus;
- divide every component of the experimental vector by $\phi_{r,max}$;
- carry out the complex-to-real conversion as previously illustrated;
- return the normalized mode shape vector in terms of amplitude and phase; alternatively, return the modal displacement with sign (+ if the phase is 0°, − if it is 180°).

The experimentally identified mode shapes have to be graphically displayed, because the visual inspection of the estimated mode shapes represents the simplest method for a preliminary check of the modal identification results. Two approaches exist for the graphical display of mode shape estimates. The static display provides a picture of the mode shape, eventually superimposed to the undeformed configuration of the structure (Fig. 4.7). This is the display format used in reports.

Taking into account the measurement directions of the sensors installed on the structure and their positions, the deformed shape is obtained by assigning to each measured point in each measured direction a displacement proportional to the corresponding component of the mode shape vector. The scaling constant is set in a way that the various modal displacements are appreciable but not too large, otherwise the basic geometry of the structure might appear heavily altered. The sign of the mode shape component determines if the measured point is moving in-phase (+) or out-of-phase (−) with respect to the reference direction of the sensor.

The static display is able to represent only real modes. As a consequence, a preliminary complex-to-real conversion of the estimated mode shapes is necessary. The visual inspection of complex mode shapes by static plots can be, therefore, misleading. Fortunately, normal or nearly normal modes are typically encountered in practical applications. Plotting animated mode shapes overcomes the limitations of static display. Animated plots simulate the swing of the structure according to the selected mode shape, so they can effectively represent also the complex modes.

One of the main drawbacks inherent in the visual inspection of the identified mode shapes is related to the fact that the identified model is incomplete, since measurements are carried out in a few points. The number of measurement points is typically much lower (by some order of magnitudes) than the number of DOFs adopted, for instance, in numerical models. Since there are several unmeasured DOFs during tests, in the grid of points adopted to represent the geometry of the structure some of them will always be characterized by null modal displacements.

This effect, caused by the finite number of measurement channels, has to be taken into account in the visual inspection of mode shapes. In fact, those points probably exhibit some displacements, which are not represented in the plots.

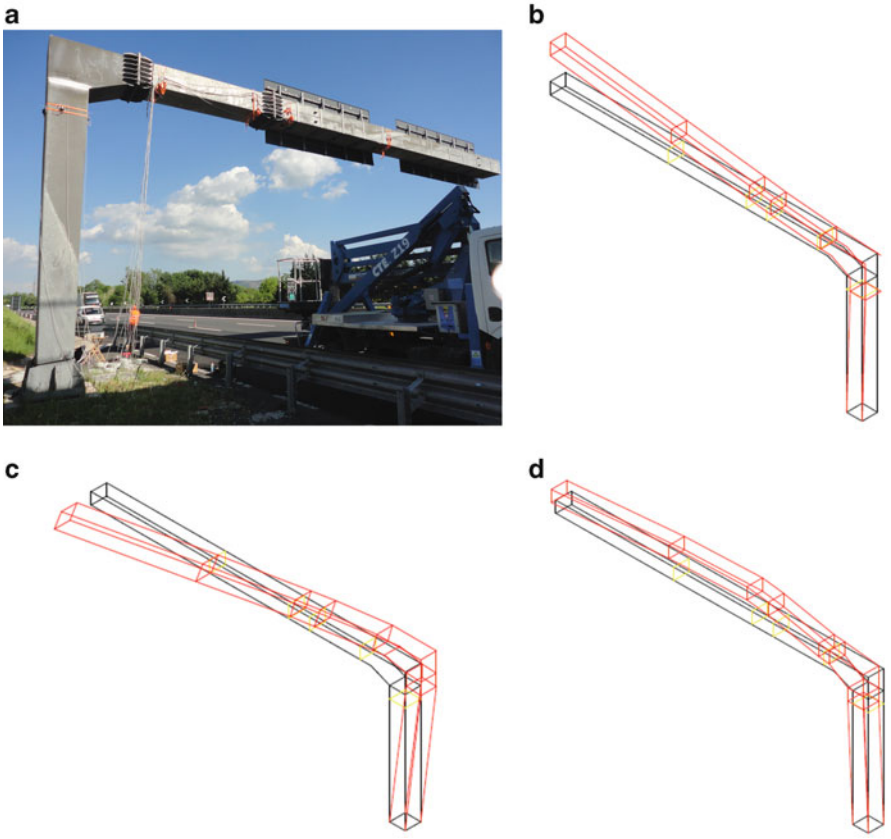

Fig. 4.7 Steel structure for road sign (**a**) and static display of some of its experimentally estimated mode shapes (**b**–**d**)

Neglecting the effect of incomplete measurements can lead to misleading results in the interpretation of the experimental mode shapes. In some cases interpolation of modal displacements or consideration of some constraints (for instance, the presence of rigid diaphragms) can compensate the lack of information about some modal displacements in the experimental estimates.

However, erroneous plots are obtained if, for instance, the assumption of constrained DOFs is not verified or interpolation of modal displacements is applied in the case of a structure characterized by the presence of joints or abrupt changes in its section. In summary, an effective display of the identified mode shapes is always the result of a good choice of the sensor layout and the installation of a sufficient number of sensors to ensure the observability of the modes of interest (see also Chap. 3).

In the extreme case, when the adopted sensor layout is too coarse with respect to the geometric complexity of the structure under test, there are problems not only in

displaying the deformation patterns but also in the analysis of the deformed shapes. In fact, an insufficient number of sensors leads to the well-known problem of spatial aliasing (Ewins 2000) with the related problems of distinction of the various modes, which appear very similar each other. An effective tool to assess (ex post) the quality of the adopted sensor layout is introduced in Sect. 4.8.2.2.

4.8.2 Quality Checks and Comparisons

4.8.2.1 Natural Frequencies

Validation of modal identification results mainly relies on consistency checks obtained by comparing the experimental estimates provided by different OMA methods. If the experimental estimates provided by the different methods are in good agreement each other, they can eventually be compared with the results of numerical models of the structure under investigation. Comparisons and correlations between experimental and numerical estimates of the modal properties represent the primary tools to verify numerical models. A *verified model* is a model that includes all the necessary features to provide an acceptable representation of the actual dynamic behavior of the structure. A verified model can eventually undergo some adjustments to make its dynamic properties closer to the experimental values. The calibration of a numerical model based on experimental estimates of the modal properties is referred to as *model updating*. This is one of the main applications of modal testing. Even if most of the necessary tools to compare numerical and experimental results are discussed in this section, the interested reader can refer to the literature (Friswell and Mottershead 1995, Mottershead et al. 2011, Ewins 2000) for an extensive discussion about model updating techniques, which are beyond the scope of the present book.

Natural frequencies can be compared by a simple tabulation, quantifying the relative scatter, expressed in percent, as follows:

$$\Delta f_n = \frac{f_{2,n} - f_{1,n}}{f_{1,n}} \cdot 100 \tag{4.298}$$

where $f_{1,n}$ and $f_{2,n}$ are the two values of the natural frequency for the n-th mode under comparison; $f_{1,n}$ and $f_{2,n}$ can be either experimental estimates, obtained from two different OMA methods, or represent the numerical and the experimental estimate of the experimental frequency of the n-th mode, respectively.

An alternative approach to compare two sets of natural frequency estimates consists of plotting the natural frequencies in the second set against the natural frequencies of the first set in a Cartesian plane (Fig. 4.8). The first set holds the reference natural frequency estimates (for instance, those provided by a certain OMA method, or average values of the estimates obtained from different methods) while the second set holds the values of the natural frequencies that have to be compared with the corresponding estimates in the first dataset. The natural frequencies in the second set can be experimental estimates obtained from a

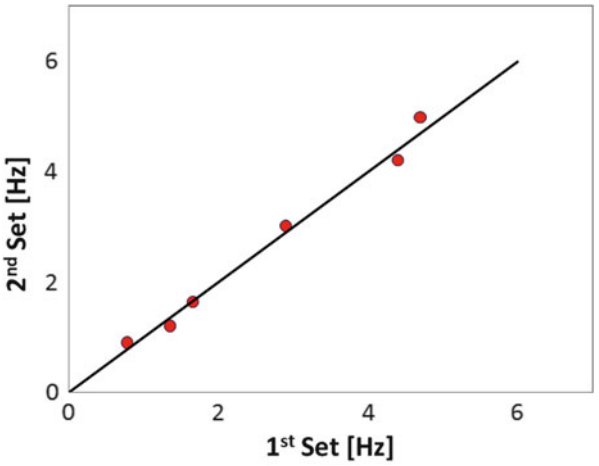

Fig. 4.8 Comparison of natural frequencies

different OMA method or the values predicted by a numerical model. In the ideal case of very good correlation between the two sets of natural frequencies, the points lie very close to the line passing through the origin of the axes with 45° slope. However, mainly in the case of the comparison between numerically predicted and experimentally estimated natural frequencies, it may happen that the points lie along a different line or they are fairly scattered with respect to the 45° line. Depending on how the points are distributed, it is possible to determine the reasons for the deviations. For instance, about the comparison between numerically predicted natural frequencies and the corresponding experimental estimates, if the numerical model is representative of the actual behavior of the structure, only small and randomly distributed deviations of the points from the 45° line are expected. When the points lie close to a line with slope different from 45°, the deviation can be addressed to erroneous setting of the material properties in the numerical model. If the points are widely scattered with respect to the 45° line, the model is unfit to represent the experimental data and a new model has to be set. Finally, if the deviations are small but all or nearly all the points lie on one side of the 45° line, they suggest the presence of a systematic error (Ewins 2000). Similar considerations can be done in the analysis of the experimental results provided by different methods.

In both cases of tabulation and graphical representation, a correct mode pairing plays a critical role in determining the results and effectiveness of the comparisons. It is not sufficient to compare two sets of ordered frequencies since there is no guarantee of one-to-one correspondence between the modes in the first set and those in the second set. For a correct mode pairing the information about the mode shapes has also to be taken into account, in order to ensure that the two natural frequency estimates under comparison are representative of the same mode. An incorrect mode pairing can lead to misleading results. The evaluation of the correlation between couples of mode shapes is based on the tools discussed in the next section.

4.8.2.2 Mode Shapes

Classical books about experimental modal analysis suggest the comparison of mode shapes through their graphical representation according to one of the methods discussed in Sect. 4.8.1; plots in the Cartesian plane similar to that discussed in Sect. 4.8.2.1 to compare natural frequencies can also be used. Even if those methods can provide a certain amount of information, for instance about poor numerical modeling (Ewins 2000), they suffer problems in the presence of some scaling errors in the data and they are inadequate to compare complex-valued mode shapes. This can lead to major errors in the analysis of results and mode pairing. A more effective comparison of mode shapes, able to deal also with complex modes, is based on some numerical indexes. The MAC (Allemang and Brown 1982) represents the most popular index to quantify the correlation between mode shapes, but it also shows some limitations. For this reason, a number of other indexes have been developed over the years. The use of MAC and other indexes to evaluate the correlation between couples of mode shapes is discussed in this section, pointing out the respective advantages and limitations. In particular, the role of those indexes in proper mode pairing, in the assessment of the quality of the adopted sensor layout and in the verification of numerical models is illustrated.

Given the two mode shape vectors under comparison, for instance the experimentally estimated mode shape $\{\phi_n^e\}$ and the numerically predicted mode shape $\{\phi_n^a\}$ of the n-th mode of the investigated structure, in the most general case of complex-valued vectors the MAC is computed as follows:

$$MAC\left(\{\phi_n^a\},\{\phi_n^e\}\right)=\frac{\left|\{\phi_n^a\}^H\{\phi_n^e\}\right|^2}{\left(\{\phi_n^a\}^H\{\phi_n^a\}\right)\left(\{\phi_n^e\}^H\{\phi_n^e\}\right)}. \tag{4.299}$$

If both vectors are real-valued, as usually happens in the presence of numerically predicted mode shapes, the transpose operator replaces the Hermitian and (4.299) can be rewritten as follows:

$$MAC\left(\{\phi_n^a\},\{\phi_n^e\}\right)=\frac{\left|\{\phi_n^a\}^T\{\phi_n^e\}\right|^2}{\left(\{\phi_n^a\}^T\{\phi_n^a\}\right)\left(\{\phi_n^e\}^T\{\phi_n^e\}\right)}. \tag{4.300}$$

The MAC index is basically a squared, linear regression correlation coefficient and it provides a measure of the consistency (degree of linearity) between the two vectors under comparison. The MAC values are bounded between 0 and 1, representing inconsistent and perfectly consistent correspondence between the two vectors, respectively. Even if the MAC between analytical and experimental mode shapes is generally used for verification and updating of finite element models, it is worth taking into account that it provides only a measure of consistency between the vectors but it does not ensure validity.

For instance, when the experimental mode shapes are measured at few locations, the incomplete information can lead to a MAC value near unity with the corresponding analytical mode shape, but the consistency between the two vectors does not ensure that the analytical mode shape is correct. If more points are measured, the consistency between analytical and experimental mode shapes can decrease to values much lower than 1.

It is also worth pointing out that the MAC is sensitive to large differences between the corresponding components of the vectors under comparison, but it is basically insensitive to small changes and small magnitudes of the modal displacements. Moreover, the MAC is not able to distinguish between random errors and systematic deviations from the reference mode shape components. Notwithstanding the previous limitations, the MAC is by far the most used index for mode shape comparisons.

Taking into account the relative scatter between the natural frequencies (4.298) and the consistency of the mode shape vectors (4.299), an effective mode pairing is possible. The information about the mode shapes plays a primary role for a correct mode pairing above all in the case of closely spaced modes, when proper matching between analytical and experimental mode shapes can be difficult if only the information about the natural frequencies is available.

When the mode shapes under comparison exhibit a consistent, linear relationship, it is possible to compute the *modal scale factor* (MSF) as follows:

$$MSF\left(\{\phi_n^e\},\{\phi_n^a\}\right)=\frac{\left(\{\phi_n^a\}^H\{\phi_n^e\}\right)}{\left(\{\phi_n^a\}^H\{\phi_n^a\}\right)} \tag{4.301}$$

if the analytical mode shape is considered as reference, or as:

$$MSF\left(\{\phi_n^a\},\{\phi_n^e\}\right)=\frac{\left(\{\phi_n^e\}^H\{\phi_n^a\}\right)}{\left(\{\phi_n^e\}^H\{\phi_n^e\}\right)} \tag{4.302}$$

if the experimental mode shape is considered as reference. The MSF does not provide information about the quality of the fit, but it only gives the scale factor between consistent vectors.

An alternative index to assess the mode shape correlation is represented by the *Normalized Modal Difference* (NMD) (Waters 1995, Maia et al. 1997):

$$NMD\left(\{\phi_n^a\},\{\phi_n^e\}\right)=\sqrt{\frac{1-MAC\left(\{\phi_n^a\},\{\phi_n^e\}\right)}{MAC\left(\{\phi_n^a\},\{\phi_n^e\}\right)}} \tag{4.303}$$

The NMD basically represents a close estimate of the average difference between the components of the two vectors $\{\phi_n^a\}$ and $\{\phi_n^e\}$. It appears much more sensitive to mode shape differences than the MAC and, therefore, it is sometimes used to better remark the differences between highly correlated mode shapes.

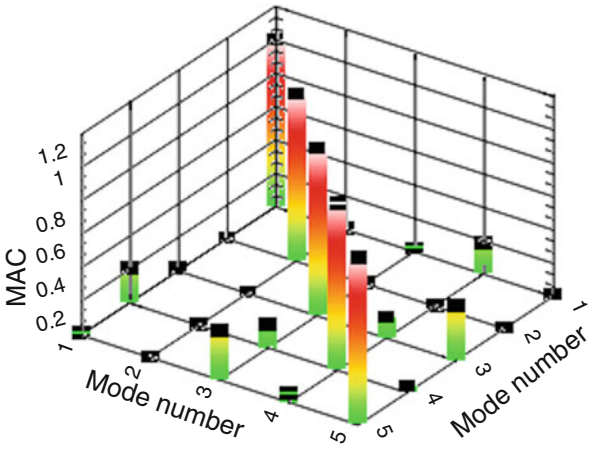

Fig. 4.9 Graphical representation of MAC matrix

In practical applications, given N_m^e experimentally identified modes and N_m^a numerically predicted modes, the $N_m^e \times N_m^a$ MAC matrix (Fig. 4.9) is computed. Assuming without loss of generality that $N_m^e = N_m^a$, if the numerical and experimental mode shape vectors are consistent the MAC matrix will show values close to 1 along its main diagonal, where the MAC is computed for mode shapes corresponding to the same mode, and close to 0 elsewhere, where the MAC is related to two different modes.

When the MAC matrix is different from this ideal case, for instance because of the presence of low MAC values along the main diagonal or of off-diagonal terms characterized by large values of the MAC, a supplement of investigation is needed since these anomalies can be the result of poor modeling, poor analysis of the experimental data, inappropriate choice of the DOFs included in the correlation or incorrect mode pairing.

MAC values between mode shapes corresponding to the same mode are always expected to be slightly lower than 1 in practical applications, due to the unavoidable uncertainties associated to the experimental estimates and the approximations inherent in numerical models. However, when the objective of the comparison is simply a verification of the numerical model, values of MAC in excess of 0.8–0.9 can be accepted as indicators of good consistency, while values less than 0.1–0.2 can be accepted as indicators of poor consistency. These limit values for the MAC must not be regarded in absolute terms, since there are some applications that demand high levels of consistency and some others that can accept lower MAC values, depending on the final use of the verified or updated model.

The MAC index is a measure of the overall consistency between two vectors, but it gives no information about the scatter between corresponding DOFs. When the information about the spatial distribution of the degree of correlation is of interest, extensions of the MAC have to be considered.

The Coordinate Modal Assurance Criterion (COMAC) (Ewins 2000) has been developed to identify the DOFs that yield low MAC values. In the case of

real-valued mode shapes and a set of N_m couples of paired experimental-numerical mode shapes, the COMAC associated to the r-th DOF can be computed as follows:

$$COMAC_r = \frac{\sum_{j=1}^{N_m} \left| \phi_{r,j}^a \cdot \phi_{r,j}^e \right|^2}{\sum_{j=1}^{N_m} \left(\phi_{r,j}^a \right)^2 \cdot \sum_{j=1}^{N_m} \left(\phi_{r,j}^e \right)^2} \tag{4.304}$$

where $\phi_{r,j}^a$ and $\phi_{r,j}^e$ denote the r-th component of the j-th analytical and experimental mode shape, respectively. Thus, the COMAC preserves the information about the individual DOFs. Low values of COMAC indicate poor correlation.

An Enhanced Coordinate Modal Assurance Criterion (ECOMAC) has also been proposed (Hunt 1992) to overcome the potential problems caused by erroneous calibration scaling or definition of the orientation of the sensors. In particular, the erroneous definition of sensor orientations causes the inversion of the sign of the associated components of the experimental mode shapes. Given a set of N_m couples of paired experimental-numerical mode shapes, the ECOMAC associated to the r-th DOF can be computed as follows:

$$ECOMAC_r = \frac{\sum_{j=1}^{N_m} \left| \phi_{r,j}^a - \phi_{r,j}^e \right|}{2N_m}. \tag{4.305}$$

Thus, the ECOMAC basically represents a measure of the average difference between the vector components corresponding to a certain DOF.

The role of the MAC index in the verification of numerical models has been already introduced. However, it can be used also to check the effectiveness of the adopted sensor layout and to assess the consistency between mode shape estimates provided by different OMA methods.

For instance, the effectiveness of sensor layout can be assessed through the computation of the AutoMAC matrix of the experimental mode shape estimates provided by a given OMA method. The entries of this matrix are represented by the values of the MAC obtained when a set of experimental mode shapes are correlated with themselves. Thus, the AutoMAC matrix is a symmetric matrix characterized by values all equal to 1 along the main diagonal. When the off-diagonal terms are all close to 0, the adopted sensor layout is effective in distinguishing the different modes; on the contrary, the presence of large off-diagonal terms means that similar mode shape vectors have been obtained for distinct modes. This requires a supplement of investigation to define the reasons of the correlation. It could be due to the fact that the orthogonality condition of the modes with respect to the mass matrix cannot be translated into a perfectly diagonal AutoMAC matrix. However, it is frequently an indicator of problems, such as spatial aliasing or spurious modes erroneously included into the set of identified physical modes. Including additional

sensors and eventually changing the measurement positions to enhance the observability of the different modes can solve the problems related to spatial aliasing and poor discrimination of the modes.

The consistency between mode shape estimates provided by different OMA methods can be assessed by the construction of the CrossMAC matrix. It is basically a MAC matrix but both the sets of vectors under comparison are made by experimental mode shape estimates. The two sets of experimental mode shapes have been obtained from the application of different OMA techniques. If the two set of mode shape estimates are consistent, a CrossMAC matrix characterized by values very close to 1 along the main diagonal and close to 0 elsewhere is obtained, provided that the AutoMAC matrices of the two sets of experimental mode shapes are approximately diagonal (absence of large off-diagonal terms).

4.9 Stabilization Diagrams for Parametric OMA Methods

An appropriate parameter setting in parametric OMA methods requires some prior knowledge about the order of the model to identify all modes in the analyzed frequency range. As a consequence, the number of modes has to be estimated in advance based on a physical insight or from the peaks in the output power spectra or in the singular value plots obtained by SVD of the output PSD matrix at all discrete frequency values.

More formal procedures are based on the comparison of models characterized by different orders according to some predefined criteria, which can eventually include penalties to avoid overfit (Ljung 1999). In the case of SSI methods it has also been shown that the order of the model can theoretically be determined from the experimental data as the rank of the Toeplitz matrix of correlations (Sect. 4.5.3.1) or of the projection matrix (Sect. 4.5.3.2) provided that the condition expressed by (4.207) is fulfilled. Unfortunately, due to noise and modeling inaccuracies, it often happens that no clear gap is visible in the sequence of the singular values of those matrices, thus resulting in serious problems for the determination of the correct model order. This is due to the fact that the factorization properties given by (4.208) and (4.239) do not exactly hold in the case of a finite number of data points. However, in the case of experimental/operational modal analysis the final objective is the identification of accurate and reliable modal parameter estimates rather than a good model as such. As a consequence, in practical applications a conservative approach is adopted based on the overspecification of the order of the model, which is set large enough to ensure the identification of all physical modes.

The amount of overspecification mainly depends on the characteristics of the analyzed dataset. In any case overmodeling introduces spurious poles, which have to be separated from the physical poles. This makes the modal parameter estimation more complicated. Spurious modes can be:

- noise modes: they are represented, for instance, by poles of the excitation system and, as such, they are due to physical reasons;

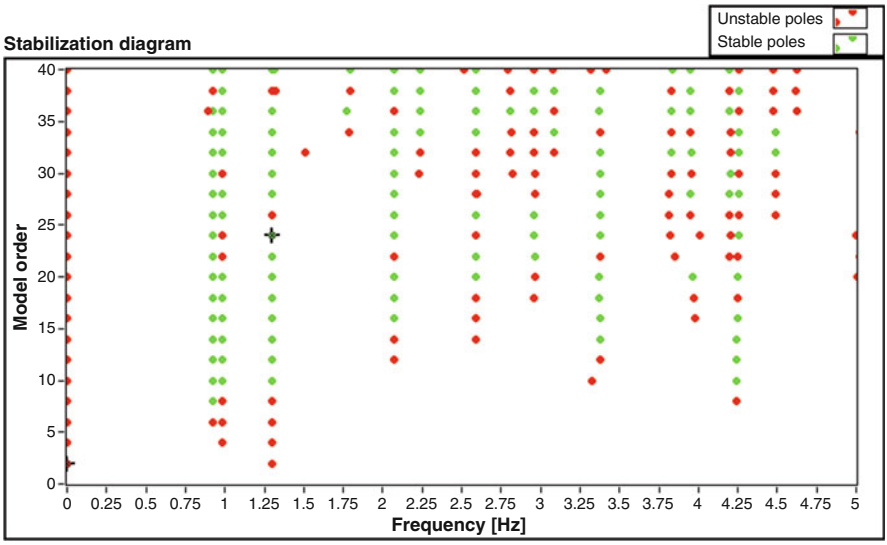

Fig. 4.10 Stabilization diagram

- mathematical modes: they are created by the model in addition to the physical poles to ensure the mathematical description of the measured data, which are inevitably affected by slight imperfections (measurement noise, computational noise, modeling inaccuracies); thus, they are the result of the overestimation of the order of the model.

The separation of the physical poles from the spurious mathematical ones can take advantage of the construction of the so-called *stabilization diagram* (Fig. 4.10). It shows the poles obtained for different model orders as a function of their frequency. By tracking the evolution of the poles for increasing model orders, the physical modes can be identified from alignments of stable poles, since the spurious mathematical poles tend to be more scattered and typically do not stabilize. The alignments of stable poles can start at lower or higher values of the model order, depending on the level of excitation of the modes.

The construction of the stabilization diagram is based on the comparison of the poles associated to a given model order with those obtained from a one-order lower model. Only the poles that fulfill assigned user-defined stabilization criteria are labeled as stable. Typical stability requirements are expressed by the following inequalities:

$$\left(\frac{|f(n)-f(n+1)|}{f(n)}\right) < 0.01 \tag{4.306}$$

$$\left(\frac{|\xi(n)-\xi(n+1)|}{\xi(n)}\right) < 0.05 \tag{4.307}$$

$$\left[1 - MAC(\{\phi(n)\}, \{\phi(n+1)\})\right] < 0.02. \tag{4.308}$$

In other words, (4.306) implies that the scatter between the estimates of the natural frequency at two subsequent model orders has to be lower than 1 % for a pole to be labeled as stable. Similar conditions on damping ratios and mode shapes are expressed by (4.307) and (4.308), respectively.

If all the conditions expressed by the previous inequalities are satisfied, the pole is labeled as stable. In the case of two stage methods, when the information about mode shapes is not available, the stabilization criteria apply to natural frequency and damping ratio estimates, only. It is worth pointing out that the relative criteria to assess the stability of the poles have to be used with caution. In fact, they can be particularly severe in the case of lightly damped modes, when the damping ratios are small and their percentage variations can be larger than the preset limit.

After the identification of the alignments of stable poles, eventual noise modes can be discarded according to physical criteria based on the expected damping ratio or the expected properties and aspect of the mode shapes.

It is worth pointing out that a bias of the modes can sometimes occur at low orders of the model. The estimates are biased since the poles represent a combination of different modes. This phenomenon is denoted by the splitting of a certain alignment of stable poles in the stabilization diagram into two separate columns from a certain model order. Thus, only if the maximum model order in the stabilization diagram has been set large enough, the bias of the modes can be identified. In this case, the modal parameters have to be estimated from the two alignments of poles generated after the splitting.

In the case of SSI methods, the stabilization diagram can be efficiently constructed once the factorization property given by (4.208) for Cov-SSI or (4.239) for DD-SSI has been computed for the maximum order of the model. In fact, models of lower order can be directly obtained by excluding an increasing number of singular values and vectors in the computation of $[O_i]$ and $[\Gamma_i]$ or $\left[\hat{S}_i\right]$ (Peeters 2000). Moreover, the poles in complex conjugate pairs allow plotting the stabilization diagram considering only those characterized by positive imaginary component (and, therefore, positive damped frequency). As a result, the state-space model provides modal parameters for a number of modes equal to half of its order (Magalhaes and Cunha 2011).

In the case of OMA methods based on least squares estimators (LSCE, LSCF, and their poly-reference versions), coefficient constraint and basis function have a relevant influence on the discrimination between physical and mathematical modes. In fact, an appropriate choice of the constraint applied to the coefficients with respect to the adopted basis function can force the mathematical poles to be unstable (positive real part, negative damping) while the physical modes are stable (negative real part, positive damping). As a result, the distinction between

mathematical and physical poles is simplified, because it is based on the sign of damping. Mathematical poles are forced to be unstable by adopting the following combinations of coefficient constraint and basis function (Cauberghe et al. 2005):

- the lowest-order coefficient is unitary and the basis function is z^{-1};
- the highest-order coefficient is unitary and the basis function is z.

When the adopted basis function is z^{-1}, the denominator coefficients in the LSCF method are computed as follows:

$$\{\theta_d\} = \begin{bmatrix} 1 \\ -\left[M_{(2:n+1,2:n+1)}\right]^{-1}\left[M_{(2:n+1,1)}\right] \end{bmatrix} \tag{4.309}$$

where $[M_{(2:n+1,2:n+1)}]$ is the submatrix made by the last n rows and n columns of $[M]$ (4.134), while $[M_{(2:n+1,1)}]$ is the submatrix made by the last n rows and the first column of $[M]$. In the case of the p-LSCF method, instead, the denominator coefficients are computed as follows:

$$[\alpha] = \begin{bmatrix} [I_l] \\ -\left[M_{(l+1:(n+1)l,\,l+1:(n+1)l)}\right]^{-1}\left[M_{(l+1:(n+1)l,\,1:l)}\right] \end{bmatrix} \tag{4.310}$$

where $[M_{(l+1:(n+1)l,\,l+1:(n+1)l)}]$ is the submatrix made by the last nl rows and nl columns of $[M]$ (4.167), while $[M_{(l+1:(n+1)l,\,1:l)}]$ is the submatrix made by the last nl rows and the first l columns of $[M]$. In this last case, the roots of the denominator polynomial are the eigenvalues of the following companion matrix:

$$[A] = \begin{bmatrix} -[A_n]^{-1}[A_{n-1}] & -[A_n]^{-1}[A_{n-2}] & \cdots & -[A_n]^{-1}[A_1] & -[A_n]^{-1}[A_0] \\ [I] & [0] & \cdots & [0] & [0] \\ \vdots & \vdots & \ddots & \vdots & \vdots \\ [0] & [0] & \cdots & [I] & [0] \end{bmatrix}. \tag{4.311}$$

In Sect. 4.4.3.2, the procedure for mode shape estimation in the context of the p-LSCF method has been discussed. Another approach consists in the conversion of the RMFD model into a state-space model (Magalhaes and Cunha 2011). In this case, the model coefficients have to be rearranged into the output influence matrix as follows:

$$[C] = \begin{bmatrix} [B_{n-1}] - [B_n][A_n]^{-1}[A_{n-1}] & \cdots & [B_0] - [B_n][A_n]^{-1}[A_0] \end{bmatrix} \tag{4.312}$$

where:

$$\left[B_j\right] = \begin{bmatrix} \langle B_{1,j} \rangle \\ \vdots \\ \langle B_{o,j} \rangle \\ \vdots \\ \langle B_{l,j} \rangle \end{bmatrix}. \tag{4.313}$$

The theoretical derivations can be found elsewhere (Reynders 2009). Once the matrices $[A]$ and $[C]$ are known from (4.311) and (4.313), the modal parameters are obtained as described in Sect. 4.5.3.1.

The combination coefficient constraint-basis function has an influence on damping ratio estimates only in the case of discrete-time models. The superior quality of the stabilization diagram, that simplifies its interpretation, explains why discrete-time models are preferred over continuous-time models.

Some authors (Peeters and Van der Auweraer 2005, Cauberghe 2004) suggest the application of p-LSCF in combination with positive power spectra instead of one-sided spectra, because this yields very clear stabilization diagrams. The improvement in the quality of stabilization can be appreciated by comparing the plots shown in Fig. 4.11. They represent the stabilization diagrams obtained from the application of p-LSCF to one-sided spectra (Fig. 4.11a) and positive power spectra (Fig. 4.11b) estimated from the same dataset. However, the accuracy of mode shape estimates might be negatively affected when positive power spectra are used. For this reason, the comparison of the mode shape estimates obtained from the application of p-LSCF to positive power spectra with those obtained from one-sided spectra is recommended.

4.10 Applications

4.10.1 Basic Frequency Domain

Task. Develop software for output-only modal identification based on the Basic Frequency Domain (Peak Picking) method. Alternatively, install and use the software in "Chapter 4/BFD". Use the data in "Sample record 12 channels – sampling frequency 10 Hz.txt" in the folder "Chapter 2/Correlation" of the disk accompanying the book. Data in the file are organized in columns: time is in the first column; data are in the next 12 columns. Assume that the data have been collected on a framed structure made by three floors and that four sensors per floor have been installed according to the layout shown in Fig. 4.12. Assume that the time series in the file are ordered for increasing sensor number (excluding the column of time, the first column holds the data from sensor #1, the second column holds the data from sensor #2, and so on; the last column holds the data from sensor #12).

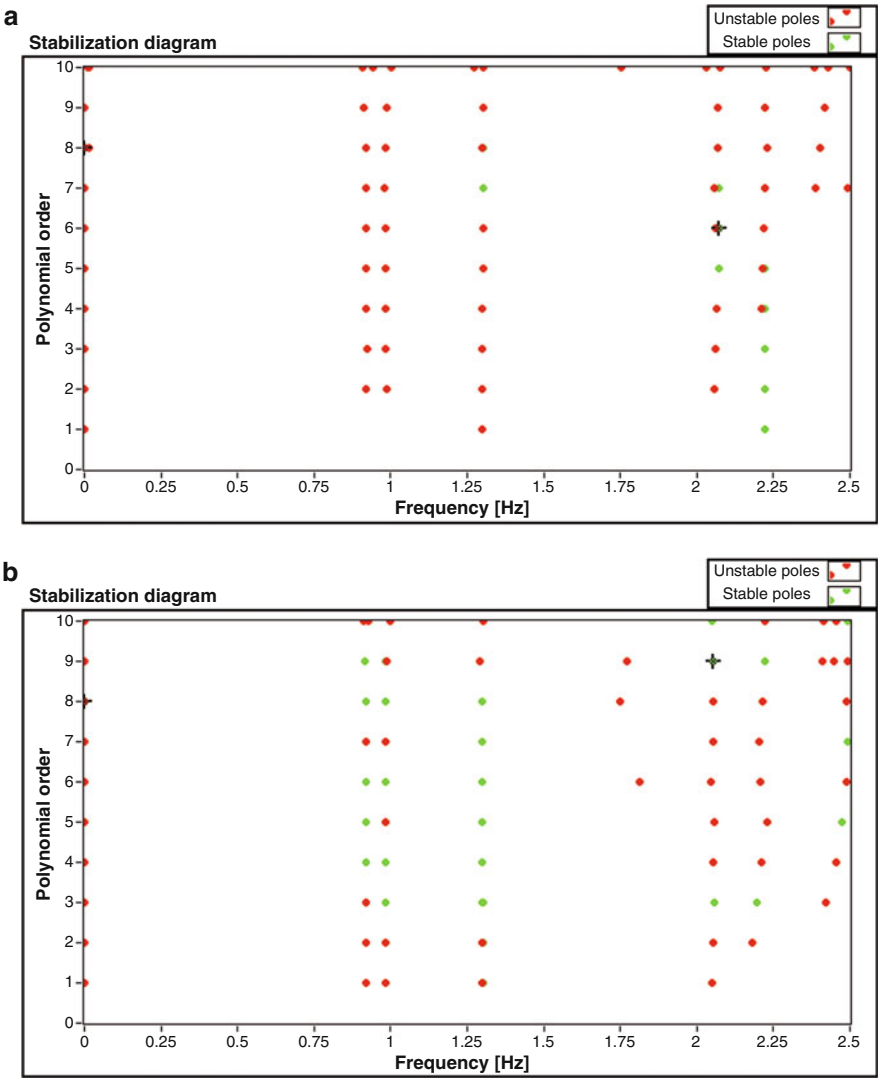

Fig. 4.11 Stabilization diagram obtained from the application of p-LSCF to one-sided spectra (**a**) and positive power spectra (**b**)

Suggestions. Starting from the sample code for computation of power spectra developed in Chap. 2, develop software for output-only modal identification based on the BFD (Peak Picking) method. It should be able to carry out the following operations (adoption of state machine architecture or event structure is recommended):

- At start-up, load the data and set the main analysis parameters (window, number of segments, decimation factor, overlap);
- Compute the PSD matrix and show its trace in a plot to identify the peaks that can be recognized as possible structural modes (possible structural modes can be eventually identified also as recurrent peaks in the auto-power spectra);

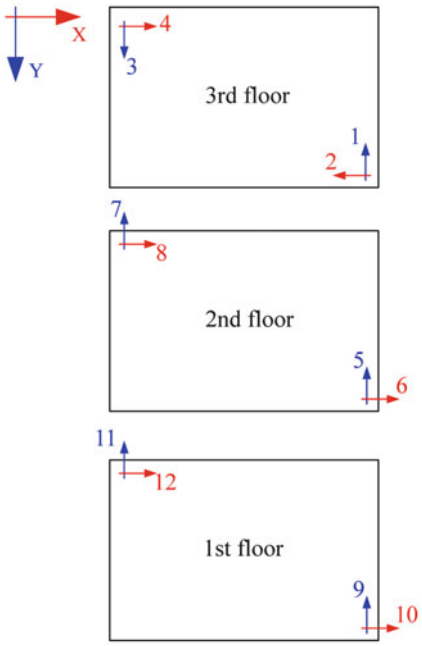

Fig. 4.12 Sensor layout for applications

- After having identified the peak frequencies, select a reference channel and compute its auto-power spectrum and the cross-power spectra with all the remaining channels;
- Show the spectra in terms of amplitude and phase and the coherence functions;
- Collect the values of amplitude, phase, and coherence at the previously identified peak frequencies; take advantage of the coherence plots to identify structural modes and to define the nature (bending, torsion) of the mode; if certain peaks are missing in the auto-power spectrum of the reference channel, repeat the previous steps with a different choice of the reference channel in order to identify also those modes;
- Normalize the mode shape vectors so that the component with maximum amplitude is equal to 1;
- Create a report of modal identification results in terms of natural frequencies and mode shapes.

It is worth pointing out that the accuracy of natural frequency estimates depends on the frequency resolution; thus, long records of the structural response to ambient vibrations are recommended to compute spectra characterized by a large number of averages and a fine frequency resolution (in the order of 0.01 Hz).

Use the BFD method to identify at least the three fundamental modes of the structure. Create a report with the identified natural frequencies and mode shape estimates; plot the mode shapes considering the floors as rigid diaphragms. Compute the AutoMAC matrix (Sect. 4.8.2.2).

Table 4.1 Mode shape estimate for the first mode (0.92 Hz—channel #2 as reference)

Amplitude	Phase	Normalized mode shape
6.31E−06	−0.02	−0.114
5.49E−05	0.00	−0.990
2.11E−05	−0.03	−0.380
5.54E−05	3.14	1.000
4.44E−06	−0.03	−0.080
4.19E−05	−3.14	0.756
1.10E−05	3.11	0.198
4.24E−05	3.14	0.764
3.36E−06	0.00	−0.061
1.82E−05	−3.13	0.329
5.27E−06	3.12	0.095
1.90E−05	−3.13	0.343

Table 4.2 Mode shape estimate for the second mode (0.98 Hz—channel #1 as reference)

Amplitude	Phase	Normalized mode shape
7.42E−0.5	0.00	−0.828
6.54E−06	−0.27	−0.073
8.96E−05	−3.12	1.000
1.85E−05	3.05	0.207
4.60E−05	0.00	−0.513
6.01E−06	2.92	0.067
5.52E−05	0.01	−0.616
9.03E−06	2.99	0.101
1.86E−05	−0.02	−0.207
1.64E−06	2.80	0.018
2.12E−05	0.00	−0.236
4.21E−06	3.02	0.047

Results obtained by the Authors of this book by applying the BFD method are reported in Tables 4.1, 4.2, and 4.3 as reference. The identified mode shapes are also shown in Fig. 4.13, based on the assumption of rigid diaphragms. Real-valued normalized mode shapes were constructed as discussed in Sect. 4.8.1. Channel #2 was selected as reference for the identification of the first and the third mode, while channel #1 was the reference for the identification of the second mode.

Sample software. Sample software to carry out output-only modal identification based on the BFD method can be found in "Chapter 4/BFD" of the disk accompanying the book.

Table 4.3 Mode shape estimate for the second mode (1.30 Hz—channel #2 as reference)

Amplitude	Phase	Normalized mode shape
4.62E−05	−3.13	1.000
8.58E−06	0.00	−0.186
4.17E−05	−3.12	0.903
6.43E−07	2.88	0.014
2.79E−05	−3.13	0.603
5.36E−06	3.14	0.116
2.49E−05	0.02	−0.539
1.32E−06	0.09	−0.029
1.01E−05	−3.13	0.218
2.16E−06	−3.14	0.047
8.91E−06	0.02	−0.193
7.27E−07	0.03	−0.016

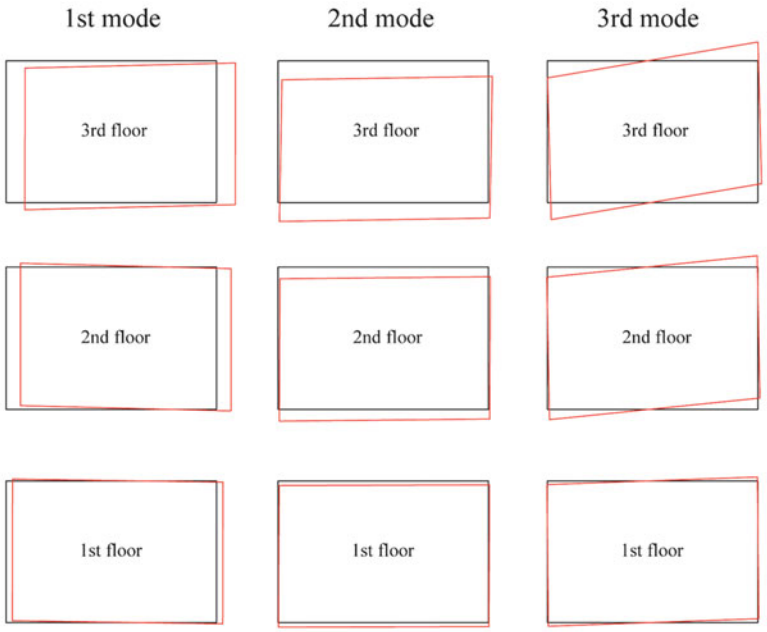

Fig. 4.13 Plots of the identified mode shapes

4.10.2 Frequency Domain Decomposition

Task. Develop software for output-only modal identification based on the FDD method. Alternatively, install and use the software in "Chapter 4/FDD". Repeat the identification of the fundamental modes of the structure of Sect. 4.10.1. Operational response data are in "Sample record 12 channels – sampling frequency 10 Hz.txt" in

the folder "Chapter 2/Correlation" of the disk accompanying the book. Organization of data in the file has been described in Sect. 4.10.1. Sensor layout is shown in Fig. 4.12.

Suggestions. The previously developed software for Peak Picking can be easily extended to carry out output-only modal identification according to the FDD method. Here is the list of the main tasks in software development:

- At start-up, load the data and set the main analysis parameters (window, number of segments, decimation factor, overlap);
- Compute the PSD matrix, organizing the data into an array of $l \times l$ square matrices; each matrix holds the values of the power spectra at a certain frequency line in the form of complex values;
- At each frequency line compute the SVD of the complex-valued PSD matrix; concatenation of the vectors of the singular values obtained at the various discrete frequencies yields the singular value plots;
- Plot all the singular values as a function of frequency in the same plot; create and use cursors to identify the peaks corresponding to structural modes; the peak frequency can be considered an estimate of the natural frequency (for lightly damped systems) as in the case of the BFD method; the peaks are usually selected in the first singular value plot, unless repeated modes are present;
- Collect the singular vectors associated to the selected singular values at the various frequencies; normalize these vectors so that the component characterized by the largest amplitude is set equal to 1; with a few exceptions for closely spaced modes (Sect. 4.4.2), the singular vectors at the peak frequencies are good mode shape estimates;
- Create a report of modal identification results in terms of natural frequencies and mode shapes.

It is worth noting that also in the case of FDD the accuracy of natural frequency estimates depends on the frequency resolution; thus, long records of the structural response to ambient vibrations are recommended to obtain high quality singular value plots as a result of spectra characterized by a large number of averages and a fine frequency resolution (in the order of 0.01 Hz). Natural frequency estimates independent of the frequency resolution and damping estimates can be obtained by the EFDD method. In this case, the following additional steps have to be included in the previous list before reporting:

- For each peak frequency, compare the singular vector associated to the selected peak frequency with the singular vectors at the nearby frequencies; retain all the singular values in the vicinity of the peak whose singular vectors yield a MAC (4.109) with the singular vector associated to the peak frequency larger than a user-defined MAC Rejection Level (usually, 0.8); the selected singular values belong to the SDOF Bell function of the considered mode;
- Compute the IFT of the SDOF Bell functions to obtain the approximated SDOF correlation functions (Sect. 4.4.2);
- For each correlation function, select the portion characterized by large amplitude (removing the tails where the influence of noise is relevant, and eventually neglecting also the first cycle) and estimate the damping ratio by the logarithmic

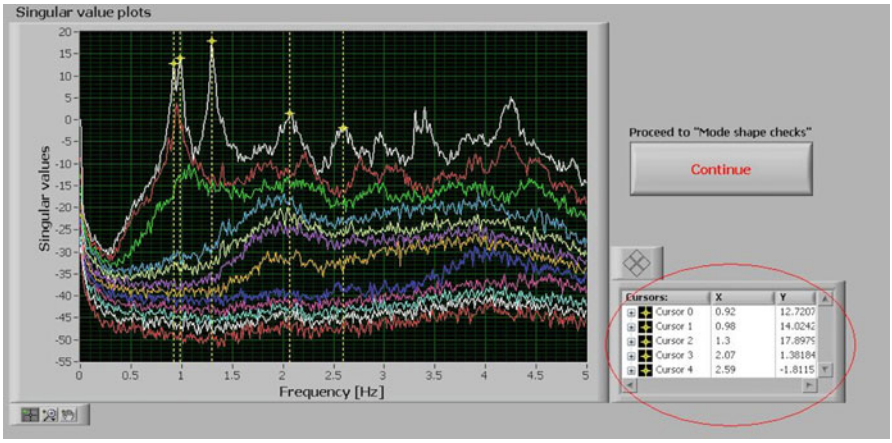

Fig. 4.14 Singular value plots and cursor legend (in the *oval*)

decrement technique; get an estimate of the damped frequency independent of the frequency resolution from the number of zero crossing points in the selected interval; use the estimates of damped frequency and damping ratio to compute the natural frequency (4.110).

Use the FDD method to identify the three fundamental modes of the structure. Cursors can be added by right-clicking on the cursor legend (marked by the oval in Fig. 4.14) and selecting "Create Cursor – Single-Plot"; cursors are attached to one of the singular value plots by right-clicking on the cursor legend and selecting "Snap To" and the number of the plot.

Since the fundamental modes are normal, real-valued mode shapes can be easily recovered from the (normalized) complex-valued singular vectors (Sect. 4.8.1). Compute the AutoMAC (Sect. 4.8.2.2). Compare the obtained results with the corresponding natural frequency and mode shape estimates obtained from BFD (Sect. 4.10.1). Report the results of the comparison in a table showing, for each mode, the frequency scatter between the natural frequency estimates (4.298) and the CrossMAC (Sect. 4.8.2.2) between corresponding mode shapes. Use COMAC (4.304) or ECOMAC (4.305) to identify the DOFs causing the major differences in the mode shape estimates provided by the two methods.

Sample software. Sample software to carry out output-only modal identification based on the FDD method can be found in "Chapter 4/FDD" of the disk accompanying the book.

4.10.3 Least Squares Complex Frequency

Task. Develop software for output-only modal identification based on the LSCF method. Alternatively, install and use the software in "Chapter 4/LSCF". Repeat the identification of the fundamental modes of the structure of Sect. 4.10.1.

Operational response data are in "Sample record 12 channels – sampling frequency 10 Hz.txt" in the folder "Chapter 2/Correlation" of the disk accompanying the book. Organization of data in the file has been described in Sect. 4.10.1. Sensor layout is shown in Fig. 4.12.

Suggestions. The previously developed software for Peak Picking can be extended to carry out output-only modal identification according to the LSCF method. Here is the list of the main tasks in software development:

- At start-up, load the data and set the main analysis parameters (window, number of segments, decimation factor, overlap, maximum polynomial order for the construction of the stabilization diagram);
- Compute the PSD matrix;
- Select the z-domain basis function: z_f (4.116) or z_f^{-1};
- Assuming that z_f has been adopted as basis function (in the case of z_f^{-1} the implementation steps are the same; the only difference is in the coefficient constraint and, therefore, in the formulation for computation of the denominator coefficients; refer to Sect. 4.9 for more details), compute z_f^j (j = 0, . . ., n, where n denotes the polynomial order) at all discrete frequency lines and build the matrices $[\Gamma_k]$ (4.126) and $[\Upsilon_k]$ (4.127) for k = 1, . . ., $l \times l$;
- Compute the matrices $[R_k]$ (4.129), $[S_k]$ (4.130), and $[T_k]$ (4.131) for k = 1, . . ., $l \times l$;
- Compute the (n + 1) × (n + 1) matrix $[M]$ as follows:

$$[M] = \sum_{k=1}^{l \cdot l} \left([T_k] - [S_k]^H [R_k]^{-1} [S_k] \right) \tag{4.314}$$

- Compute $\{\theta_d\}$ (4.135);
- Use "Polynomial Roots.vi" under "Mathematics – Polynomial" in the Functions Palette to compute the roots z_r;
- Convert the poles from discrete time to continuous time (4.136);
- Remove the unstable poles (Sect. 4.9);
- Compute natural frequencies (4.137) and damping ratios (4.139) from the remaining poles;
- Repeat the last eight steps for different model orders and plot the stabilization diagram reporting the poles as a function of frequency for different model orders (Sect. 4.9);
- Identify the alignments of stable poles in the stabilization diagram, which correspond to structural modes; select a pole for each identified structural mode;
- Use the selected poles (holding the information about natural frequencies and damping ratios) to compute the residues according to the LSFD method (4.147); rearrange the vector $\{R_k\}$ into the $l \times l$ residue matrices $[R_j]$;
- Compute the SVDs of the residue matrices $[R_j]$ (4.148); for each SVD the first singular vector yields a mode shape estimate;

- Normalize the mode shape vectors so that the component with maximum amplitude is equal to 1;
- Create a report of modal identification results in terms of natural frequencies and mode shapes.

Appropriately replacing the equations (Sect. 4.4.3.2), the p-LSCF method can be implemented in a similar way.

Use the LSCF method to identify the three fundamental modes of the structure. Since they are normal modes, real-valued mode shapes can be easily recovered from the (normalized) complex-valued singular vectors (Sect. 4.8.1). Compute the AutoMAC matrix (Sect. 4.8.2.2). Compare the obtained results with those provided by FDD or BFD. In particular, compute the scatters between corresponding natural frequency estimates (4.298) and the CrossMAC matrix (Sect. 4.8.2.2).

Sample software. Sample software to carry out output-only modal identification based on the LSCF method can be found in "Chapter 4/LSCF" of the disk accompanying the book.

4.10.4 Stochastic Subspace Identification

Task. Develop software for output-only modal identification based on the Cov-SSI method. Alternatively, install and use the software in "Chapter 4/Cov-SSI". Repeat the identification of the fundamental modes of the structure of Sect. 4.10.1. Operational response data are in "Sample record 12 channels – sampling frequency 10 Hz. txt" in the folder "Chapter 2/Correlation" of the disk accompanying the book. Organization of data in the file has been described in Sect. 4.10.1. Sensor layout is shown in Fig. 4.12.

Suggestions. The software implementation of the Cov-SSI algorithm for output-only modal identification is based on the following steps:

- At start-up, load the data and eventually set the filter parameters and the decimation factor;
- Compute the PSD matrix and show its trace in a plot to estimate the number of structural modes in the frequency range under investigation; set the number of block rows accordingly; the condition expressed by (4.207) must be fulfilled; the product $l \times \mathrm{i}$ defines the limit value of the maximum model order that can be adopted in the construction of the stabilization diagram; however, the maximum model order in the stabilization plot is usually much lower than $l \times \mathrm{i}$, and it is defined so that only a subset of the singular values and vectors of the block Toeplitz matrix of correlations ((4.206), (4.211), and (4.212)) is retained;
- Compute the SVD of the block Toeplitz matrix of correlations ((4.206), (4.211), and (4.212)) and define the maximum model order in the construction of the stabilization diagram (Sect. 4.9);
- From the retained subset of singular values and vectors of the block Toeplitz matrix of correlations compute the observability matrix $[O_i]$ (4.213) and the reversed controllability matrix $[\Gamma_i]$ (4.214); the first l rows of $[O_i]$ and the last

l rows of $[\Gamma_i]$ yield the output influence matrix $[C]$ and the next state-output covariance matrix $[G]$, respectively;

- Compute the state matrix $[A]$ from (4.216) and (4.217); alternatively, it can be computed according to (4.218) and (4.219), with the weights given by (4.220) or (4.224);
- The poles in discrete time are obtained by the eigenvalue decomposition of $[A]$ (4.77); they have to be converted from discrete time to continuous time (4.136) in order to compute natural frequency (4.137) and damping ratio (4.139) from each pole; the corresponding mode shapes are obtained from the eigenvectors of $[A]$ according to (4.79);
- Repeat the last three steps for different model orders and plot the stabilization diagram reporting the poles as a function of frequency for different model orders (Sect. 4.9); in this case, also the information about the mode shapes (4.308) is used for the construction of the stabilization diagram;
- Identify the alignments of stable poles in the stabilization diagram, which correspond to structural modes; select a pole for each identified structural mode;
- Normalize the mode shape vector associated to each pole so that the component with maximum amplitude is equal to 1;
- Create a report of modal identification results in terms of natural frequencies and mode shapes.

DD-SSI can be implemented in a similar way according to the following list of steps:

- The first two steps are the same of Cov-SSI; the only difference is that the block Toeplitz matrix of correlation is replaced by the block Hankel matrix of raw data (4.229);
- Compute the LQ factorization of the block Hankel matrix of the outputs and the projections $[P_i]$ and $[P_{i-1}]$ ((4.234), (4.235), (4.236), and (4.237));
- Compute the SVD of $[P_i]$ (4.240) and define the maximum model order in the construction of the stabilization diagram;
- From the retained subset of singular values and vectors of $[P_i]$ compute the observability matrix $[O_i]$ (4.241) and the Kalman filter state sequence $\left[\hat{S}_i\right]$ (4.242);
- Compute $\left[\hat{S}_{i+1}\right]$ from (4.244);
- Compute the state matrix $[A]$ and the output influence matrix $[C]$ from (4.246); alternatively, the state matrix can be computed directly from the observability matrix according to (4.219) or (4.252), while the first l rows of $[O_i]$ yield the output influence matrix;
- The poles in discrete time are obtained by the eigenvalue decomposition of $[A]$ (4.77); they have to be converted from discrete time to continuous time (4.136) in order to compute natural frequency (4.137) and damping ratio (4.139) from each pole; the corresponding mode shapes are obtained from the eigenvectors of $[A]$ according to (4.79);
- Repeat the last four steps for different model orders and plot the stabilization diagram reporting the poles as a function of frequency for different model orders (Sect. 4.9); in this case, also the information about the mode shapes (4.308) is used for the construction of the stabilization diagram;

- Proceed as in the case of Cov-SSI (last three steps) to select the parameters of the structural modes and create a report of modal identification results.

Use the Cov-SSI method to identify the three fundamental modes of the structure. Since they are normal modes, real-valued mode shapes can be easily recovered from the (normalized) complex-valued singular vectors (Sect. 4.8.1). Compute the AutoMAC matrix (Sect. 4.8.2.2). Compare the obtained results with those provided by FDD and LSCF. In particular, compute the scatters between corresponding natural frequency and damping ratio (LSCF/Cov-SSI only) estimates, and the CrossMAC matrices (Sect. 4.8.2.2) with the mode shape estimates provided by LSCF and FDD.

Sample software. Sample software to carry out output-only modal identification based on the Cov-SSI method can be found in "Chapter 4/Cov-SSI" of the disk accompanying the book.

4.10.5 Second Order Blind Identification

Task. Install and use the software in "Chapter 4/SOBI" for output-only modal identification according to the SOBI method. Identify the modes of the structure of Sect. 4.10.1 in the range 0–5 Hz. Compare the results provided by SOBI with those obtained from Cov-SSI or any other method yielding complex-valued mode shape estimates. Operational response data are in "Sample record 12 channels – sampling frequency 10 Hz.txt" in the folder "Chapter 2/Correlation" of the disk accompanying the book. Organization of data in the file has been described in Sect. 4.10.1. Sensor layout is shown in Fig. 4.12.

Suggestions. When SOBI is used for output-only modal identification, mode shapes are directly obtained from the mixing matrix (Sect. 4.5.4). Natural frequencies and damping ratios can be estimated from the auto-correlations of the sources as follows:

- for each correlation function, select the portion characterized by large amplitude (removing the tails where the influence of noise is relevant, and eventually neglecting also the first cycle);
- get an estimate of the damping ratio by the logarithmic decrement technique;
- get an estimate of the damped frequency independent of the frequency resolution from the number of zero crossing points in the selected interval;
- use the estimates of damped frequency and damping ratio to compute the natural frequency (4.110).

Use the Cov-SSI method to identify also the higher modes of the structure. Among them, the mode at 2.59 Hz shows appreciable imaginary parts in the mode shape components (Fig. 4.15). Comparison of the modal parameter estimates provided by Cov-SSI with those obtained from SOBI results in a good agreement for the fundamental modes. The mode at 2.07 Hz cannot be properly identified by SOBI. About the mode at 2.59 Hz, SOBI yields a mode shape estimate characterized by a CrossMAC with the corresponding estimate by Cov-SSI that is

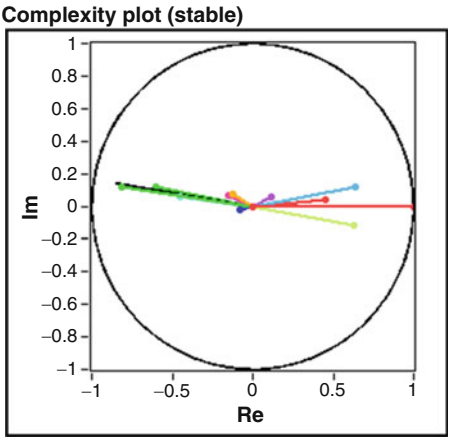

Fig. 4.15 Complexity plot of the mode at 2.59 Hz (mode shape estimate obtained from Cov-SSI)

slightly lower than the CrossMAC values obtained for the fundamental modes. The difference can be addressed to the fact that SOBI forces the mode shape estimates to be real-valued.

Sample software. Sample software to carry out output-only modal identification based on the SOBI method can be found in "Chapter 4/SOBI" of the disk accompanying the book.

4.10.6 Influence of Sensor Layout

Task. Remove channels #3, #7, and #11 from the dataset in "Sample record 12 channels – sampling frequency 10 Hz.txt" in the folder "Chapter 2/Correlation" of the disk accompanying the book and update the sensor layout shown in Fig. 4.12. Repeat the identification of the modes of the structure of Sect. 4.10.1 by a method of your choice among the previous ones. Compare the AutoMAC matrices before and after the removal of the above-mentioned channels.

Suggestions. Even if both translations and torsions are still observable after sensor removal, the presence of large off-diagonal elements in the AutoMAC matrix highlights that the new layout is less effective than the previous one in distinguishing some of the modes.

References

Allemang RJ, Brown DL (1982) A correlation coefficient for modal vector analysis. In: Proc 1st international modal analysis conference, November 8–10, 1982, Orlando, FL

Allemang RJ, Brown DL (1998) A unified matrix polynomial approach to modal identification. J Sound Vib 211(3):301–322

Andersen P (1997) Identification of civil engineering structures using vector ARMA models, Ph.D. thesis. University of Aalborg, Aalborg

Andersen P, Brincker R (1999) Estimation of modal parameters and their uncertainties. In: Proc XVII international modal analysis conference, February 8–11, 1999, Kissimmee, FL

Andersen P, Brincker R, Kirkegaard PH (1996) Theory of covariance equivalent ARMAV models of civil engineering structures. In: Proc XIV international modal analysis conference, February 12–15, 1996, Dearborn, MI

Ans B, Hérault J, Jutten C (1985) Adaptive neural architectures: detection of primitives. In: Proc COGNITIVA'85, June 4–7, 1985, Paris

Aoki M (1987) State space modeling of time series. Springer, Berlin

Asmussen JC, Brincker R, Ibrahim SR (1999) Statistical theory of the vector random decrement technique. J Sound Vib 226(2):329–344

Bartlett MS (1946) The theoretical specification and sampling properties of autocorrelated time-series. J R Stat Soc 8(1):27–41, Supplement

Belouchrani A, Abed-Meraim K, Cardoso JF, Moulines E (1997) A blind source separation technique using second-order statistics. IEEE Trans Signal Process 45:434–444

Bendat JS, Piersol AG (2000) Random data: analysis and measurement procedures, 3rd edn. Wiley, New York, NY

Brincker R, Andersen P (1999) ARMA models in modal space. In: Proc XVII international modal analysis conference, February 8–11, 1999, Kissimmee, FL

Brincker R, Andersen P (1999) Ambient response modal analysis for large structures. In: Proc 6th Int Congr on Sound and Vib, July 5–8, 1999, Copenhagen

Brincker R, Zhang L (2009) Frequency domain decomposition revisited. In: Proc 3rd international operational modal analysis conference, May 4–6, 2009, Portonovo

Brincker R, Krenk S, Kirkegaard PH, Rytter A (1992) Identification of dynamical properties from correlation function estimates. Bygningsstatiske Meddelelser 63(1):1–38

Brincker R, Zhang L, Andersen P (2001) Modal identification of output-only systems using frequency domain decomposition. Smart Mat Struct 10:441–445

Cardoso JF, Souloumiac A (1996) Jacobi angles for simultaneous diagonalization. SIAM J Matrix Anal Appl 17:161–164

Cauberghe B (2004) Applied frequency-domain system identification in the field of experimental and operational modal analysis, Ph.D. thesis. Vrije Universiteit Brussels, Brussels

Cauberghe B, Guillaume P, Verboven P, Vanlanduit S, Parloo E (2005) On the influence of the parameter constraint on the stability of the poles and the discrimination capabilities of the stabilisation diagrams. Mech Syst Signal Process 19:989–1014

Chelidze D, Zhou W (2006) Smooth orthogonal decomposition-based vibration mode identification. J Sound Vib 292:461–473

Chopra AK (2000) Dynamics of structures – theory and applications to earthquake engineering, 2nd edn. Prentice Hall, Upper Saddle River, NJ

Cole HA (1968) On-the-line analysis of random vibrations. In: Proc AIAA/ASME 9th structures, structural dynamics and materials Conf, April 1–3, 1968, Palm Springs, CA

Cole HA (1973) On-line failure detection and damping measurement of aerospace structures by random decrement signatures. NASA contractor report CR22-05

Comon P (1994) Independent component analysis, a new concept? Signal Process 36:287–314

De Troyer T, Guillaume P, Steenackers G (2009a) Fast variance calculation of polyreference least-squares frequency-domain estimates. Mech Syst Signal Process 23:1423–1433

De Troyer T, Guillaume P, Pintelon R, Vanlanduit S (2009b) Fast calculation of confidence intervals on parameter estimates of least-squares frequency-domain estimators. Mech Syst Signal Process 23:261–273

Devriendt C, Guillaume P (2007) The use of transmissibility measurements in output-only modal analysis. Mech Syst Signal Process 21(7):2689–2696

Devriendt C, Guillaume P (2008) Identification of modal parameters from transmissibility measurements. J Sound Vib 314:343–356

Devriendt C, De Sitter G, Vanlanduit S, Guillaume P (2009) Operational modal analysis in the presence of harmonic excitations by the use of transmissibility measurements. Mech Syst Signal Process 23:621–635

Devriendt C, Steenackers G, De Sitter G, Guillaume P (2010) From operating deflection shapes towards mode shapes using transmissibility measurements. Mech Syst Signal Process 24:665–677

Even J, Moisan E (2005) Blind source separation using order statistics. Signal Process 85:1744–1758

Ewins DJ (2000) Modal testing: theory, practice and application, 2nd edn. Research Studies Press Ltd., Baldock

Feeny BF, Kappagantu R (1998) On the physical interpretation of proper orthogonal modes in vibrations. J Sound Vib 211:607–616

Felber AJ (1993) Development of a hybrid bridge evaluation system, Ph.D. thesis. University of British Columbia, Vancouver

Franklin GF, Powell JD, Workman ML (2006) Digital control of dynamic systems, 3rd edn. Ellis-Kagle Press, Half Moon Bay, CA

Friswell MI, Mottershead JE (1995) Finite element model updating in structural dynamics. Kluwer Academic Publishers, Dordrecht

Gade S, Møller NB, Herlufsen H, Konstantin-Hansen H (2005) Frequency domain techniques for operational modal analysis. In: Proc 1st international operational modal analysis conference, April 26–27, 2005, Copenhagen

Golub GH, Van Loan CF (1996) Matrix computations, 3rd edn. The Johns Hopkins University Press, Baltimore, MD

Gouttebroze S, Lardies J (2001) On using the wavelet transform in modal analysis. Mech Res Comm 28(5):561–569

Han J-G, Ren W-X, Xu X-X (2005) Wavelet-based modal parameter identification through operational measurements. In: Proc 1st international operational modal analysis conference, April 26–27, 2005, Copenhagen

Hanson D, Randall RB, Antoni J, Thompson DJ, Waters TP, Ford RAJ (2007) Cyclostationarity and the cepstrum for operational modal analysis of mimo systems – Part I: modal parameter identification. Mech Syst Signal Process 21(6):2441–2458

Herlufsen H, Andersen P, Gade S, Møller N (2005) Identification techniques for operational modal analysis – an overview and practical experiences. In: Proc 1st international operational modal analysis conference, April 26–27, 2005, Copenhagen

Hermans L, Van Der Auweraer H (1999) Modal testing and analysis of structures under operational conditions: industrial applications. Mech Syst Signal Process 13(2):193–216

Heylen W, Lammens S, Sas P (1998) Modal analysis theory and testing. Katholieke Universiteit Leuven, Leuven

Ho BL, Kalman RE (1966) Effective construction of linear state-variable models from input/output data. Regelungstechnik 14:545–548

Hunt DL (1992) Application of an enhanced coordinate modal assurance criterion (ECOMAC). In: Proc 10th international modal analysis conference, February 3–7, 1992, San Diego, CA

Ibrahim SR (1977) Random decrement technique for modal identification of structures. J Spacecraft Rockets 14(11):696–700

Ibrahim SR, Mikulcik EC (1977) A method for direct identification of vibration parameters from the free response. Shock Vib Bul 47:183–198

Ibrahim SR, Brincker R, Asmussen JC (1996) Modal parameter identification from responses of general unknown random inputs. In: Proc 14th international modal analysis conference, February 12–15, 1996, Dearborn, MI

Jacobsen N-J, Andersen P, Brincker R (2008) Applications of frequency domain curve-fitting in the EFDD technique. In: Proc 26th international modal analysis conference, February 4–7, 2008, Orlando, FL

James GH, Carne TG, Lauffer JP, Nord AR (1992) Modal testing using natural excitation. In: Proc 10th international modal analysis conference, February 3–7, 1992, San Diego, CA

James GH, Carne TG, Lauffer JP (1995) The natural excitation technique (next) for modal parameter extraction from operating structures. J Anal Exp Modal Anal 10(4):260–277

Juang J-N (1994) Applied system identification. PTR Prentice Hall, Englewood Cliffs, NJ
Juang J-N, Pappa RS (1985) An eigensystem realization algorithm for modal parameter identification and model reduction. AIAA J Guid Contr Dynam 8:620–627
Kailath T (1980) Linear systems. Prentice Hall, Englewood Cliffs, NJ
Katayama T (2005) Subspace methods for system identification. Springer, London
Kerschen G, Golinval JC (2002) Physical interpretation of the proper orthogonal modes using the singular value decomposition. J Sound Vib 249:849–865
Kerschen G, Golinval JC, Vakakis AF, Bergman LA (2005) The method of proper orthogonal decomposition for dynamical characterization and order reduction of mechanical systems: an overview. Nonlin Dynam 41:147–170
Kerschen G, Poncelet F, Golinval JC (2007) Physical interpretation of independent component analysis in structural dynamics. Mech Syst Signal Process 21:1561–1575
Lardies J, Gouttebroze S (2002) Identification of modal parameters using the wavelet transform. Int J Mech Sci 44:2263–2283
Ljung L (1999) System identification: theory for the user, 2nd edn. Prentice Hall, Upper Saddle River, NJ
Magalhaes F, Cunha A (2011) Explaining operational modal analysis with data from an arch bridge. Mech Syst Signal Process 25:1431–1450
Maia NMM, Silva JMM, He J, Lieven NAJ, Lin RM, Skingle GW, To W-M, Urgueira APV (1997) Theoretical and experimental modal analysis. Research Studies Press, Taunton
McNeill SI, Zimmerman DC (2008) A framework for blind modal identification using joint approximate diagonalization. Mech Syst Signal Process 22:1526–1548
Mohanty P (2005) Operational modal analysis in the presence of harmonic excitations, Ph.D. thesis. Technische Universiteit Delft, Delft
Mottershead JE, Link M, Friswell MI (2011) The sensitivity method in finite element model updating: a tutorial. Mech Syst Signal Process 25(7):2275–2296
Olsen P, Brincker R (2013) Using random response input in Ibrahim Time Domain. In: Proc XXXI International Modal Analysis Conference, February 11–14, 2013, Garden Grove, CA
Pandit SM (1991) Modal and spectrum analysis: data dependent systems in state space. Wiley, New York, NY
Pandit SM, Wu SM (1983) Time series and system analysis with applications. Wiley, New York, NY
Pappa RS, Elliott KB, Schenk A (1992) A consistent mode indicator for the eigensystem realization algorithm. NASA Report TM-107607
Peeters B (2000) System identification and damage detection in civil engineering, Ph.D. thesis. Katholieke Universiteit Leuven, Leuven
Peeters B, De Roeck G (1999) Reference-based stochastic subspace identification for output-only modal analysis. Mech Syst Signal Process 13(6):855–878
Peeters B, Van der Auweraer H (2005) PolyMAX: a revolution in operational modal analysis. In: Proc 1st international operational modal analysis conference, April 26–27, 2005, Copenhagen
Pintelon R, Guillaume P, Rolain Y, Schoukens J, Van Hamme H (1994) Parametric identification of transfer functions in the frequency domain – a survey. IEEE Trans Automat Contr 39(11):2245–2260
Pintelon R, Guillaume P, Schoukens J (2007) Uncertainty calculation in (operational) modal analysis. Mech Syst Signal Process 21:2359–2373
Poncelet F, Golinval JC, Kerschen G, Verhelst D (2007) Output-only modal analysis using blind source separation techniques. Mech Syst Signal Process 21:2335–2358
Rainieri C, Fabbrocino G, Cosenza E (2010) Some remarks on experimental estimation of damping for seismic design of civil constructions. Shock Vib 17:383–395
Reynders E (2009) System identification and modal analysis in structural mechanics, Ph.D. thesis. Katholieke Universiteit Leuven, Leuven
Reynders E, Houbrechts J, De Roeck G (2012) Fully automated (operational) modal analysis. Mech Syst Signal Process 29:228–250

Reynders E, Pintelon R, De Roeck G (2008) Uncertainty bounds on modal parameters obtained from stochastic subspace identification. Mech Syst Signal Process 22:948–969

Richardson M, Schwarz B (2003) Modal parameter estimation from operating data. Sound Vib 302:1–8

Rodrigues J, Brincker R, Andersen P (2004) Improvement of frequency domain output-only modal identification from the application of the random decrement technique. In: Proc XXII international modal analysis conference, January 26–29, 2004, Dearborn, MI

Ruzzene M, Fasana A, Garibaldi L, Piombo B (1997) Natural frequencies and dampings identification using wavelet transform: application to real data. Mech Syst Signal Process 11(2):207–218

Schoukens J, Pintelon R (1991) Identification of linear systems: a practical guide to accurate modeling. Pergamon Press, London

Shih CY, Tsuei YG, Allemang RJ, Brown DL (1988) Complex mode indication function and its applications to spatial domain parameter estimation. Mech Syst Signal Process 2(4):367–377

Srikantha Phani A, Woodhouse J (2007) Viscous damping identification in linear vibration. J Sound Vib 303:475–500

Tamura Y, Suganuma S-Y (1996) Evaluation of amplitude-dependent damping and natural frequency of buildings during strong winds. J Wind Eng Ind Aerodyn 59:115–130

Tong L, Liu RW, Soon VC, Huang YF (1991) Indeterminacy and identifiability of blind identification. IEEE Trans Circ Syst 38:499–509

Van Overschee P, De Moor B (1993) Subspace algorithm for the stochastic identification problem. Automatica 29(3):649–660

Van Overschee P, De Moor B (1996) Subspace identification for linear systems: theory - implementation – applications. Kluwer Academic Publishers, Dordrecht

Vandiver JK, Dunwoody AB, Campbell RB, Cook MF (1982) A mathematical basis for the random decrement vibration signature analysis technique. J Mech Des 104(2):307–313

Verboven P (2002) Frequency-domain system identification for modal analysis, Ph.D. thesis. Vrije Universiteit Brussels, Brussels

Verboven P, Guillaume P, Cauberghe B, Vanlanduit S, Parloo E (2005) A comparison of frequency-domain transfer function model estimator formulations for structural dynamics modeling. J Sound Vib 279(3–5):775–798

Vold H, Kundrat J, Rocklin T, Russell R (1982) A multi-input modal estimation algorithm for mini-computers. SAE Trans 91(1):815–821

Waters TP (1995). Finite element model updating using measured frequency response functions, Ph.D. thesis. University of Bristol, Bristol

Yi J-H, Yun C-B (2004) Comparative study on modal identification methods using output-only information. Struct Eng Mech 17(3–4):445–466

Zhang L, Wang T, Tamura Y (2005) A frequency-spatial domain decomposition (FSDD) technique for operational modal analysis. In: Proc 1st international operational modal analysis conference, April 26–27, 2005, Copenhagen

Zhang L, Brincker R, Andersen P (2005) An overview of operational modal analysis: major development and issues. In: Proc 1st international operational modal analysis conference, April 26–27, 2005, Copenhagen

Zhou W, Chelidze D (2007) Blind source separation based vibration mode identification. Mech Syst Signal Process 21:3072–3087